CHANGES (*Creating Habitat, Acidification reduction, Nitrogen bio-extraction, Guarding our shorelines, Erosion control, Sequestering carbon)*

Progress Report for Peconic Estuary Partnership, March 2026

EXECUTIVE SUMMARY

Coastal communities, ecosystems, and fisheries face multiple concurrent, compounding and complex environmental threats in the 20th century. Sea level rise poses a significant and escalating threat to coastal communities. Habitat loss has resulted in the collapse of critical fisheries. The overloading of nitrogen from anthropogenic sources has degraded water quality and contributed to the decline of fisheries and aquaculture. Ocean acidification represents an additional threat to shellfisheries. Still, creative expansion of bivalve populations and marine habitats offers an opportunity to mitigate these threats, while enhancing fisheries. Oyster, seagrasses, and kelp aquaculture can contribute significantly to coastal economies and economic growth and may offer valuable natural defenses against the storm surge and sea-level rise while also offering opportunities to mitigate ocean acidification. The overarching objective of this project is to utilize combinations of kelp, oysters, and seagrasses to bioextract nitrogen, sequester carbon, mitigate ocean acidification, protect shorelines, enhance fisheries and biodiversity, and improve water quality/clarity. The first phase of the project was designed to identify locations that would be ideal for the development of a living shoreline that would creating habitat, combat ocean acidification, actively bio-extract reduction nitrogen, protect shorelines, and sequester carbon.

During 2023 and 2024, six locations across the Peconic Estuary were evaluated for water quality (temperature salinity, dissolved oxygen, light penetration, chlorophyll *a*, total nitrogen) sediment composition (grain size distribution, organic matter content, depth of muds), and growth and survival performance of kelp, seagrass and oysters. The data has combined to provide a clear sense regarding locations that would be ideal for kelp, seagrass, and oysters. Among the sites considered, Menatic Creek was deemed inappropriate as it had poor water and sediment quality (high chlorophyll *a* and total nitrogen, low dissolved oxygen and water clarity, muddy, fine-grained sediments) and yielded poor kelp and seagrass survival and growth, although the oyster population did well at this location. Some other sites were deemed to be too marginal for full scale restoration projects including Ganet Creek, Sag Harbor Cove, and the South Ferry/Shelter Island Sound site. These locations had fair water and sediment quality, fair kelp growth, varied seagrass growth, but generally good oyster growth. Sag Harbor Cove was the best among the marginal sites, but may not be appropriate due to the presence of widgeon grass. Two sites that were studied in 2024 that seemed ideal for restoration were the Barcelona Point/Northwest Harbor site and the east side of North Haven. These sites had excellent water quality and sediment quality (low chlorophyll *a* and total nitrogen, high dissolved oxygen and water clarity, coarser grained, low organic matter sediments), had the best kelp growth, excellent seagrass growth and survival, and good oyster growth and survival.

During 2025, deployments of oysters, kelp, and eelgrass were expanded at the two most promising sites (i.e., Barcelona Point and East North Haven), and monitoring continued at these sites and Sag Harbor Cove. Kelp yields were greatly enhanced in 2025 compared to 2024, with the yields found at Barcelona Point (4.6 kg m^{-1}) marking the second highest kelp yield the Gobler Lab has achieved

in the Peconic Estuary over the past five years. In part, this can be attributed to the use of gametophyte cultures for the production of seedstock, which allowed for the earlier seeding of lines in the field (i.e. November vs. December) as compared to the traditional seedstock production method whereby spores are released from wild-collected kelp tissue. Spore-derived seedstock, however, also performed well in 2025, suggesting that environmental conditions were better for kelp in 2025. Oyster deployments were expanded with the addition of three more oyster cages at each site, as well as three spat-on-shell bags. Spat-on-shell bags are typically used by oyster restoration practitioners to build restored oyster reefs, and their use here allowed us to begin to evaluate this restoration strategy for these sites. Oyster continued to thrive at the study sites in 2025, with high survival and growth. The eelgrass patches planted in 2024 continued to persist and even expand in aerial coverage in 2025, and the new patches transplanted in 2025 also survived throughout the year.

INTRODUCTION

Oyster, seagrasses, and kelp aquaculture significantly contributes to coastal economies and economic growth in the US (NOAA, 2024). Regarding oyster and kelp, these industries generate revenue through the direct sale of harvested products (Gentry et al., 2017). Kelp also holds promise as a fertilizer and source of biostimulants for emerging agricultural markets (Kim et al., 2019). Seagrasses play a critical role as a nursery habitat for many important shellfish and finfish fisheries (Heck et al., 2003). Aquaculture operations for crops such as oyster and kelp create jobs in coastal communities, spanning farm labor, processing, distribution, and supporting industries like boatbuilding and equipment supply (Jolly and Klonts, 2020). Furthermore, these forms of aquaculture can enhance tourism and recreation by attracting visitors interested in sustainable seafood and recreational fishing opportunities associated with restored habitats (Hicks et al., 2004; Jolly and Klonts, 2020). Moreover, restoration of shellfisheries can play a key role in boosting regional economies. For example, the Shinnecock Bay Restoration Program was shown to contribute tens of millions of dollars to the regional economy by restoring the hard clam fishery in Shinnecock Bay (Gobler et al., 2022). By diversifying coastal economies and providing sustainable alternatives to wild-capture fisheries, oyster and seagrass restoration, and kelp aquaculture, can support economic resilience and long-term economic growth in coastal regions.

Sea level rise, driven by thermal expansion of warming ocean waters and melting ice sheets, poses a significant and escalating threat to coastal communities. As sea levels rise, inundation of low-lying communities becomes more frequent and severe, leading to coastal erosion, and damage to infrastructure (IPCC, 2021). Furthermore, sea level rise exacerbates the impacts of storm surges, increasing the risk of flooding and destruction during extreme weather events (Kopp et al., 2017). The combined effects of these processes threaten the economic stability of coastal communities, necessitating adaptation and mitigation strategies to minimize future losses and displacement (Bosello & De Cian, 2014).

Oyster reefs, seagrass meadows, and aquaculture kelp lines can offer valuable natural defenses against the combined threats of storm surge and sea-level rise for coastal communities. Oyster reefs, with their complex three-dimensional structure, act as natural breakwaters, dissipating wave energy and reducing storm surge height (Scyphers et al., 2011). Similarly, seagrass meadows, by stabilizing sediments and creating friction against water flow, attenuate wave action and lessen the impact of storm surge (Paul, 2018). Furthermore, the vertical structure of kelp forests cultivated on aquaculture lines can also provide a similar wave-buffering effect, reducing wave height and energy reaching the shore (Bodycomb et al., 2023). These natural and nature-based features not only offer immediate protection against storm surge but also contribute to long-term coastal resilience in the face of sea-level rise by trapping sediment and building elevation, effectively combating erosion and maintaining critical intertidal habitats (Phillips, 2018). Integrating these ecosystem-based approaches into coastal management strategies offers

a sustainable and cost-effective way to enhance coastal protection and adapt to the challenges of sea level rise.

Finally, seagrass meadows, kelp forests, and to a lesser extent oyster reefs are recognized as "blue carbon" ecosystems that sequester carbon and mitigate the threat of ocean acidification. It is clear that kelp and seagrasses absorb substantial amounts of carbon from the atmosphere and seawater through photosynthesis, effectively reducing the concentration of CO_2 (Duarte and Krause-Jensen, 2017; Duarte et al., 2025). The carbon is then stored in their biomass, as well as in the sediments beneath seagrasses and within the complex three-dimensional structure of kelp forests (Macreadie et al., 2019; Duarte et al., 2025). This process not only sequesters carbon but also helps to buffer against ocean acidification by increasing pH levels in the surrounding waters (Hendriks et al., 2014). By locally reducing CO2 concentrations and increasing pH, seagrasses and kelp can create refugia for marine organisms that are vulnerable to the impacts of ocean acidification, including oysters (Young et al., 2022). Protecting and restoring these valuable ecosystems is therefore crucial for both carbon mitigation and adaptation strategies in the face of climate change.

OBJECTIVE AND TASKS:

The overarching objective of this project is to utilize combinations of kelp, oysters, and seagrasses to bioextract nitrogen, sequester carbon, mitigate ocean acidification, protect shorelines, enhance biodiversity, and improve water quality/clarity.

Tasks of this project are to: 1. Perform benthic and pelagic site evaluations to assess the suitability of multiple sites across the eastern Peconic Estuary for the aquaculture of kelp, the establishment of restored oyster reefs and /or oyster aquaculture in cages, and for eelgrass restoration. 2. Perform experimental and pilot scale deployment of aquacultured kelp, oyster cages (i.e. aquaculture method) and shell bags (restoration method),and eelgrass shoots and seeds. 3. Quantify carbon sequestration, nitrogen bioextraction, and shoreline protection afforded by sundry experimental and pilot scale approaches, and 4. To estimate carbon sequestration, nitrogen bioextraction, and shoreline protection afforded by full scale deployments.

METHODS

Approach

Restoration/aquaculture activities, and the associated monitoring, were conducted at three of the original six study sites: Barcelona Point (BP), East North Haven (ENH), and Sag Harbor Marina (SHM) (Figure 1). Kelp was cultivated and monitored at all three of these sites. Oyster, summer seaweed (i.e. *Ulva sp.*) and eelgrass deployments and monitoring were expanded at the two most promising sites, BP and ENH. Following the expanded deployments at BP and ENH, the field

design, heading shoreward from the outer edge of the restoration area, consisted of 1) four shallow-water staked kelp lines, (two gametophyte-derived and two spore-derived), 2) six low-profile bottom oyster cages, 3) three spat-on-shell (SOS) oyster reef bags, and 4) transplanted seagrass patches and seed (Figures 2 & 3). Monitoring of each restoration component (i.e. kelp, oysters, and eelgrass), along with water quality and wave energy, was conducted throughout the year following the methods described in the subsections below.

Water Quality Monitoring

Water quality monitoring was conducted using various instruments for both discrete and continuous data collection. Continuous dissolved oxygen (mg L^{-1}), temperature (°C), and pH sensors (HOBO data loggers) were deployed at the midpoint of the second kelp line during the kelp growing season and were deployed on the top of the third low-profile bottom cage during the oyster growing season (Figure 2). All HOBOware continuous monitoring instruments were programmed to log at 10-minute intervals and were serviced in the field and data offloading accord on a bi-weekly basis. To complement the continuous measurements, discrete water temperature (°C), DO (mg L^{-1}), and salinity (ppt) was measured using a Handheld multiparameter meter during each site visit. Water samples were collected monthly for dissolved nutrients (DNUTS) to obtain total nitrogen on filtered (0.2 µm) polysulfide capsule. Site water was collected and quantified in triplicate on filtered combusted glass fiber filters (CGFF) on site and frozen for later analyzed fluorometrically (Parsons, 2013).

Wave Energy

Wave action impact was continuously measured using a RBR*solo³* D: pressure (depth) wave attenuation sensor inside and outside the restoration area, set to 17-minute bursts intervals for a ~14-day period in 2024 at four of the study sites and for a ~20-day period in 2025 and 2026 at the East North Haven study site. Inside the restoration area, wave attenuation sensors were placed on the shoreward side of the low-profile cages (Figure 2). Outside the conservation, the sensor was paced in open unprotected water to the side of the restoration area (Figure 2). The hydrodynamic measurements recorded included tidal slope (m $hour^{-1}$), average wave height (meters), maximum wave height (meters), and wave energy (J m^{-2}).

Kelp

At each cultivation site, kelp lines were seeded with seedstock produced in the Gobler Lab kelp hatchery by two different methods: spore-derived and gametophyte-derived. For spore-derived seedstock, reproductive parental tissue was collected by SCUBA divers off Montauk Point in early November of 2024. Following collection, reproductive kelp blades were immediately brought back to the lab where the sorus tissue was excised, cleaned, and desiccated overnight in

a refrigerator. The following day, the prepared tissue was placed in 10 °C filtered seawater to induce spore release, and the spores were set onto spools of string in aquarium tanks at known setting densities. The spools of seedstring were grown in aquarium in f/2 nutrient enriched sterilized seawater under controlled environmental conditions (10 °C; 12:12 light-dark cycle), with weekly water changes performed until the juvenile sporophytes were large enough (~2 mm) to seed kelp lines at the field sites, which occurred in December, approximately 5 to 6 weeks after the initial spore release. In NY waters, reproductive kelp tissue typically cannot be found in wild kelp populations until late October/early November, and spore-derived seedstock is therefore typically not ready for field deployment until December.

For gametophyte-derived seedstock, cultures of kelp gametophytes (a microscopic life stage of kelp) were painted onto spools of seedstring, which were then cared for in the kelp hatchery following the same methods as for spore-derived seed spools. The gametophyte cultures were purchased from Greenwave and painted onto seed spools in October, and were ready for deployment to the field sites in November, a month earlier than the spore-derived seedstock. In NY waters, reproductive kelp tissue typically cannot be found in wild kelp populations until late October/early November, and spore-derived seedstock is therefore typically not ready for field deployment until December. Gametophyte cultures, on the other hand, can be maintained year-round, allowing for the earlier production of seedstock that can be deployed as soon as water temperatures are cool enough (i.e. < 15 °C).

Kelp biomass growth and the carbon and nitrogen (CN) content of kelp tissue were monitored on a monthly basis from December through May by collecting triplicate samples from each open-water kelp line deployed at each site. For each sample, all kelp biomass, including blade, stipe, and holdfast, was excised from a 15 cm length of line, and transported back to the Southampton Marine Station laboratory on ice packs in coolers. Upon arrival, the samples were first cleaned of biofouling and spun in a salad spinner to remove excess water before the following measurements were made: wet weight, average kelp blade length, blade width, and stipe length. Following these measurements, the samples were dried at 60 °C in a laboratory drying oven. After complete drying, each sample was prepared and weighed for analysis of CN content on a combustion elemental analyzer at Stony Brook University's Center for Clean Water Technology. When growth ceased and kelp tissues began to decay in late spring, all kelp lines were harvested and brought to the Stony Brook – Southampton campus for drying and/or composting.

Summer Seaweeds

In year one of this project (2024), two endemic warm water species of macroalgae, *Agardhiella subulata* and *Ulva sp.* were deployed for cultivation trials at each of the six study sites. Species specific cultivation methods, based on prior cultivation experiments, were used, including: 1) commercial mussel socks utilized in the cultivation of *Agardhiella subulate*, and 2) modified commercial oyster grow out bags utilized in the cultivation of *Ulva sp.*. For both species, cultivation involved the vegetative propagation of wild-collected parental tissue over multiple

two-week intervals during the summer. Overall growth was poor for both species, but based on the results the decision was made to focus on the surface cultivation of *Ulva sp.* in summer 2025.

Ulva sp. was cultivated at the East North Haven site from early June to early August in 2025. To cultivate *Ulva sp.*, six replicate floating oyster grow-out bags (36" x 18" x 3") were each stocked with 20-grams of *Ulva sp.* that was wild-collected from Shinnecock Bay. The oyster bags were made of semi-rigid 4-mm polyethylene mesh, and were made to float by attaching plastic, air-filled, cylindrical floats (3" diameter) to each long side. The bags opened and closed on one side using stainless steel clips, and a bridle-clip system was using to attach the bags along a ~20-foot-long horizontal rope (Proflex ½" three-strand) that was anchored at either end using screw-down anchors. This deployment method allowed bags to rise and fall with the tide. The trawl line of floating bags was positioned seaward of bottom oyster cages.

To accommodate rapid growth, all but 20 grams of *Ulva sp.* was completely harvested from each grow-out bag and replaced every three to four weeks from June to August, an approach the Gobler Lab had iteratively discovered maximized yields of *Ulva sp.* in Long Island coastal waters. In total, three rounds of *Ulva sp.* cultivation experiments were conducted at the East North Haven study site in 2025. The first experiment ran for 21 days from June 4th to June 25th, the second experiment ran for 28 days from July 23rd to August 20th, and the third experiment ran for 24 days from August 20th to September 13th. At the end of each cultivation round, *Ulva sp.* was removed from bags, cleaned of biofouling, spun in a salad spinner to remove excess water, and weighed. After obtaining each sample whole wet weight (grams), 20grams of the original parental tissue was redeployed. Excess biomass was then placed in a labeled Ziplock bag containing site water, placed in a cooler with icepacks and transported back to Stony Brook University- Southampton Marine Science Research Station. Once samples arrived at the Marine Science Research Station, samples were individually placed in a seawater bath, and any residual biofouling was removed. The sample was then placed into a salad spinner and spun down to remove the excess seawater. Samples whole wet weight (grams) was then obtained and placed into a drying oven at 60°C for a one-week desiccation period. Whole dry weights (grams) were then obtained, and each sample was ground to a fine powder using a sterile mortar and pestle. Each sample was then stored in a sterile Falcon tube and stored in a drying oven at 60°C for nitrogen-carbon content analysis.

Oysters

Oyster spat-on-shell (SOS) was deployed in triplicate cages at each of the six study sites to monitor survival and growth. The low-profile wire cages (103 cm x 56 cm x 27 cm), typically used by the oyster aquaculture industry, were customized to hold one standard oyster grow-out bag (4 mm mesh size), with 6-inch legs to elevate the bag above the sediments (Figure 4). Oysters were deployed in each cage using two separate methods that differed in the level of predator protection. First, SOS oysters were placed inside mesh grow-out bags inside of the oyster cages, as would typically be done by commercial oyster farmers. Second, SOS oysters

were placed in soft Vexar mesh sleeves that were affixed to the top exterior surface of the cages. Vexar mesh sleeves are often used by oyster restoration practitioners to construct shell bags to build oyster reefs, and this deployment method better represented the conditions oyster spat may experience in a restoration setting as opposed to an aquaculture setting, particularly regarding predator exposure. While the aquaculture method (grow-out bags) helps protect small oyster spat from large predators like crabs, whelk, and starfish, the restoration method (Vexar mesh sleeves) does not. Seven shells with known starting quantities and sizes of oyster spat were placed in each replicate bag/sleeve for each treatment at each site.

Spat-on-shell was deployed to the field sites on July 12th, 2024, and monitored every four to five weeks through October 4th, 2024. The oysters were left to overwinter in the cages and were next monitored on March 3rd, 2025. On this date, the oyster deployment at Sag Harbor Marina was terminated and the three oyster cages were removed and relocated to the Barcelona point site to expand the oyster deployment there. Additionally, three new oyster cages were deployed to East North Haven on July 23rd, 2025 to expand the deployment there, with a new cohort of SOS added to these cages. Standard monitoring proceeded from June 25th, 2025 through October 22nd, after which the cages were periodically checked and monitored through the winter of 2025-2026. At each monitoring time point, the number of live and dead spat were counted on each shell, and the shell heights of live oyster spat were measured. In addition, the shells of dead oysters were inspected for predator damage, and the presence of predators on or in the bags/sleeves was recorded.

Oysters were sampled from the East North Haven site in January 2026 to measure tissue and shell weights as well as the carbon and nitrogen content in the tissue and shell. Additionally, the tissue and shell weight measurements were used to calculate condition index. Seven oysters were removed from each replicate bag inside and outside of each cage, for both cohorts of oysters (i.e, 21 oysters from each treatment from each cohort). Oysters were then transported in a cooler with ice packs back to the Stony Brook-Southampton Marine Science Research Station for processing. A total of twenty-one oysters from each group were processed and measured for the following; 1) shell height, length, and width, 2) whole weight (g), 3) shell weight (g), 4) wet tissue weight (g), 5) dry shell weight (g), 6) dry tissue weight (g), 7) gonad ripeness which is indicated by the presence or absence of gametes in a gonad tissue smear, and 8) sex. Wet samples were placed in a drying oven for a one-week desiccation period at 60°C. Condition index was calculated using the Lawrence and Scott (1982) method where the internal shell cavity capacity is determined gravimetrically by subtracting the shell weight (g) from the whole weight (g) of the living oyster:

$$\text{Condition Index (CI)} = \frac{\text{dry soft tissue wt (g)} \times 100}{\text{internal shell cavity capacity (g)}}$$

After the one-week desiccation period at 60°C, the samples were then removed, and the dry weight (g) of both the tissue and shell were obtained. Samples were then ground to a fine powder in a sterile mortar and pestle for later percent nitrogen-carbon content analysis.

Seagrass

The sites that were selected for further study from the 2024 sites were the East North Haven (ENH) and Barcelona Point (BP) sites. On 7/9/2025, six large sods were sampled from Shinnecock Road eelgrass meadow in Eastern Shinnecock Bay, and transported by boat to the Peconic bays, where three were planted at ENH and three at BP. At both sites, growth remained from the experiment in 2024, and the 2025 sods were planted to supplement and expand upon existing eelgrass. At both sites, new sods were planted to the right of existing growth (Figure 2).

At ENH, two marker buoys 5.4 m apart mark the edges of the planting zone – the 2024 plantings covered the 2.7 m on the left, and even spacing of the three new patches was attempted within the 2.7 m of space on the right – on 7/9/2025, conditions led to very limited visibility at this site, and although they remained oriented to the transect between the marker buoys, the spacing of the new plantings was not quite equal. Consequently, upon returning for further monitoring later in the summer, the researchers were unable to distinguish between patches 3 (old growth) and 4 (new growth). What likely occurred was the two patches growing together into one – patch 4 had been planted in rough conditions and low visibility, very near patch 3. As the conditions settled and the patch settled in the coming weeks, it likely stabilized itself by associating with the existing rhizome structure present from site three, and this promoted further growth of the two patches together. Although monitoring data was recorded separately for patches 3 and 4 on 7/9/2025, subsequent data collection measured only the combined patch as the two separate patches could no longer be distinguished. This combined patch is referred to as ENH_3 throughout the remainder of the study period, and the data reported for this patch on 7/9/2025 was calculated as averages of the values from ENH_3 and ENH_4 taken on that day. Likewise, between the end of the study period in 2024 and the beginning of the study period in 2025, the original patches ENH_1 and ENH_2 had grown together and were indistinguishable. This combined patch is referred to as ENH_2 in the figures and data.

To plant a sod, the bin containing it was lowered onto the sediment, and two divers scooped out a few inches of sand in a roughly rectangular area. They then worked together to slide the sod from the holding bin into the depression in the sand and pile more sand from the area on top of the new planting, ensuring that rhizome masses were buried instead of exposed to the water column.

At BP, the same process was followed. The distance between the two marker buoys at this site is 5.8 m, so the three new plantings were spaced as evenly as possible on the 2.9 m of the right half of the transect. These transects were set up behind other hardware relevant to this project – cages and bags holding oysters that were arranged in the same orientation, placed to shelter grass plantings from wave and wake action. However, on 7/9/2025, not all of the oyster hardware that would eventually be used had yet been placed in the field, so some estimation was necessary based on the researcher's understanding of where those would eventually be. At the conclusion

of planting at each site, diagrams were drawn (Figure 1) and GPS waypoints recorded for the buoys at the end of each transect.

On the last monitoring day of the season, eelgrass seeds were planted at ENH and BP. These seeds had been collected from various projects throughout the summer and had been stored in refrigerated seawater to prevent premature germination. Into each of 12 small burlap drawstring bags, ~125 seeds were scooped, and the bag was soaked in seawater for several minutes prior to burial to allow the fibers to saturate and expand. After the fibers had reached equilibrium, 6 seed bags were planted at each of the two sites, in a unique configuration determined by the layout of the existing growth. Instead of planting the seeds within existing patches of seagrass, as was previously suggested, bags were buried on the edges of patches. This change was made to minimize damage to the existing patches, some of which were quite small and fragile.

The seed-planting process consisted of a diver on SCUBA digging a small ovular pit in the sand with their hands, placing a seed pouch in the center of the depression, securing the bag with a 12-inch sod staple, and burying the material with sand from the surrounding area. Conducting this process in the middle of an existing patch would have necessitated disturbing and breaking rhizome structures, or even live shoots at patches where the grass was dense enough, which is why the change to a side-by-side planting orientation was made. Furthermore, the 6 bags were planted in each site in association with the patches that "needed the most help". For example, at BP, patches 1-3 exhibited 80 – 100 % coverage, while patches 4 – 6 were well below 50%. Therefore, more seed patches were buried in association with patches 4 – 6 than 1 – 3. The layout of seed plantings can be seen in Fig. 1.

Monitoring of seagrass health and growth was conducted at each site every several weeks for the entirety of the eelgrass growing season, starting on the day of out-planting. On 7/9/2025, researchers on SCUBA assessed the percent cover of *Zostera marina*, *Ruppia spp.,* and non-seagrass macroalgae, as well as shoot counts, 5 shoot lengths, and recorded the number of unrooted shoots (before resecuring those loose shoots in the sediment) at each quadrat at each site. On the next day of monitoring, this protocol was expanded to include sampling of a dozen eelgrass shoots at each site, which were subsequently worked up in the lab for epiphytic load, dry weight of leaves, and shoot morphometrics by leaf. This expanded monitoring protocol was carried out on 7/31/25, 8/20/25, 9/11/25, and 10/2/25. Each monitoring day, researchers wrote notes on the general condition of the plantings and any observed changes in layout and growth patterns. Results from the monitoring are shared and discussed in subsequent sections.

RESULTS AND INTERPRETATION

Water quality

Discrete water temperature readings at Barcelona Point, East North Haven, and Sag Harbor Marina were similar over the two-year period from January 2024 to January 2026 (Figure 5).

Continuous temperature readings, however, indicated greater temperature fluctuations at the East North Haven site, potentially due to exposure of the sensors at extreme low tides, and/or sensor malfunction (Figure 6). Warmest daytime temperatures during summer at the Barcelona Point and East North Haven sites exceeded 25°C, a level known to be stressful to seagrass when sustained for more than one week (NYSDEC, 2009).

Discrete salinity readings ranged between 21 and 31 ppt over the two-year period across the three sites (Figure 7). Salinity was typically lowest at SHM, except for periodic dips in salinity observed at BP and ENH most likely associated with precipitation events. At all three sites, salinity was generally higher in 2025 than 2024 (Figure 7).

Discrete dissolved oxygen (DO) levels were similar among sites, ranging from 6.3 to 17.8 (mg L^{-1}) over the two-year monitoring period (Figure 8). Based on the discrete data alone, the dissolved oxygen levels did not appear to fall below the NYSDEC chronic DO minimum (4.8 mg L^{-1}) or acute DO minimum (3.0 mg L^{-1}). The chronic dissolved oxygen (DO) standard in New York State is a regulatory benchmark set for certain marine waters to protect their designated uses, such as shellfishing, fishing, and recreation. For Class SA, SB, and SC waters, the chronic DO standard is 4.8 mg L^{-1}, with an allowable excursion to not less than 3.0 mg L^{-1} (i.e. acute DO minimum) for certain periods of time. This standard applies year-round and is continuously enforceable. The continuous DO measurements, however, gave a more complete picture of the large daily fluctuations and diel cycles of DO at the study sites, with DO frequently falling below chronic levels and sometimes acute levels during nighttime hours when photosynthesis and the production of oxygen by macroalgae and sea grasses does not occur (Figure 9). Among the sites, DO fell below chronic and acute levels most frequently at Sag Harbor Marina, and least frequently at Barcelona Point (Figure 9).

Similarly, pH also exhibited large daily fluctuations that followed diel cycles with higher pH found in the daytime hours when macroalgae and seagrasses remove dissolved CO_2 from the water during photosynthesis, and lower during nighttime hours when respiration dominates and CO_2 is released (Figure 10). During summer, nocturnal pH occasionally fell below 7.1 at BP and ENH, a level known to be stressful to bivalves (Ringwood and Keppler, 2002; Gazeau et al., 2007; Bressan et al., 2014; Gobler and Baumann, 2016). For the majority of time, however, pH was above levels stressful for bivalves. At all sites, pH progressively declined through the year from winter to summer as waters warmed and community respiration increased, a common observation in coastal waters (Wallace et al., 2014; Wallace and Gobler, 2021).

Chlorophyll-a concentrations were similar between Barcelona Point and East North Haven, ranging from 3.5 to 14.3 *u*m L^{-1} in summer/fall 2024 and between 1.6 to 5.7 *u*m L^{-1} in summer/fall 2025 (Figure 11). Concentrations were higher during the Summer 2024 growing season compared to the Summer 2025 growing season (Figure 11). Across all dates, chlorophyll

concentrations did not exceed the USEA guidance value of 20 *u*m L^{-1}, a threshold above which is considered to be poor water quality due to algae blooms.

Kelp

Kelp lines were seeded in November (gametophyte-derived seedstock) and December (spore-derived seedstock) 2024 and growth on some lines was first detectable in December (Figure 12). Growth accelerated in March and April at all sites, with peak biomass reached on April 23 on all lines at all sites. Peak biomass yields were higher for gametophyte-derived lines at all sites (Figure 12). The highest yields along gametophyte-derived lines were obtained at Barcelona Point (4.6 kg m^{-1}), followed by Sag Harbor Marine (0.90 kg m^{-1}) and East North Haven (0.78 kg m^{-1}) (Figure 12). Barcelona Point expressed the greatest total yield with a maximum of 3 kg per meter of line. East North Haven expressed a slightly lower total yield with a maximum of 0.43 kg per meter of line. Spore-derived lines at Sag Harbor Marina experienced excessive biofouling of *Ectocapus sp.* seaweed (aka 'Slip gut') and false kelp, resulting in a loss of kelp on these lines and their consequent removal on March 24th.

The average kelp blade length (cm) and maximum blade length (cm) were also monitored during the kelp 2025 growing season. Similar to the results for line yields, blade length at peak biomass was greater on gametophyte-derived than spore-derived lines, and was greatest at Barcelona Point, followed by East North Haven and Sag Harbor Marina which were very similar (Figure 13). The average and maximum blade lengths at peak biomass of gametophyte-derived kelp were 66.4 cm and 92.8 cm at Barcelona Point, 31.7 cm and 42.6 cm at East North Haven, and 29.4 cm and 38.3 cm at Sag Harbor Marina, respectively.

Across years (2024 and 2025) and sites (BP, ENH, SHM), the nitrogen content of kelp tissue at peak line biomass ranged from 0.53% to 0.82% of the dry tissue mass, with higher tissue nitrogen content found in 2025 than 2024 (Figure 14). Nitrogen content did not differ between kelp grown at Barcelona Point and Eat North Haven in 2024 ($t=0.96$, n.s.; Figure 14a; data from Sag Harbor in 2024 is pending). In 2025, however, the nitrogen content of kelp tissue significantly varied among sites and was significantly greater at Barcelona Point than East North Haven, with neither site differing from Sag Harbor (ANOVA with Tukey tests, $F=5.21$, $p<0.02$; Figure 14b). The carbon content of kelp tissue across years and sites ranged from 22.0% to 27.3% of the dry tissue mass, with higher tissue carbon content found in 2025 than 2024 (Figure 15). Kelp tissue carbon content did not differ among sites within either year (Figure 15).

Summer Seaweeds 2025

In all three rounds of *Ulva sp.* cultivation experiments, a loss of biomass was observed, with a 100% loss of biomass in two of the rounds. The result is interesting because this grow-out

method has been used successfully by the Gobler Lab to cultivate *Ulva sp.* biomass, with growth rates between 10% to 14% per day in many locations in Long Island Sound and the South Shore Estuary. The loss of *Ulva sp.* biomass at the Peconic Estuary study sites here may reflect grazing pressure and/or poor *Ulva sp.* growth due to nutrient limitation.

Oysters

On September 17th, 2025, 406 days after deployment to the field sites, survival of the SOS for oysters inside the grow-out bags at the Barcelona Point site was 51% and for the East North Haven site, 53% (Figure 16). SOS survival for the oysters in the Vexar mesh sleeve on the outside of the cages at the Barcelona Point site was 44% and 31% at the East North Haven site (Figure 16). A two-way ANOVA was conducted to examine the effects of site and deployment method (i.e. grow-out bag vs. mesh sleeve) on oyster survival. The interaction between site and deployment method was not statistically significant ($F=2.41$, n.s.). Regarding the main effects, there was no significant difference in oyster survival between the two sites ($F=1.46$, n.s.), but the deployment method did have a significant impact on survival ($F=9.36$, $p<0.02$), with higher survival of oysters placed inside grow-out bags (i.e. commercial aquaculture method) than in Vexar mesh sleeves (restoration method) (Figure 17). One reason for this may be due to the greater predator protection provided by the commercial grow-out bags due to their smaller mesh size. While the commercial grow-out bags may have helped minimize predation from larger predators like crabs, they were not fully effective at keeping out smaller predators like oyster drills which were found at both sites. Survival of the second cohort of spat on shell that was added to new cages at East North Haven in July 2025 displayed a similar pattern to the 2024 cohort in the first several months after deployment, with mortality highest during the summer and early fall immediately after deployment, followed by a decline in mortality during late fall and winter (Figure 16). The decline in mortality during winter most likely reflects reduced predation pressure, as many of the predators on oysters are less active or dormant during winter. Additionally, as the oysters grow, there is a further reduction in predation pressure as the oysters become too big for some predators (i.e. small crabs) to break open and consume.

Similar patterns of oyster growth were observed at both sites and in both oyster deployment treatments (Figure 18). For the 2024 oyster cohort, growth rates were highest in the first growing season after deployment when the oyster spat were small, and lower in the second growing season in 2025 when the oysters were larger (Figures 18-19). In 2024 oyster growth was marginally higher in grow-out bags than Vexar mesh sleeves (two-way ANOVA; $F=4.03$, $p=0.08$; Figure 19a) and did not differ between sites (two-way ANOVA; $F=0.96$, n.s.; Figure 19a). Additionally, there was a significant interaction between the main effects (two-way ANOVA; $F=11.70$, $p<0.05$), suggesting that the impacts of deployment method on growth may be site-specific. In 2025, growth was again marginally higher in grow-out bags than Vexar mesh sleeves (two-way ANOVA; $F=3.94$, $p=0.08$; Figure 19b), and also significantly higher at

Barcelona Point than East North Haven (two-way ANOVA; $F=8.19$, $p<0.05$; Figure 19b), with no significant interaction found between site and deployment method (two-way ANOVA; $F=0.74$, n.s.; Figure 19b). The slower growth in Vexar mesh sleeves may reflect sub-lethal effects of predators, as both physical disturbances during predator foraging and/or chemical cues released by predators can cause bivalves to close up and reduce feeding, leading to lower growth (Smee & Weissburg, 2006).

Despite marginally higher shell height growth rates in oysters in aquaculture bags than Vexar mesh sleeves, no significant differences were found in dry tissue weights and dry shell weights between oysters in the two deployment treatments in January 2025 (Figure 20). This was true for both the 2024 and 2025 cohorts of oyster spat on shell. For the 2024 cohort which had been deployed at the site for ~1.5 years, dry tissue weights averaged 3.0 and 3.3 grams per oyster, and dry shell weights averaged 59.0 and 62.4 grams per oyster, in the bag and sleeve treatments respectively. For the 2025 cohort which had been deployed for ~ 5 months, dry tissue weights averaged 0.4 and 0.4 grams per oyster, and dry shell weights averaged 8.2 and 7.5 grams per oyster, in the grow-out bag and mesh sleeve treatments respectively.

Condition index ranged from 9.4 to 11.5 amongst the oyster treatments and cohorts (Figure 21). A two-way ANOVA was conducted to examine the effects of cohort and deployment method (i.e. grow-out bag vs. mesh sleeve) on oyster condition index. The interaction between cohort and deployment method was not statistically significant ($F=0.37$, n.s.; Figure 21). Regarding the main effects, there was no significant difference in condition index between the two deployment methods ($F=0.0002$, n.s.), but the two cohorts did significantly differ in condition index ($F=16.1$, $p<0.001$), with the younger cohort having higher condition (Figure 21). No gametes were discernible in visible examination of gonad tissue smears under a compound microscope in any of the oysters sampled, this is more than likely due to the fact that condition index was conducted when oysters are dormant for the winter.

The percent nitrogen in oyster tissue ranged from 7.8% to 9.8% amongst the oyster treatments and cohorts (Figure 22a). A two-way ANOVA was conducted to examine the effects of cohort and deployment method (i.e. grow-out bag vs. mesh sleeve) on oyster tissue nitrogen content. The interaction between cohort and deployment method was not statistically significant ($F=0.80$, n.s.; Figure 22a). Regarding the main effects, there was no significant difference in tissue nitrogen content between the two deployment methods ($F=0.87$, n.s.), but the two cohorts did significantly differ ($F=9.87$, $p<0.01$), with the younger cohort having higher tissue nitrogen content (Figure 22a).

The percent nitrogen in oyster shell ranged from 0.11% to 0.19% amongst the oyster treatments and cohorts (Figure 22b). A two-way ANOVA was conducted to examine the effects of cohort and deployment method (i.e. grow-out bag vs. mesh sleeve) on oyster shell nitrogen content. The

interaction between cohort and deployment method was not statistically significant (F=0.31, n.s.; Figure 22b). Regarding the main effects, there was no significant difference in shell nitrogen content between the two deployment methods (F=0.66, n.s.), or the two cohorts (F=0.11, n.s.; Figure 22b).

The percent carbon in oyster tissue ranged from 38.4% to 44.2% amongst the oyster treatments and cohorts (Figure 23a). A two-way ANOVA was conducted to examine the effects of cohort and deployment method (i.e. grow-out bag vs. mesh sleeve) on oyster tissue carbon content. The interaction between cohort and deployment method was not statistically significant (F=0.57, n.s.; Figure 23a). Regarding the main effects, there was no significant difference in tissue carbon content between the two deployment methods (F=0.13, n.s.), but the two cohorts did significantly differ (F=14.26, $p<0.001$), with the older cohort having higher tissue carbon content (Figure 23a).

The percent carbon in oyster shell ranged from 12.0% to 12.4% amongst the oyster treatments and cohorts (Figure 23b). A two-way ANOVA was conducted to examine the effects of cohort and deployment method (i.e. grow-out bag vs. mesh sleeve) on oyster shell carbon content. The interaction between cohort and deployment method was not statistically significant (F=3.17, n.s.; Figure 23b). Regarding the main effects, there was no significant difference in tissue carbon content between the two deployment methods (F=1.10, n.s.), but the two cohorts did significantly differ (F=6.85, $p<0.05$), with the older cohort having higher tissue carbon content (Figure 23b).

Compared to kelp, oyster tissue was found to have substantially higher nitrogen and carbon content (Figure 24). Oyster shell, on the other hand, contained only trace amounts of nitrogen and substantially less carbon on a per weight basis than oyster tissue (Figure 24). The mass of oyster shell, however, far exceeds the mass of oyster tissue in an oyster, making the shell an important component of overall nitrogen and carbon bioextraction and storage, despite the relatively low concentration of these elements (Table 1). Using a conservative estimate of 50 oysters m^{-2} (Peters et al. 2017), we estimate that a one-hectare restored oyster reef in the Peconic Estuary could store about 187 kg or nitrogen, and 4,525 kg of carbon.

Seagrass

Across the board, the seagrass at BP performed better than the patches at ENH. Biomass, leaf area index, average shoot length, shoot count, and percent cover of *Zostera marina* were all higher at BP than ENH, especially by the end of the study period. In July, when the new patches were planted, the 2025 patches (patches 4-6 at BP, and patches 5-6 at ENH) were relatively healthy, having been newly transplanted. Over subsequent monitoring periods, most metrics in these new patches decreased, and then started to experience a turnaround by the end of the

monitoring period. In contrast, the 2024 patches (1-3 at BP, 2-3 at ENH) were at their lowest points early in the monitoring period, and tended to increase as the monitoring period continued.

For shoot length (Figure 25), the averages at ENH stayed very steady throughout the monitoring period, especially for the pre-existing patches. The new patches were initially longer, but converged on the average lengths of the pre-existing patches by the end of the monitoring period. At BP, the trend was more complex. The 2024 patches increased in length from the beginning to the end of the monitoring period, and ended with the longest average shoot length of the study. The new patches initially had very high shoot length, but decreased through the middle of the growing period, and then diverged. Each new patch ended the season with shoot lengths corresponding to their distance from the older growth. Patch 4, closest to the 2024 patches, did relatively well, and patch 6, farthest from the 2024 patches, had the lowest shoot length across the entire study.

For shoot count (Figure 26), the trends were very similar to shoot length. The densest patches were BP 1-3, and all of the 2024 patches increased in shoot density throughout the season. All the new patches started off with high shoot density directly from transplanting, dipped in the middle of the monitoring period, and rebounded with various degrees of success. In BP, mirroring the shoot length trends, proximity to the 2024 patches determined density at the end of the season. Patch 4 had the highest density of the new patches, and patch 6 had the lowest density across the entire study. The proximity to older growth did not appear to be as important at ENH, where all patches followed generally the same trend. Both new patches rebounded to shoot counts similar to the older patches by the end of the monitoring period, and both older patches increased in density from the beginning to end of the season.

Percent cover of eelgrass (Figure 27), a factor closely associated with shoot count, mirrored the patterns described above. Percent cover for the older patches at BP started at middling levels, and was extremely high by the end of the monitoring period, with two patches at 100% cover. The newer patches did not fare as well, and decreased in end-of-season percent cover according to distance from the older patches (4 > 5 > 6). At ENH, the older patches (2 & 3) experienced an increase in percent cover throughout the growing season, and the new patches stayed relatively constant between roughly 25 – 50 % cover.

Leaf area index (Figure 28) is a metric closely associated with all of the observations already discussed, and describes the proportion of photosynthetic area to surface area of a patch. A value above one indicates >1 m^2 photosynthetic material for every m^2 of the sediment surface, and values below 1 indicate the opposite. This metric is derived from morphometric analysis of sampled eelgrass shoots and several of the measurements described above, and produces trends with less variability that give an overall indication of patch health. As shown, patches 1-3 at BP increased in health throughout the monitoring period, with patches 4-6 further decreasing in health with distance from the older patches. At ENH the older patches tended to be slightly healthier than the newer patches, but all patches followed a general trend of decreased health in the hottest part of the summer, and a rebound towards the end of the monitoring period.

Taken together, macroalgae percent cover (Figure 29) and epiphytic load (Figure 30) provide a measure of the stress experienced by the eelgrass as a result of fouling or crowding from other organisms. Throughout the growing season, ENH experienced a higher percent cover of macroalgae, and a consistently higher epiphytic load than BP. Macroalgae % cover at both sites increased throughout the monitoring period, peaking in September before falling back down. Epiphytic load decreased throughout the monitoring period at both sites, with the highest values in early August and the lowest values in September and October.

Finally, biomass of plant matter, as determined by average dry weight of 12 shoots per site, showed interesting departure from expectations based on other metrics (Figure 31). At BP it was not too dissimilar, with an increase from the beginning of the monitoring period to the end, but it peaked in late August and then slightly fell. At ENH, there was a consistent and dramatic decrease in biomass from the beginning of the monitoring period to the end, with a decrease at every time step. Averaged across 12 shoots, the dry weight of a shoot at ENH in October fell to almost a quarter of the value in early August.

Wave Energy

Wave energy was quantified at four of the six study sites in the Peconic Bays in 2024, East North Haven, Sag Harbor Marina, South Haven, and Ganet Creek and, in 2025 and 2026 at the East North Haven by using a RBR*solo*^{3} D: pressure (depth) sensor. RBR*solo*^{3} D: pressure (depth) sensor records water pressure (*dbar*) and converts the water pressure (dbar) to water depth (m) during post-processing in the Ruskin software. For the purposes of this project, variables such as tidal slope (m hour^{-1}), average wave height (m), maximum wave height (m), and wave energy (J m^{-2}) were used to assess the effectiveness of the bottom cages on wave damping. This was done by deploying a RBR*solo*^{3} D: pressure (depth) sensor behind the middlemost bottom cage and in open water, at the same level as the eel grass. Sensors were deployed for ~14-days in 2024 and for ~20-days in 2025 and 2026 and were set to record water pressure (dbar) at 17-minute interval bursts.

The tidal slope (m hour^{-1}) provides a detailed site-specific depiction of the tidal profile. This is done by using the Ruskin software to filter out the high frequency variations in pressure caused by waves. Across all study sites in 2024; the East North Haven site inside and outside the conservation area (Figure 32), for the Sag Harbor Marina site inside and outside the conservation area (Figure 33), the South Haven site inside and outside the conservation area (Figure 34), and the Ganet Creek site both inside and outside the conservation area (Figure 35), the tidal profile (m hour^{-1}) were relatively consistent. In 2025 (Figures 36) and in 2026 (Figures 37), the tidal profile (m hour^{-1}) stays consistent for the East North Haven site both inside and outside the conservation area, allowing the oysters, eel grass and macroalgae to be subject to identical water depth. The tidal profile (m hour^{-1}) also allows for an assessment of extreme tides.

The average wave height (m) provides a more defined general state/behavior of surface water both within and outside the conservation area. Lower average wave height (m) was seen inside the conservation area across the study sites in 2024; East North Haven (Figure 38), Sag Harbor Marina (Figure 39), South Haven (Figure 40), and Ganet Creek (Figure 41). In 2025 a lower average wave height (m) inside the conservation area was also observed at the East North Haven site when compared to outside the conservation area (Figure 42). In 2026 a lower average wave height (m) inside the conservation area was again observed at the East North Haven site (Figures 43).This may be indicative of shoreline protection by the bottom cages. In order to further this theory, maximum wave height (m) was then analyzed and compared.

The maximum wave height (m) displays the largest wave encountered during a recording interval which the average wave height (m) does not. In this way, wave damping caused by the bottom cages and boat wakes can be displayed graphically. In 2024, a lower maximum wave height (m) was experienced inside the conservation area compared to outside the conservation area across all study sites; East North Haven (Figures 44), Sag Harbor Marina (Figures 45), South Haven (Figures 46), and Ganet Creek (Figures 47). The South Haven and Ganet Creek study sites experienced the lowest maximum wave height (m) within the conservation area when compared to outside conservation area. It should be noted that both of these sites are either next to the Shelter Island South Haven ferry, as is the case with the South Haven site, or close to it and that both sites are subjected to large boat wakes. In 2025 at the East North Haven site, maximum wave height (m) displayed slight wave dampening inside the conservation area (Figure 48A) compared to outside the conservation area (Figure 48B). In 2026 at the East North Haven site, maximum wave height (m) again displayed slight wave dampening inside the conservation area (Figure 49A) compared to outside the conservation area (Figure 49B).

Wave energy (J m^{-2}), the total amount of kinetic and potential energy per unit surface area of a wave, was also analyzed for effectiveness of bottom cage protection of eel grass. In 2024, wave energy (J m^{-2}) was lower within the conservation area for the East North Haven (Figure 50) and South Haven (Figure 51) sites. The Sag Harbor Marina (Figure 52) and Ganet Creek sites (Figure 53) displayed slightly lower wave energy (J m^{-2}) inside the conservation. Wave energy (J m^{-2}) was recorded in 2025 (Figures 54) and in 2026 (Figures 55) at the East North Haven site both inside the conservation area and outside the conservation area. The initial wave energy (J m^{-2}) recorded in 2025 at the East North Haven site within the conservation area was similar to outside the conservation area, however, as time progressed wave energy (J m^{-2}) showed a similar trend to 2024 where there was lower wave energy (J m^{-2}) inside the conservation area compared to outside the conservation area. However, wave energy (J m^{-2}) recorded in 2026 at the East North Haven site expressed continually lower wave energy (J m^{-2}) inside the conservation area compared to outside the conservation area.

References:

Bodycomb, R., Pomeroy, A. W., & Morris, R. L. (2023). Kelp aquaculture as a nature-based solution for coastal protection: Wave attenuation by suspended canopies. Journal of Marine Science and Engineering, 11(9), 1822.

Bosello, F., & De Cian, E. (2014). Climate change, sea level rise, and coastal disasters. A review of modeling practices. *Energy Economics*, *46*, 593-605.

Duarte, C. M., Delgado-Huertas, A., Marti, E., Gasser, B., Martin, I. S., Cousteau, A., ... & Masque, P. (2025). Carbon burial in sediments below seaweed farms matches that of Blue Carbon habitats. Nature Climate Change, 1-8.

Duarte, C. M., & Krause-Jensen, D. (2017). Export from seagrass meadows contributes to marine carbon sequestration. *Frontiers in Marine Science*, *4*, 13. • Hendriks, I. E., et al. (2015). Carbon and nutrient fluxes, and CO2 buffering in a temperate seagrass meadow. *Marine Ecology Progress Series*, *520*, 1-18.

Gentry, R. R., et al. (2017). Mapping the global potential for marine aquaculture. *Nature Ecology & Evolution*, *1*(4), 189–196.

Gobler, C. J., Doall, M. H., Peterson, B. J., Young, C. S., DeLaney, F., Wallace, R. B., ... & Kulp, R. E. (2022). Rebuilding a collapsed bivalve population, restoring seagrass meadows, and eradicating harmful algal blooms in a temperate lagoon using spawner sanctuaries. *Frontiers in Marine Science*, *9*, 911731.

Heck Jr, K. L., Hays, G., & Orth, R. J. (2003). Critical evaluation of the nursery role hypothesis for seagrass meadows. *Marine Ecology Progress Series*, *253*, 123-136.

Hendriks, I. E., Olsen, Y. S., Ramajo, L., Basso, L., Steckbauer, A., Moore, T. S., ... & Duarte, C. M. (2014). Photosynthetic activity buffers ocean acidification in seagrass meadows. Biogeosciences, 11(2), 333-346.

Hicks, R. L., Haab, T. C., & Lipton, D. (2004). The economic benefits of oyster reef restoration in the Chesapeake Bay. *Final Report: Chesapeake Bay Foundation*.

IPCC. (2021). *Climate Change 2021: The Physical Science Basis. Contribution of Working Group I to the Sixth Assessment Report of the Intergovernmental Panel on Climate Change* [Masson-Delmotte, V., P. Z. Zhai, A. Pirani, S. L. Connors, N. Péan, S. Berger, N. Caud, Y. Chen, L. Goldfarb, M. I. Gomis, M. Huang, K. Leitzell, E. Lonnoy, J. B. R. Matthews, T. K.

Jolly, C. M., & Clonts, H. A. (2020). Economics of aquaculture. CRC Press. Maycock, T., Waterfield, O. Yelekçi, R. Yu, and B. Zhou (eds.)]. Cambridge University Press. In Press.

Kim, J., Stekoll, M., & Yarish, C. (2019). Opportunities, challenges and future directions of open-water seaweed aquaculture in the United States. *Phycologia*,*58*(5), 446-461.

Kopp, R. E., et al. (2017). Global and regional sea-level rise scenarios for the United States. *NOAA Technical Report NOS CO-OPS 083*.

Macreadie, P. I., Anton, A., Raven, J. A., Beaumont, N., Connolly, R. M., Friess, D. A., ... & Duarte, C. M. (2019). The future of Blue Carbon science. Nature communications, 10(1), 3998.

NYSDEC, (2009). Seagrass task force final report. New York Department of Environmental Conservation.

Parsons, T. R. (2013). A manual of chemical & biological methods for seawater analysis. Elsevier.

Paul, M. (2018). The protection of sandy shores□can we afford to ignore the contribution of seagrass?. Marine Pollution Bulletin, 134, 152-159.

Peters, J., Eggleston, J. W., Puckett, D. B., Theuerkauf, S. J. 2017. Oyster Demographics In Harvested Reefs Versus No-Take Reserves: Implications For Larval Spillover And Restoration Success. Front. Mar. Sci. 4:326. DOI : https://doi.org/10.3389/fmars.2017.00326

Phillips, J. D. (2018). Coastal wetlands, sea level, and the dimensions of geomorphic resilience. *Geomorphology*, *305*, 173-184.

Poppe, L. J., Knebel, H. J., Mlodzinska, Z. J., Hastings, M. E., & Seekins, B. A. (2000). Distribution of surficial sediment in Long Island Sound and adjacent waters: texture and total organic carbon. *Journal of Coastal Research*, 567-574.

Schumacher, B. A. (2002). Methods for the determination of total organic carbon (TOC) in soils and sediments (pp. 1-23). Washington, DC: US Environmental Protection Agency, Office of Research and Development, Ecological Risk Assessment Support Center.

Scyphers, S. B., Powers, S. P., Heck Jr, K. L., & Byron, D. (2011). Oyster reefs as natural breakwaters mitigate shoreline loss and facilitate fisheries. PloS one, 6(8), e22396.

Vargas, G. A., et al. (2017). Seagrass meadows modify ocean acidification impacts on a calcifying alga.

Yarish, C., Kim, J. K., Lindell, S., & Kite-Powell, H. (2017). Developing an environmentally and economically sustainable sugar kelp aquaculture industry in southern New England: from seed to market.

Young, C. S., Sylvers, L. H., Tomasetti, S. J., Lundstrom, A., Schenone, C., Doall, M. H., & Gobler, C. J. (2022). Kelp (Saccharina latissima) mitigates coastal ocean acidification and increases the growth of North Atlantic bivalves in lab experiments and on an oyster farm. *Frontiers in Marine Science*, *9*, 881254.

Oyster part	dry wt (g oyster^{-1})	Nitrogen content (% dry mass)	Carbon content (% dry mass)	Nitrogen (g oyster^{-1})	Carbon (g oyster^{-1})	Nitrogen capture (g hectare^{-2})	Carbon capture (g hectare^{-2})
Tissue	3.29	7.78%	44.21%	0.26	1.45	127.98	727.25
Shell	62.41	0.19%	12.17%	0.12	7.60	59.29	3797.65
Total Oyster	***65.7***			***0.37***	***9.05***	***187.27***	***4524.90***

Table 1. Calculation of the nitrogen and carbon storage potential of a restored oyster reef in the Peconic Estuary. Calculations are made from data collected on adult oysters that were deployed as spat-on-shell to the East North Haven site and grown for about 1.5 years.

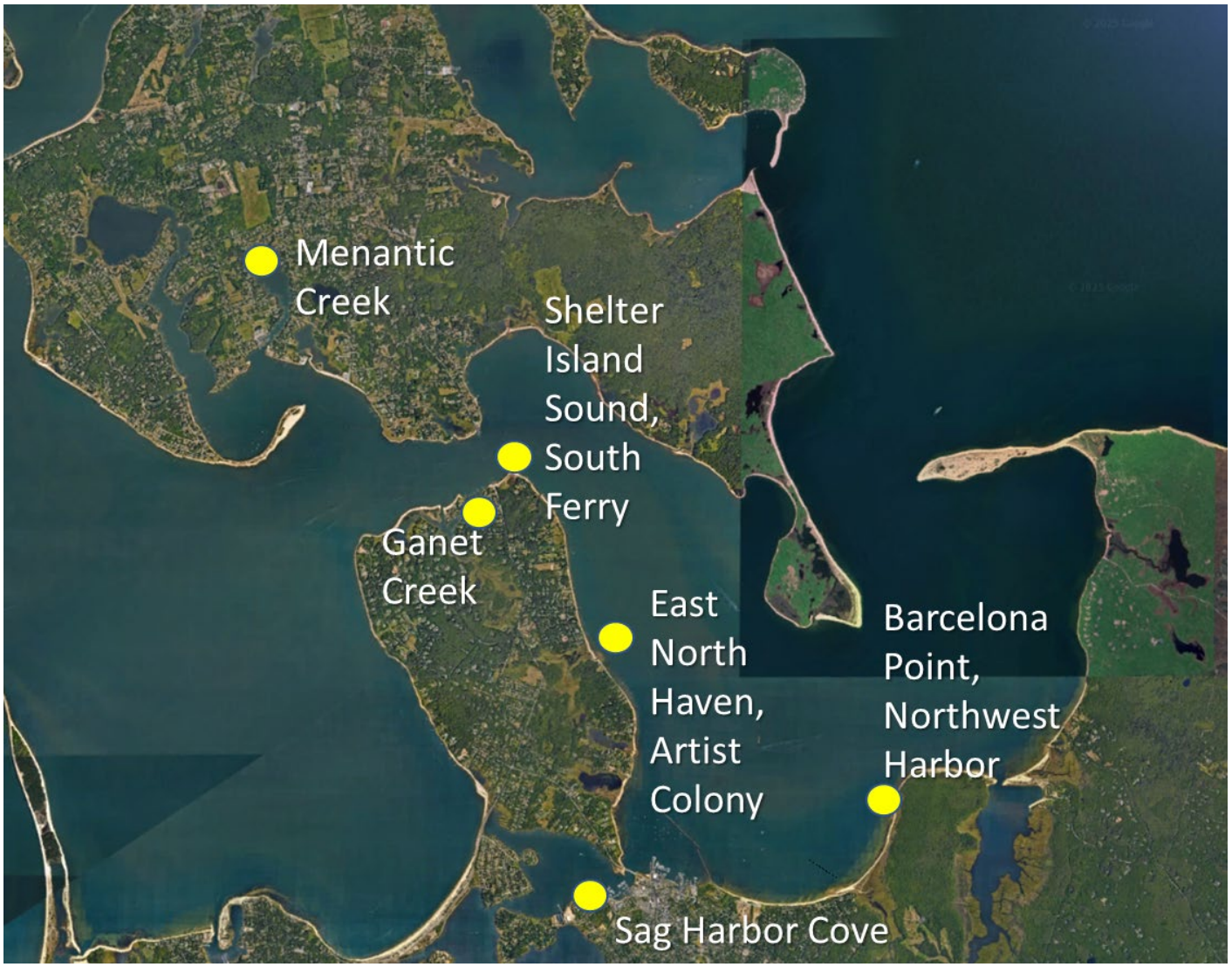
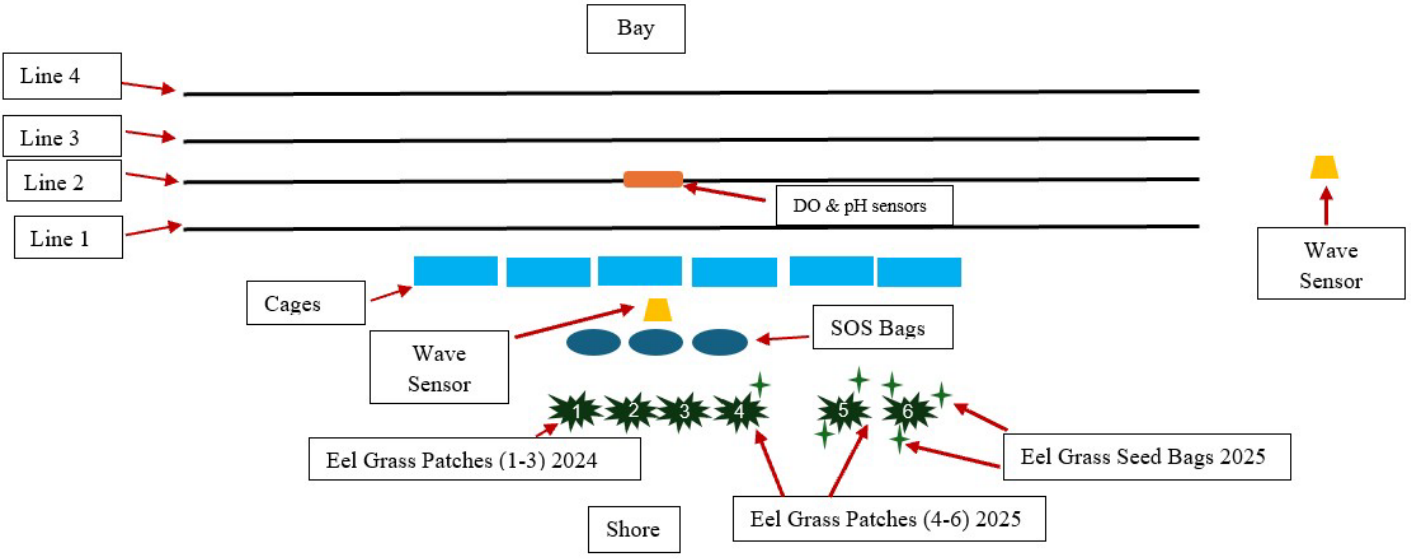


Figure 1. CHANGES study sites in the Peconic Estuary

A. Barcelona Point



B. East North Haven

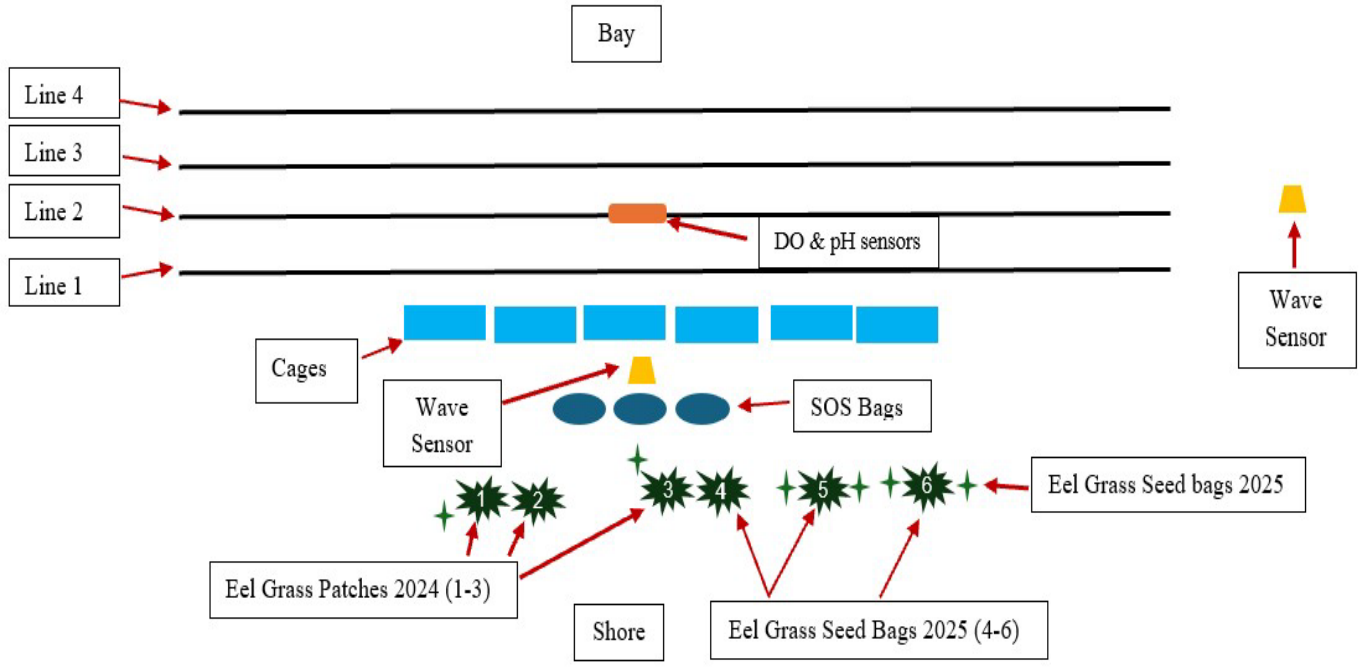


Figure 2. Field layout of the restoration area.

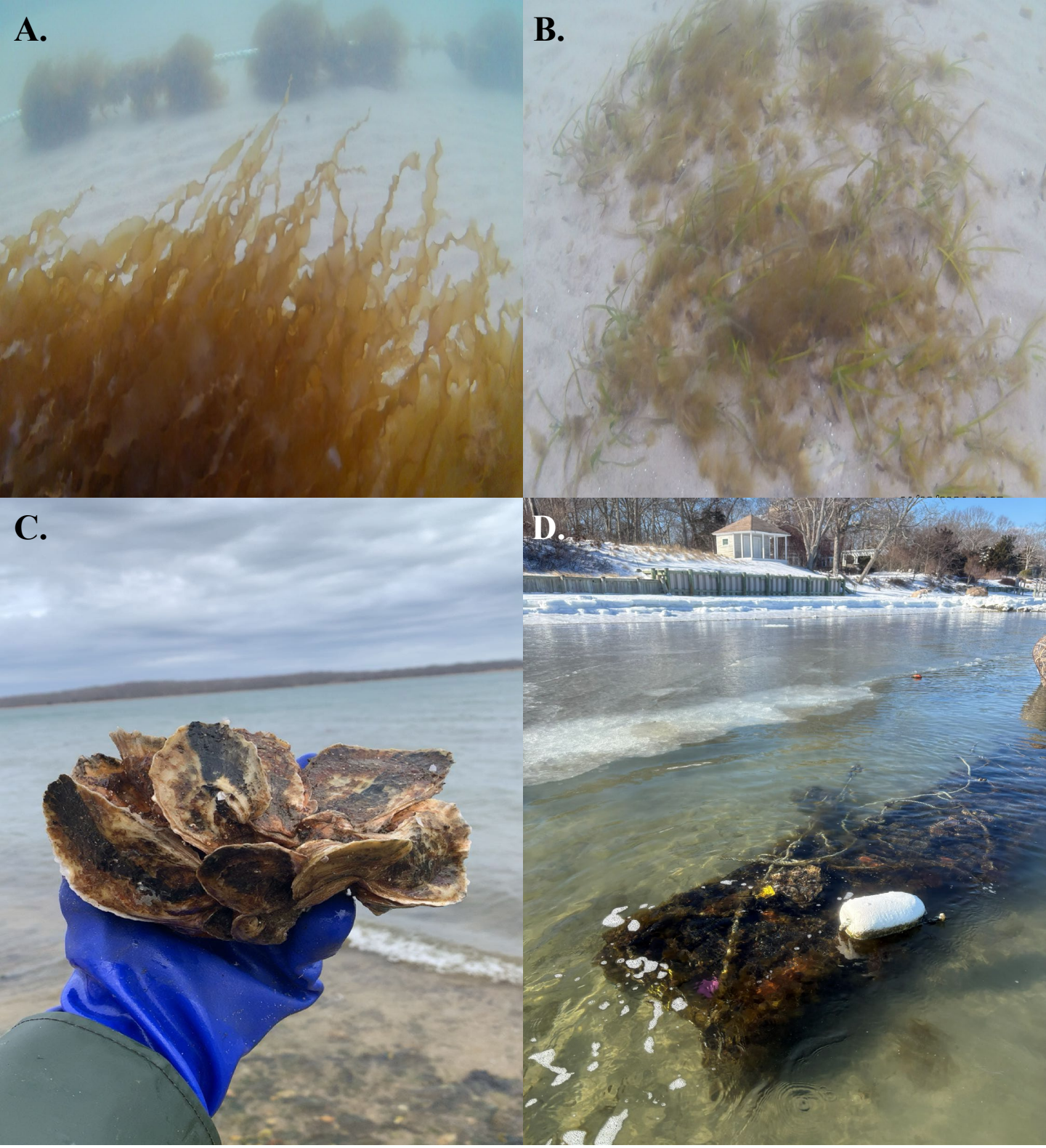


Figure 3. Photos showing the components of the restoration area, including (A) kelp in late Spring; **(B)** eel grass bed in the Summer of 2025 at the Barcelona Point study site; **(C)** Spat-on-shell oysters in late Fall 2025; **(D)** low-profile bottom cages in mid-Winter 2026 at the East North Haven study site.

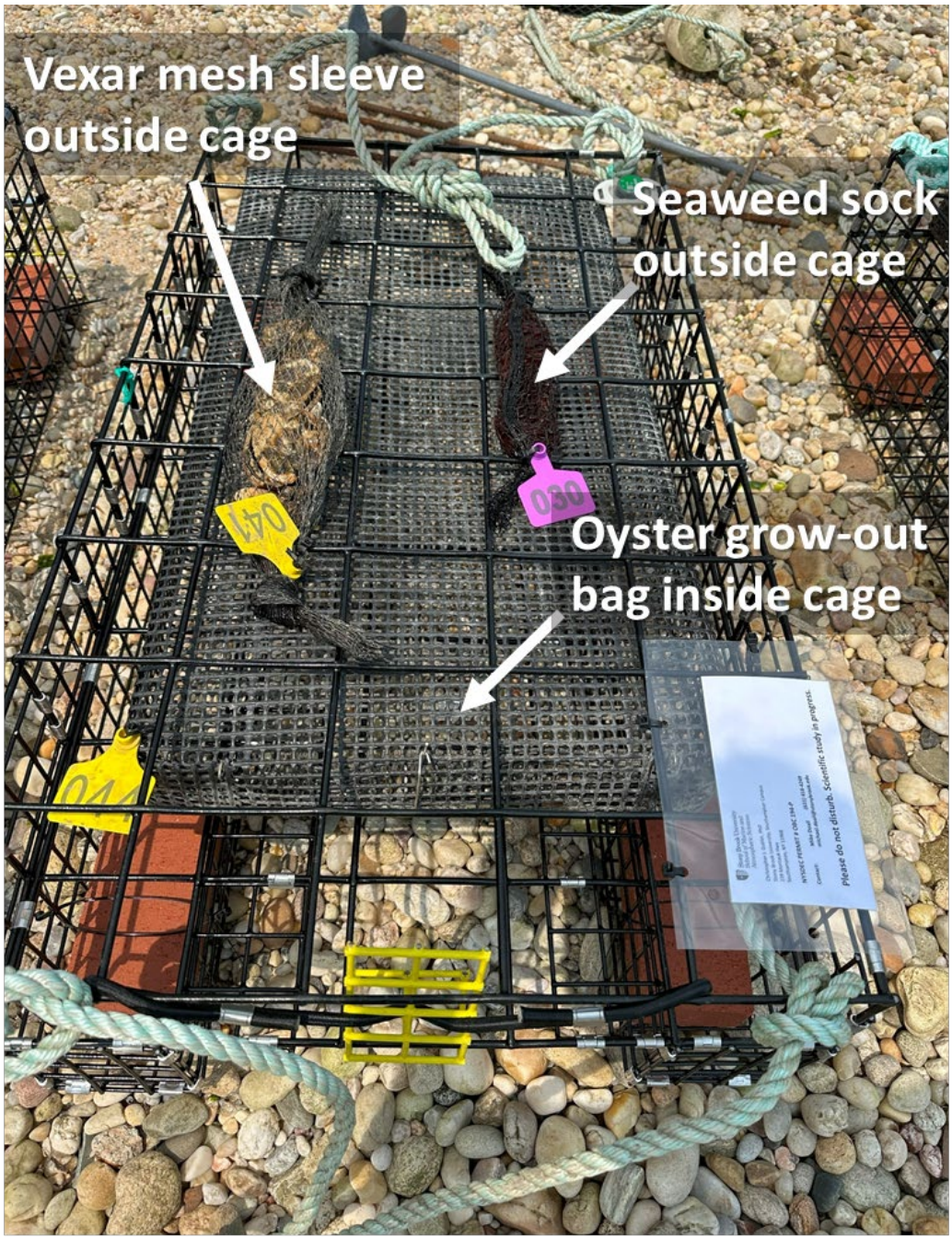


Figure 4. Photo of oyster cages deployed at the study sites. Oyster spat-on-shell (SOS) was placed in a standard aquaculture grow out bag inside the low-profile bottom cage (aquaculture method) and were also placed in a Vexar mesh sleeve, commonly used in oyster restoration, on the outside of the low-profile bottom cages (restoration method). The aquaculture bags inside the cage afforded the oysters greater protection from predators due to a smaller mesh size of the bag. Mussel socks filled with red-branching macroalgae were affixed to the top of the low-profile bottom cages. A total of six cages with this design, excluding the macroalgae, were monitored in phase two.

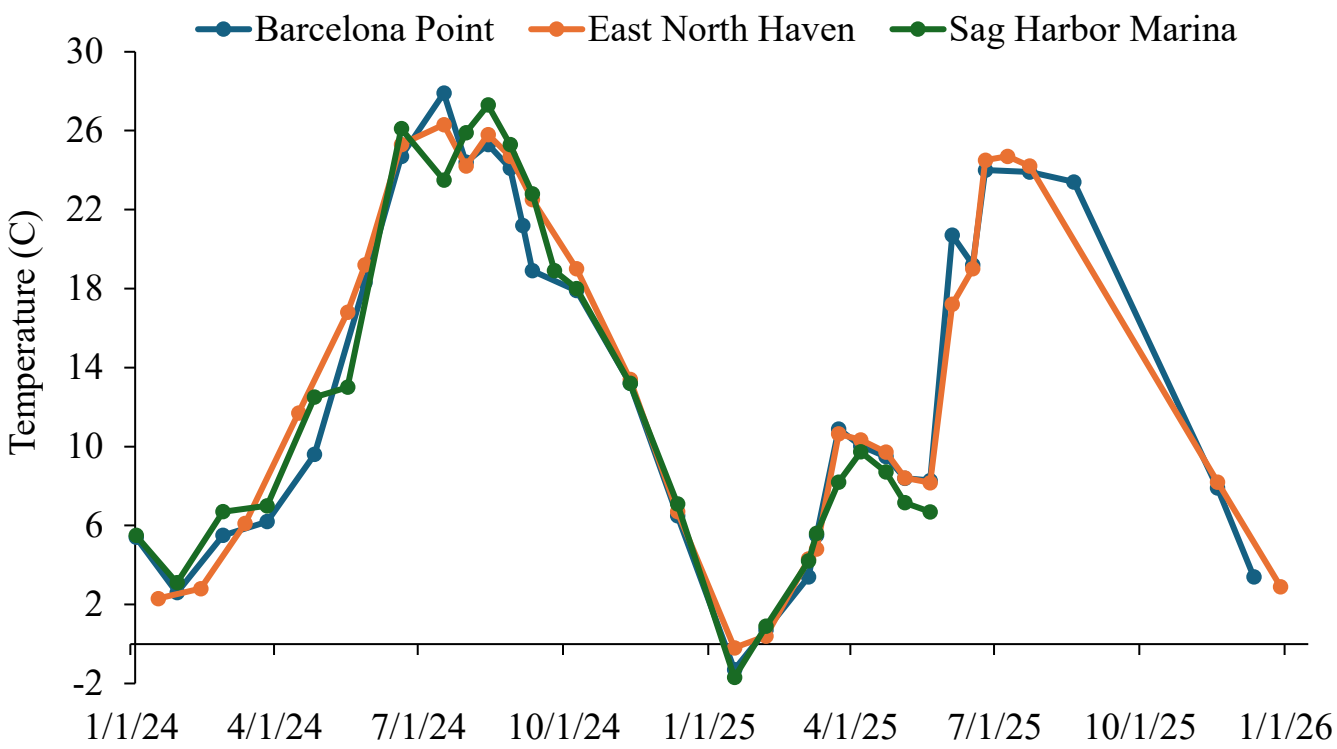


Figure 5. Discrete temperature readings at the Barcelona Point, East North Haven, and the Sag Harbor Marina study sites over a two-year time period from January 2024 to January 2026 (monitoring at Sag Harbor marina was discontinued in May 2025).

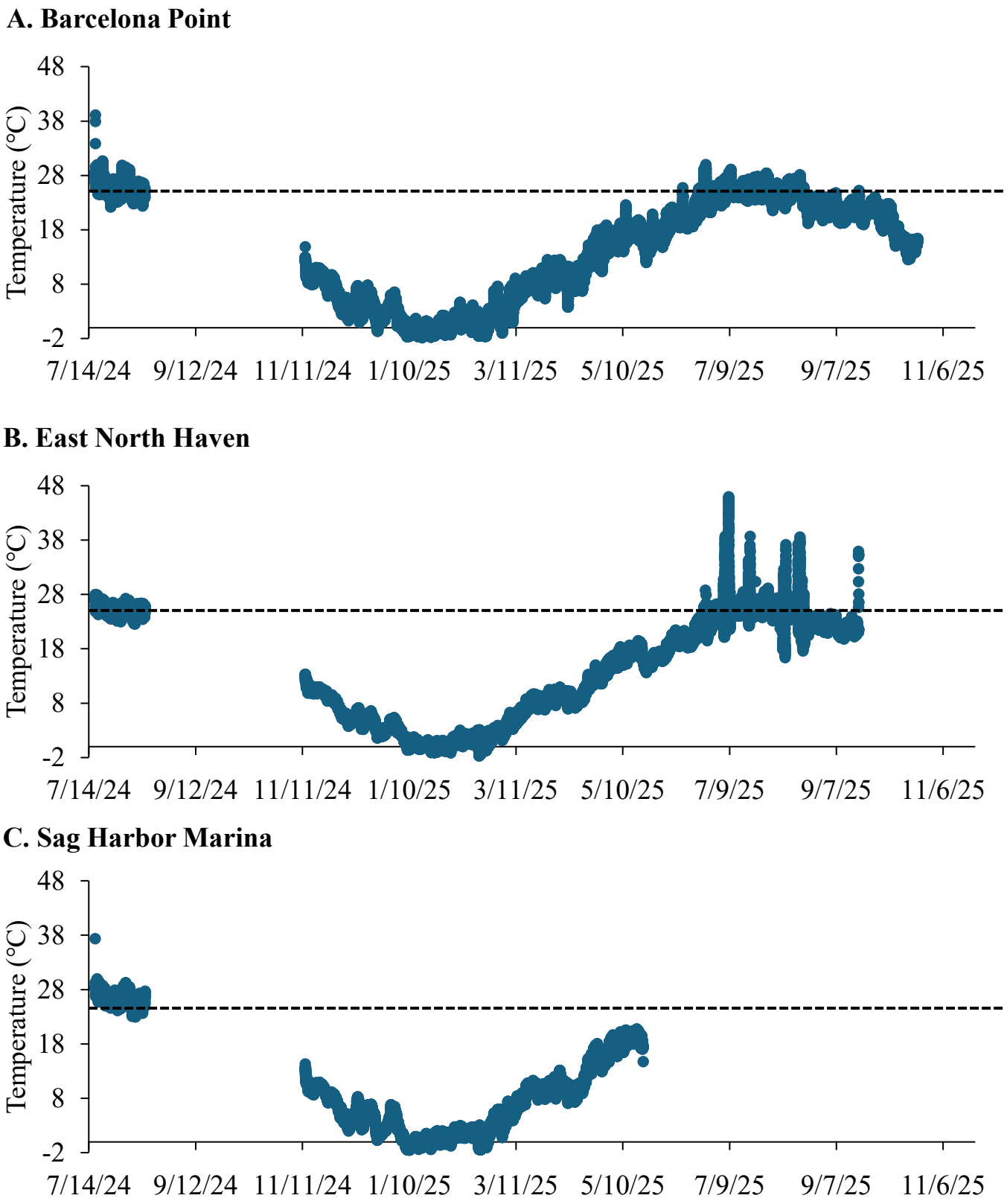


Figure 6. Continuous temperature (°C) readings taken at 10-minute intervals from July 2024 to early October 2025 for the **(A)** Barcelona Point and **(B)** East North Haven study sites, and from July 2024 to May 2025 for the **(C)** Sag Harbor Marina study site. Gaps in data indicate sensor servicing. Dotted lines mark the 25 °C level which is considered to be stressful to eelgrass.

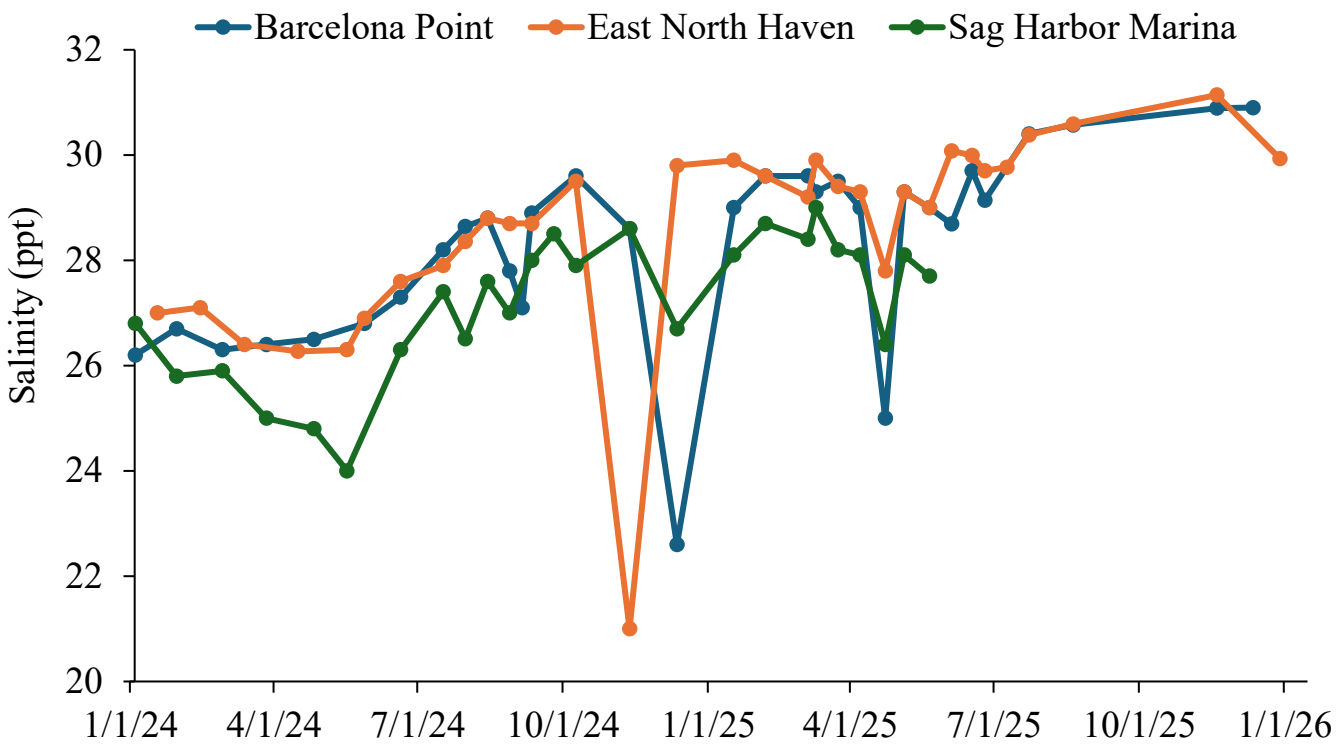


Figure 7. Discrete salinity readings (ppt) at the Barcelona Point, East North Haven, and the Sag Harbor Marina study sites over a two-year time period from January 2024 to January 2026 (monitoring at Sag Harbor marina was discontinued in May 2025).

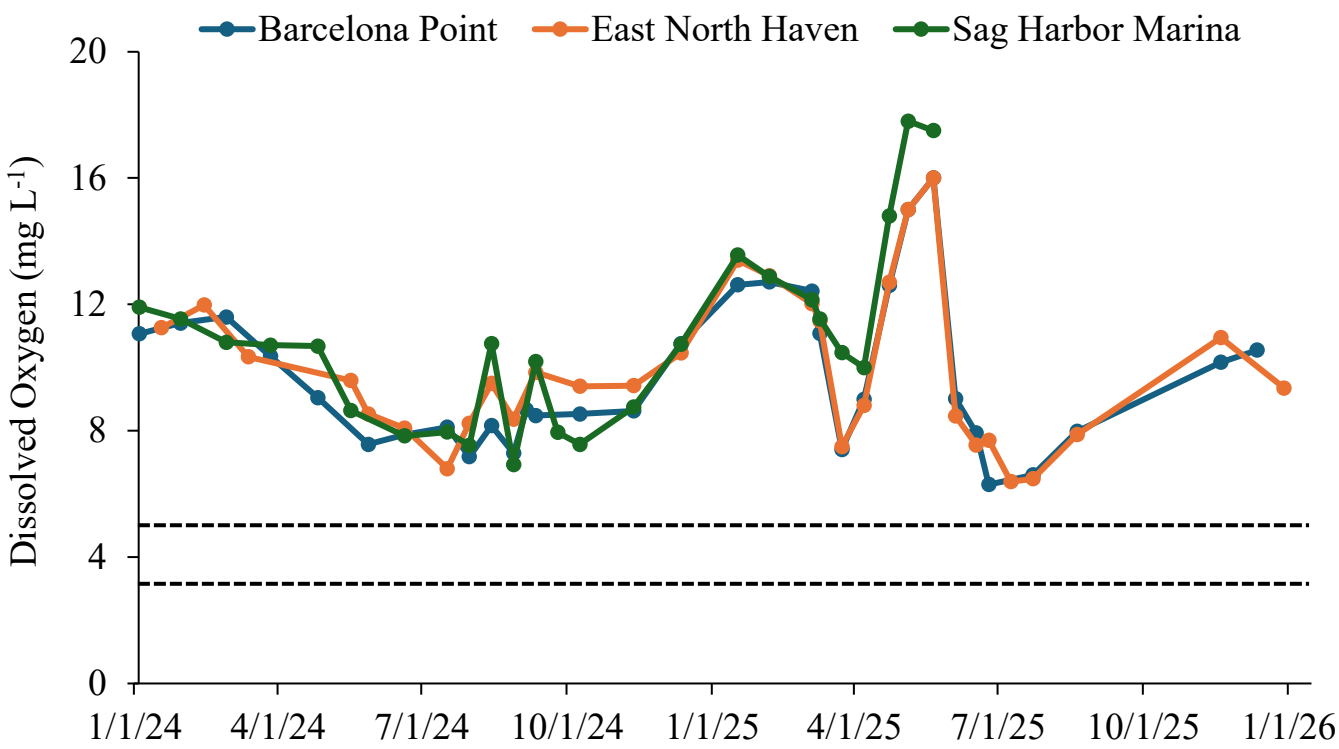


Figure 8. Discrete dissolved oxygen readings (mg L^{-1}) at the Barcelona Point, East North Haven, and the Sag Harbor Marina study sites over a two-year time period from January 2024 to January 2026 (monitoring at Sag Harbor marina was discontinued in May 2025). Dotted lines mark chronic and acute dissolved oxygen levels recognized by the NYSDEC at 4.8 mg/L and 3.0 mg/L, respectively.

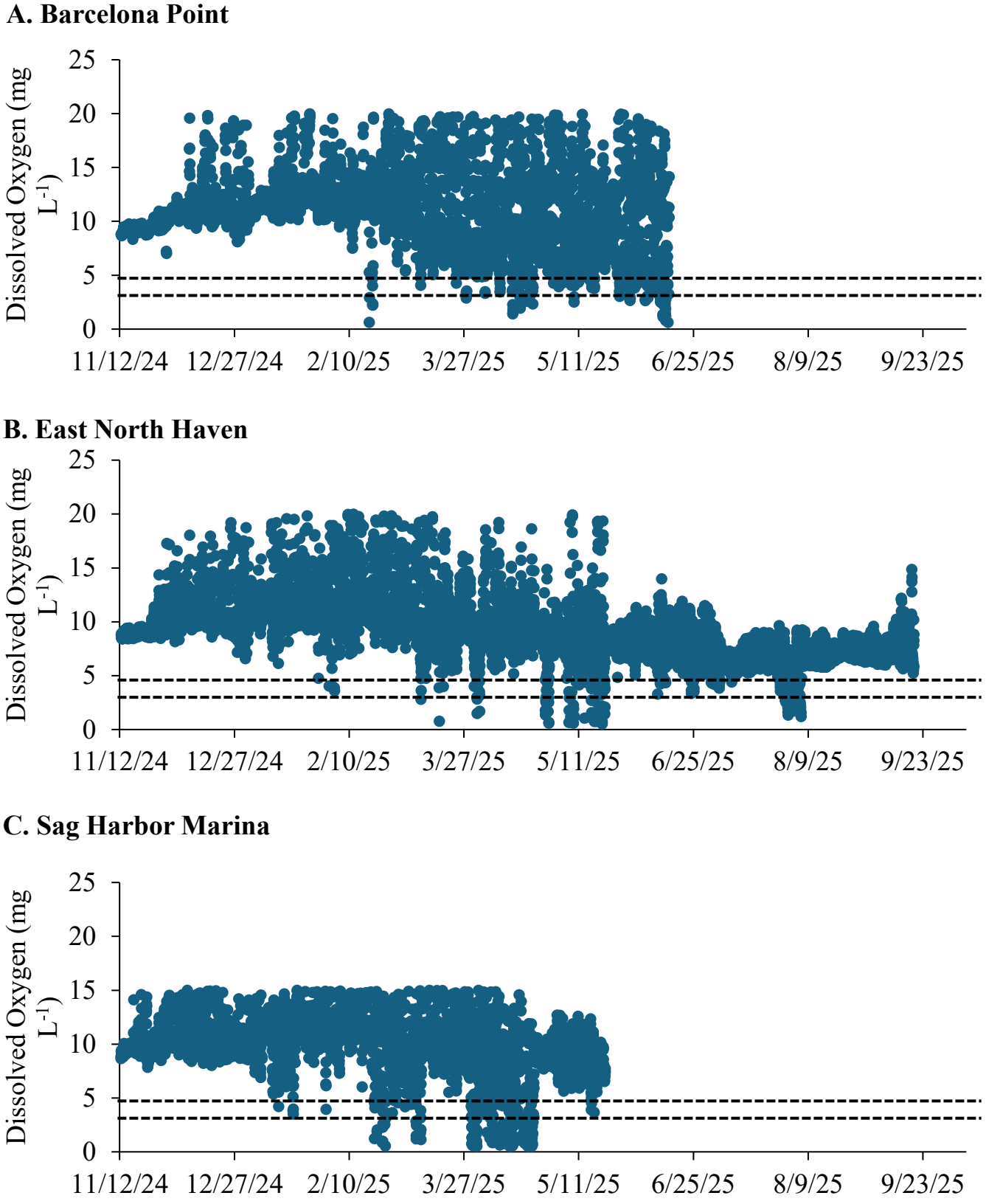


Figure 9. Continuous dissolved oxygen (mg L^{-1}) was taken at 10-minute intervals beginning November 12th, 2024, and ending in early June 2025 for the **(A)** Barcelona Point site due to sensor malfunction, early September 2025 for the **(B)** East North Haven site and, late May 2025 for the **(C)** Sag Harbor Marina site, marking the termination of Sag Harbor Marina site. Data was averaged every 60-minutes with the removal of DO levels above 20 mg L^{-1}. Dotted lines mark chronic and acute dissolved oxygen levels recognized by the NYSDEC at 4.8 mg/L and 3.0 mg/L, respectively.

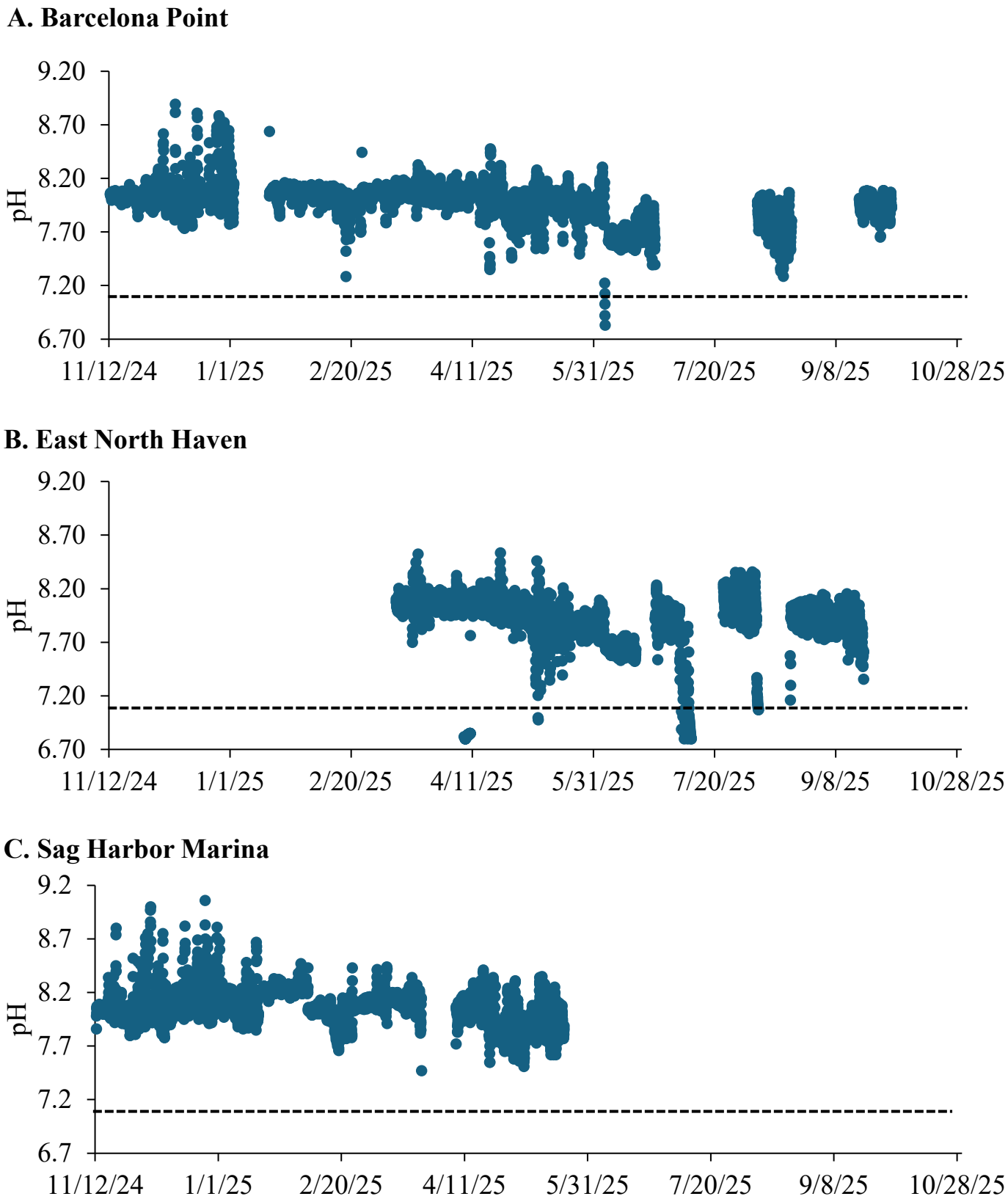


Figure 10. Continuous pH was taken at 10-minute intervals from November 12th, 2024, to late September 2025 for the **(A)** Barcelona Point site, from March 10th 2025 to late September 2025 for the **(B)** East North Haven site, and from November 12th, 2024, to Late May 2025 for the **(C)** Sag Harbor Marina study site. Data was averaged every 60-minutes. The dotted lines mark pH of 7.1, a level below which is known to be stressful to oysters.

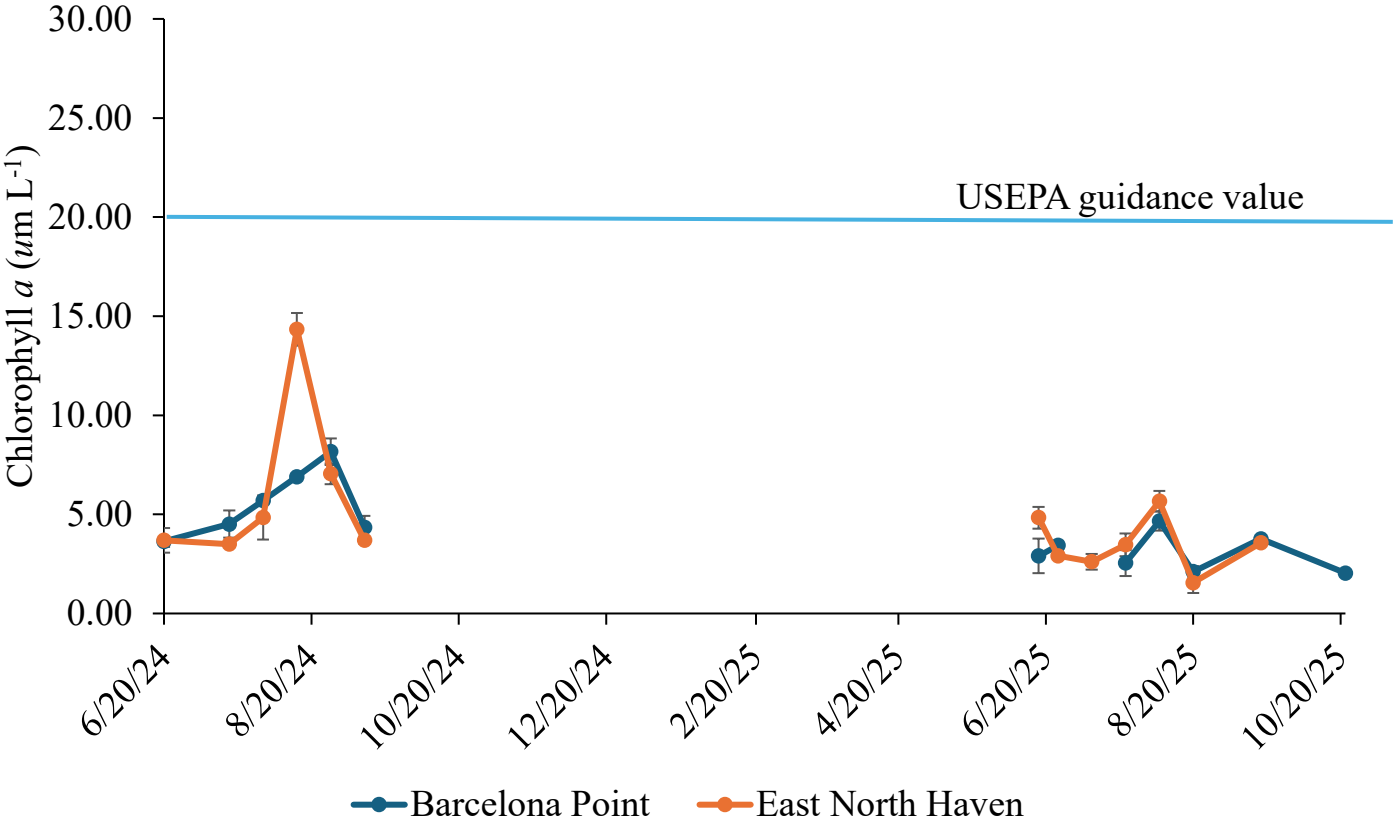


Figure 11. Discrete Chlorophyll-*a* (*u*g L^{-1}) concentrations at the Barcelona Point and the East North Haven study sites over a two-year time period from June 2024 to October 2025. Solid dark teal line marks the USEP guidance value for chlorophyll-*a* (*u*g L^{-1}) concentrations, with values above that threshold considered to be poor water quality/algae bloom.

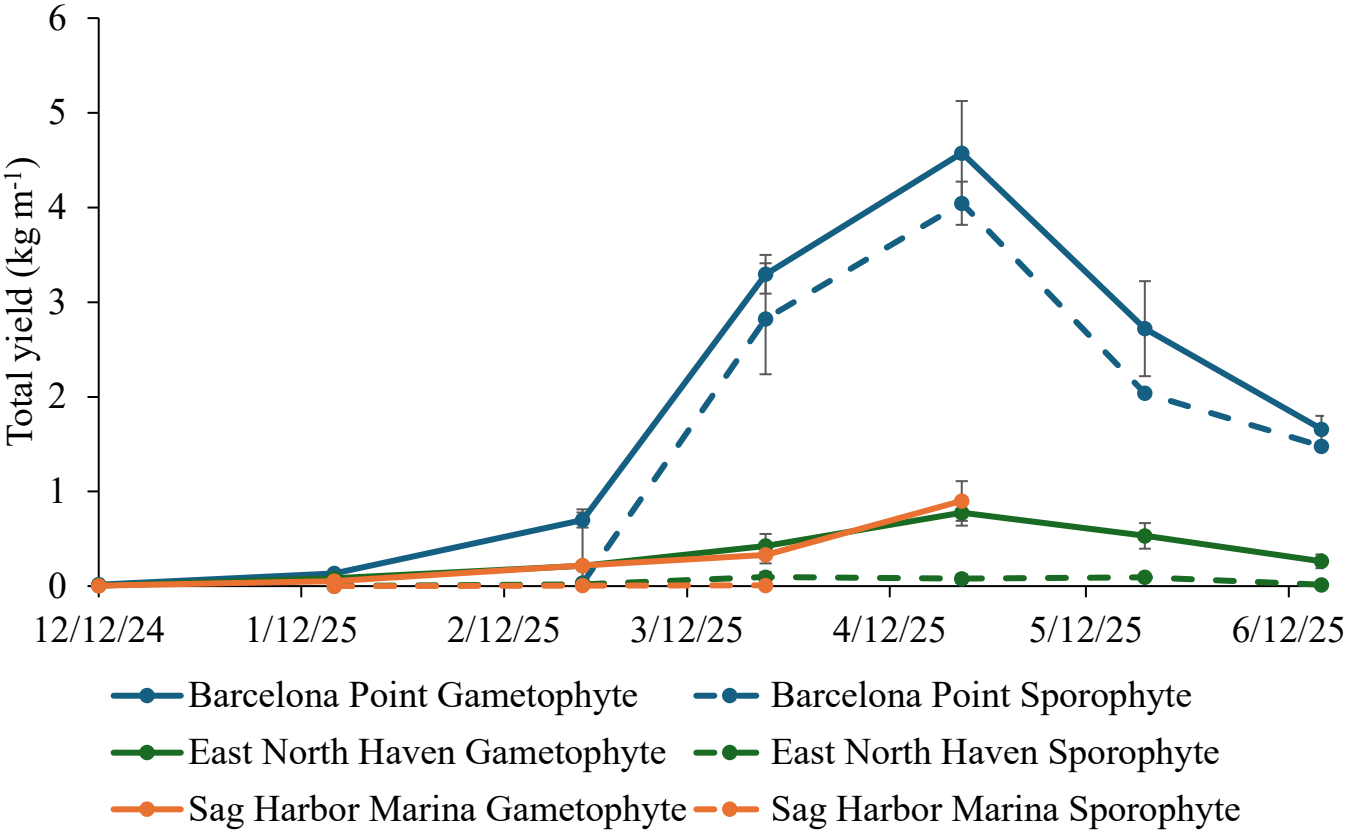


Figure 12. Yield (kg m $^{-1}$) of gametophyte and spore-derived *Saccharina latissima* during the 2025 season within the three study sites in the Peconic Estuary from the first monitoring time point in mid December 2024 to the harvest in mid-June 2025. Error bars indicate standard error.

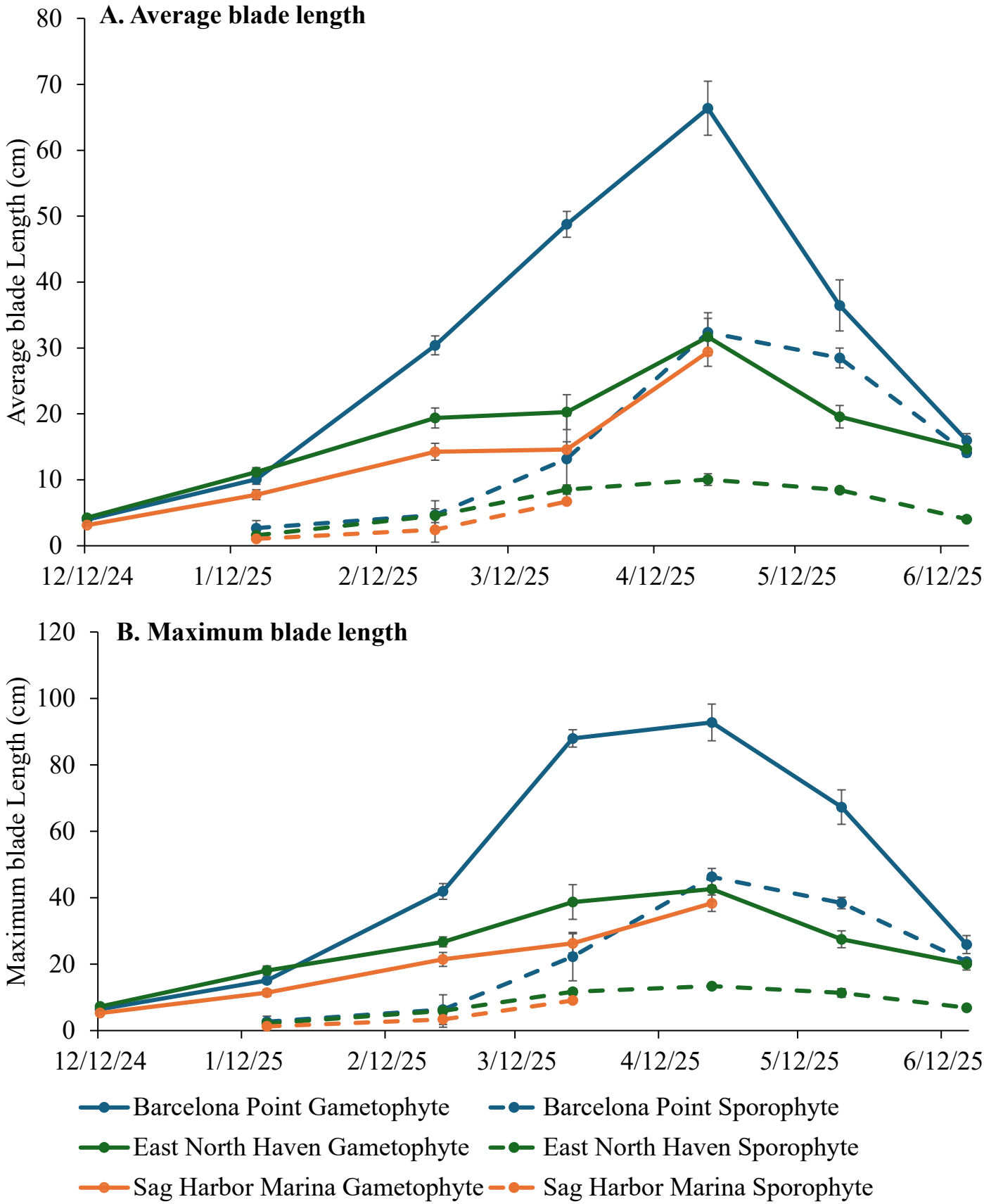


Figure 13. (A) Average blade length (cm) and **(B)** maximum blade length (cm) of gametophyte-derived and spore-derived kelp lines during the 2025 season at the three study from the first monitoring time point in mid December 2024 to the harvest in mid-June 2025. Error bars indicate standard error.

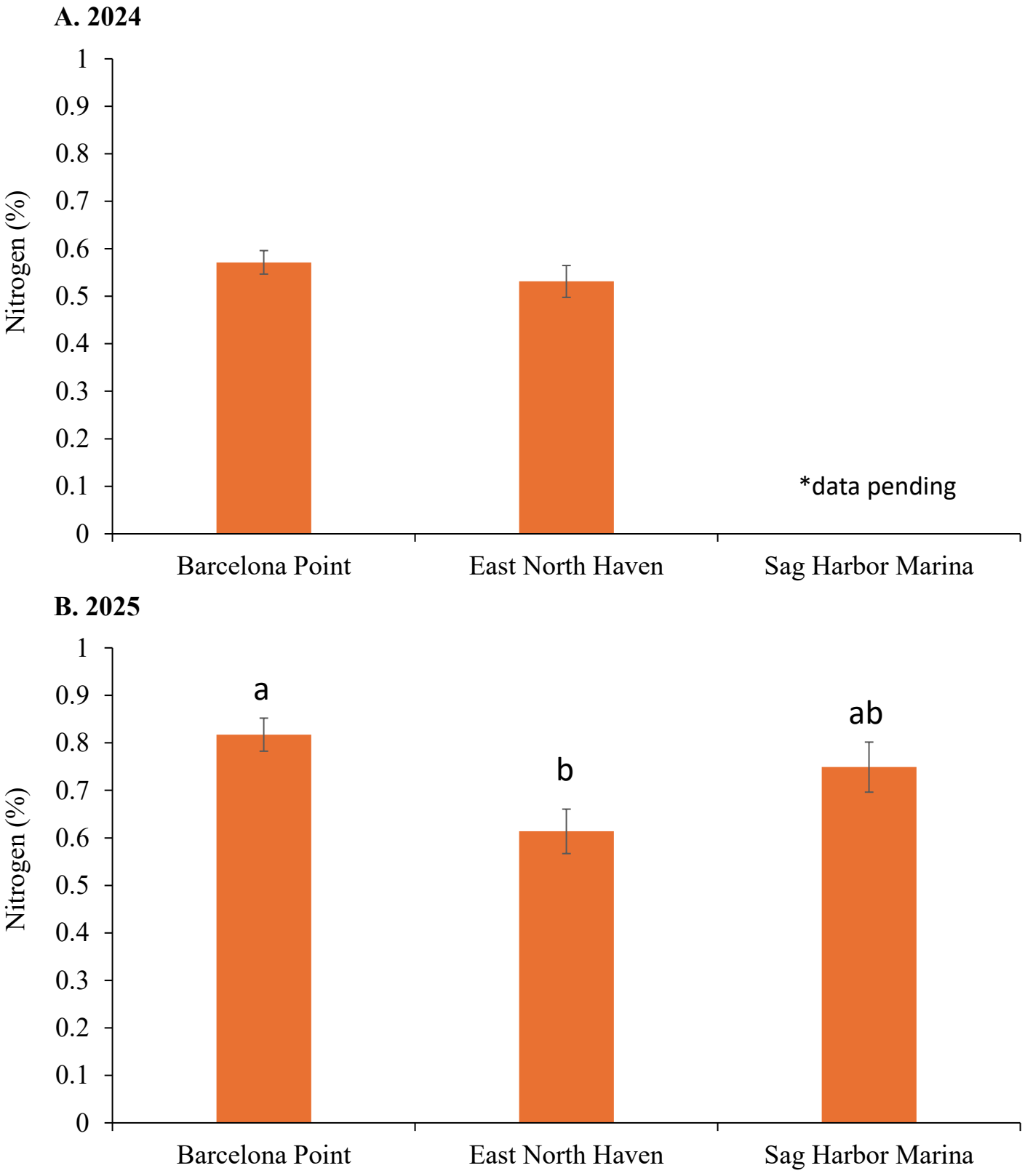


Figure 14. Nitrogen content of gametophyte-derived kelp tissue from the Barcelona Point, East North Haven, and Sag Harbor study sites at peak biomass during the **(A)** 2024 and **(B)** 2025 growing season. Data from Sag Harbor in 2024 is pending. Error bars indicate standard error. Letters above bars indicate significant differences.

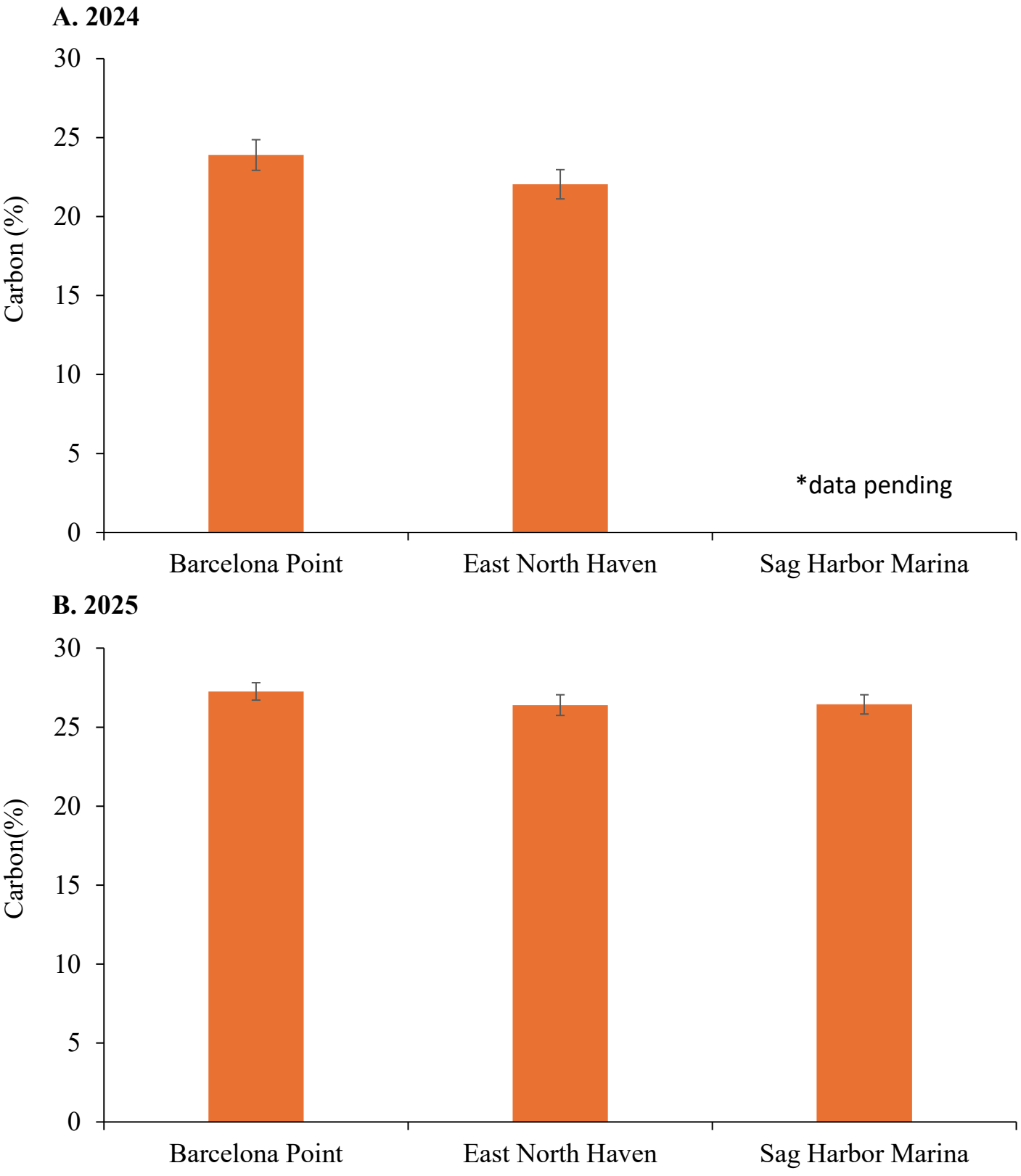


Figure 15. Carbon content of gametophyte-derive and spore-derived kelp for the Barcelona Point, East North Haven, and Sag Harbor study sites at peak biomass during the **(A)** 2024 and **(B)** 2025 growing season. Data from Sag Harbor in 2024 is pending. Error bars indicate standard error. Letters above bars indicate significant differences.

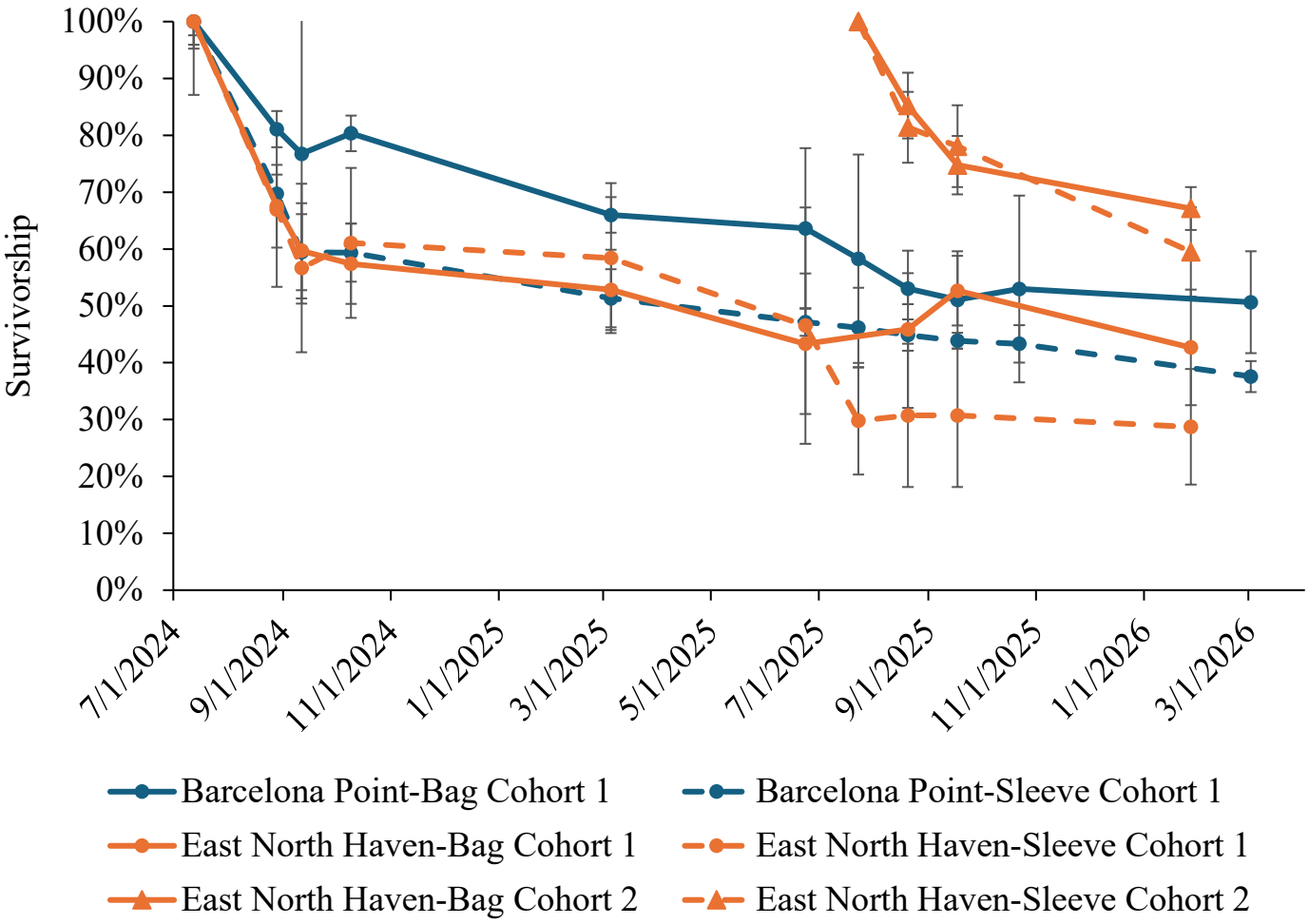


Figure 16. Survival (percent) of oysters in commercial grow-out bags in cages (aquaculture method) and Vexar mesh sleeves (restoration method) at the Barcelona Point and East North Haven study sites from July 2024 through January 2026. Error bars indicate standard error. The first cohort of oyster spat-on-shell was deployed to both sites in July 2024, and a second cohort of spat-on-shell was added to East North Haven in July 2025

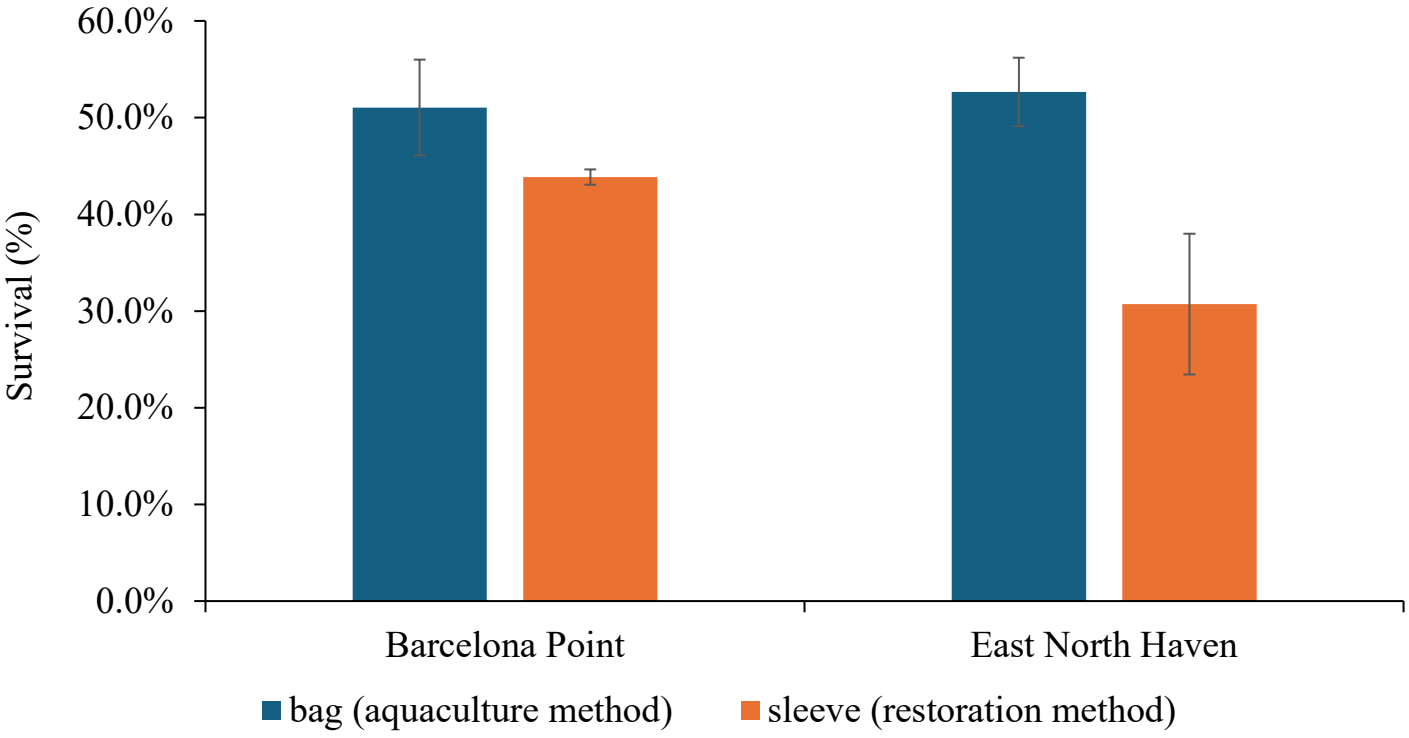


Figure 17. Survival (percent) of oysters in commercial grow-out bags in cages (aquaculture method) and Vexar mesh sleeves (restoration method) at the Barcelona Point and East North Haven study sites on September 17th, 2025, 406 days after deployment to the field sites. Error bars indicate standard error.

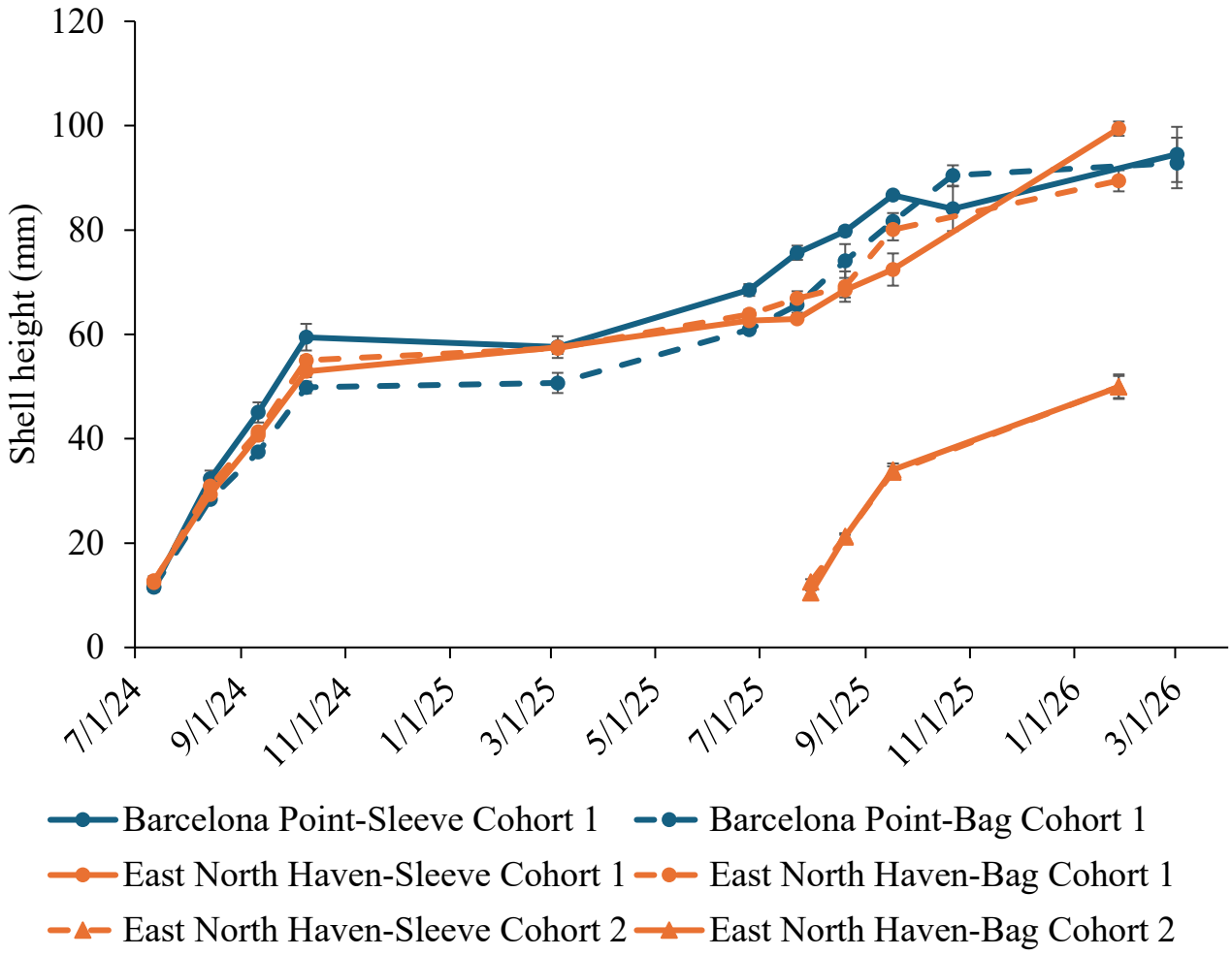


Figure 18. Growth of oysters in commercial grow-out bags in cages (aquaculture method) and Vexar mesh sleeves (restoration method) at the Barcelona Point and East North Haven study sites from July 2024 through January 2026. Error bars indicate standard error. The first cohort of oyster spat-on-shell was deployed to both sites in July 2024, and a second cohort of spat-on-shell was added to East North Haven in July 2025

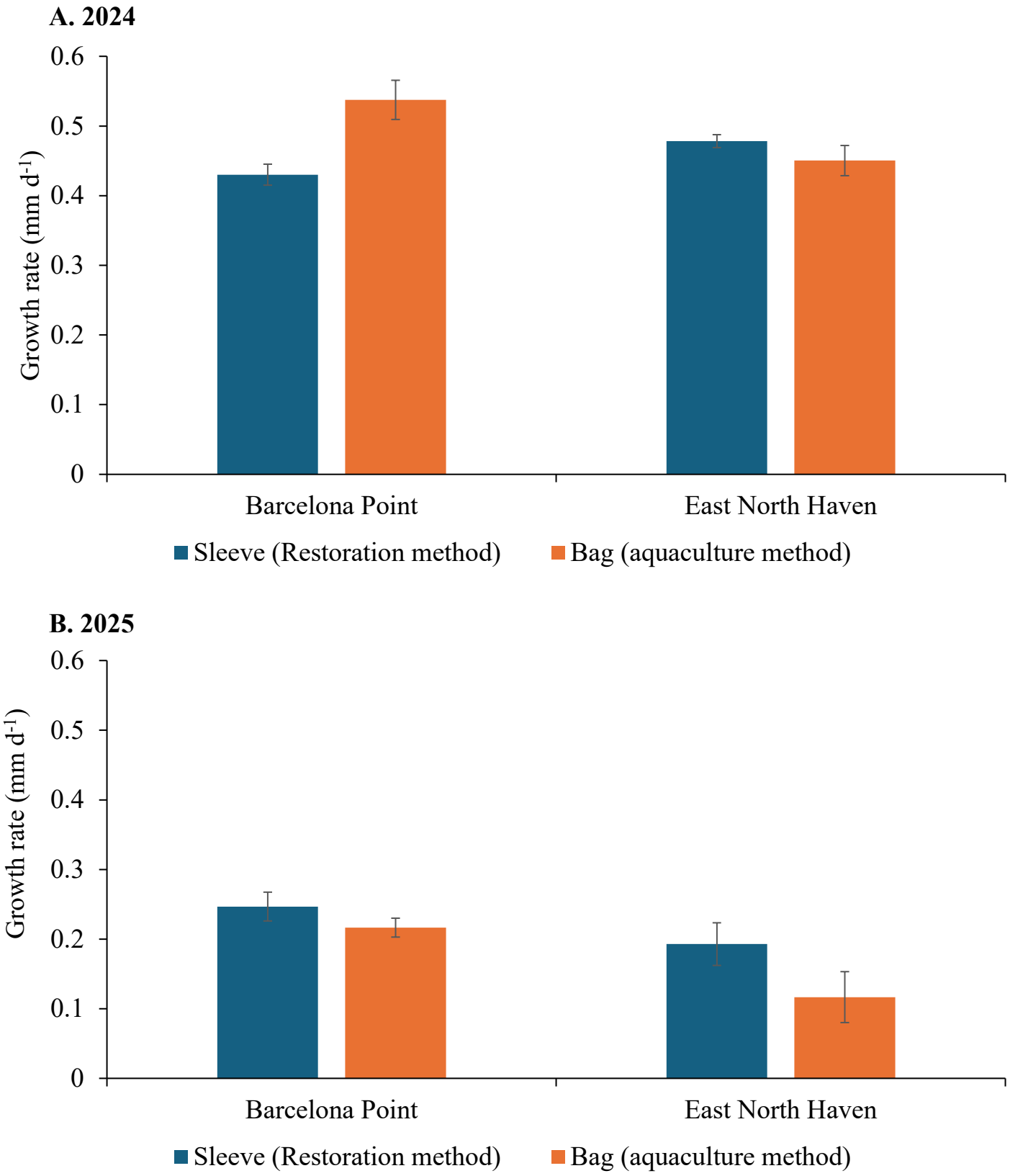


Figure 19. Growth of oysters in commercial grow-out bags in cages (aquaculture method) and Vexar mesh sleeves (restoration method) at the Barcelona Point and East North Haven study sites during the **(A)** 2024 growing season measured from July 12th to October 9th and during the **(B)** 2025 growing season from June 25th to September 17th. Error bars indicate standard error.

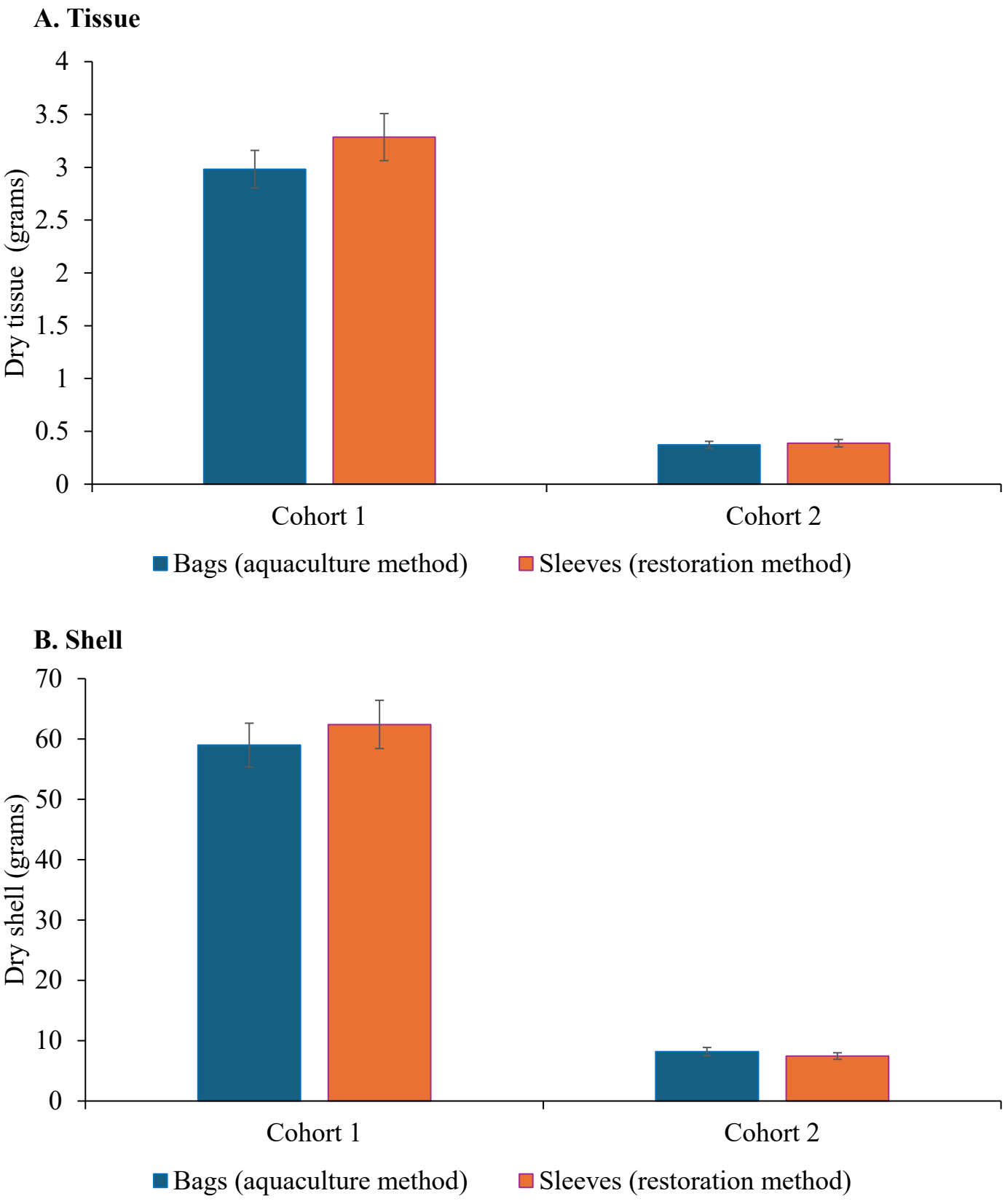


Figure 20. (A) Dry tissue and (B) dry shell weights of oysters in commercial grow-out bags in cages (aquaculture method) and Vexar mesh sleeves (restoration method) at the East North Haven study sites in January 2026. Cohort #1 oysters were deployed as Spat-on-shell in June 2024, and cohort #2 oysters were deployed as spat-on-shell in July 2025. Error bars indicate standard error.

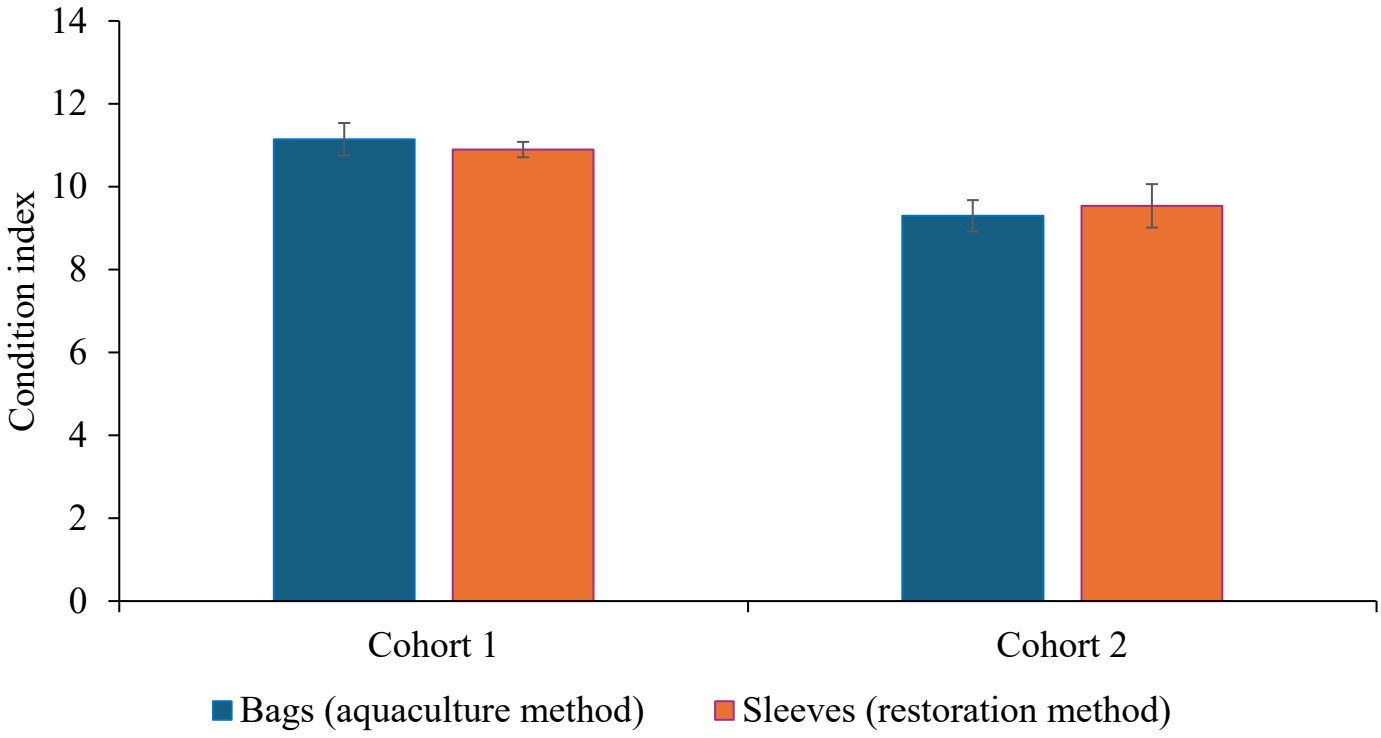


Figure 21. Condition index of oysters in commercial grow-out bags in cages (aquaculture method) and Vexar mesh sleeves (restoration method) at the East North Haven study sites in January 2026. Cohort #1 oysters were deployed as Spat-on-shell in June 2024, and cohort #2 oysters were deployed as spat-on-shell in July 2025. Error bars indicate standard error.

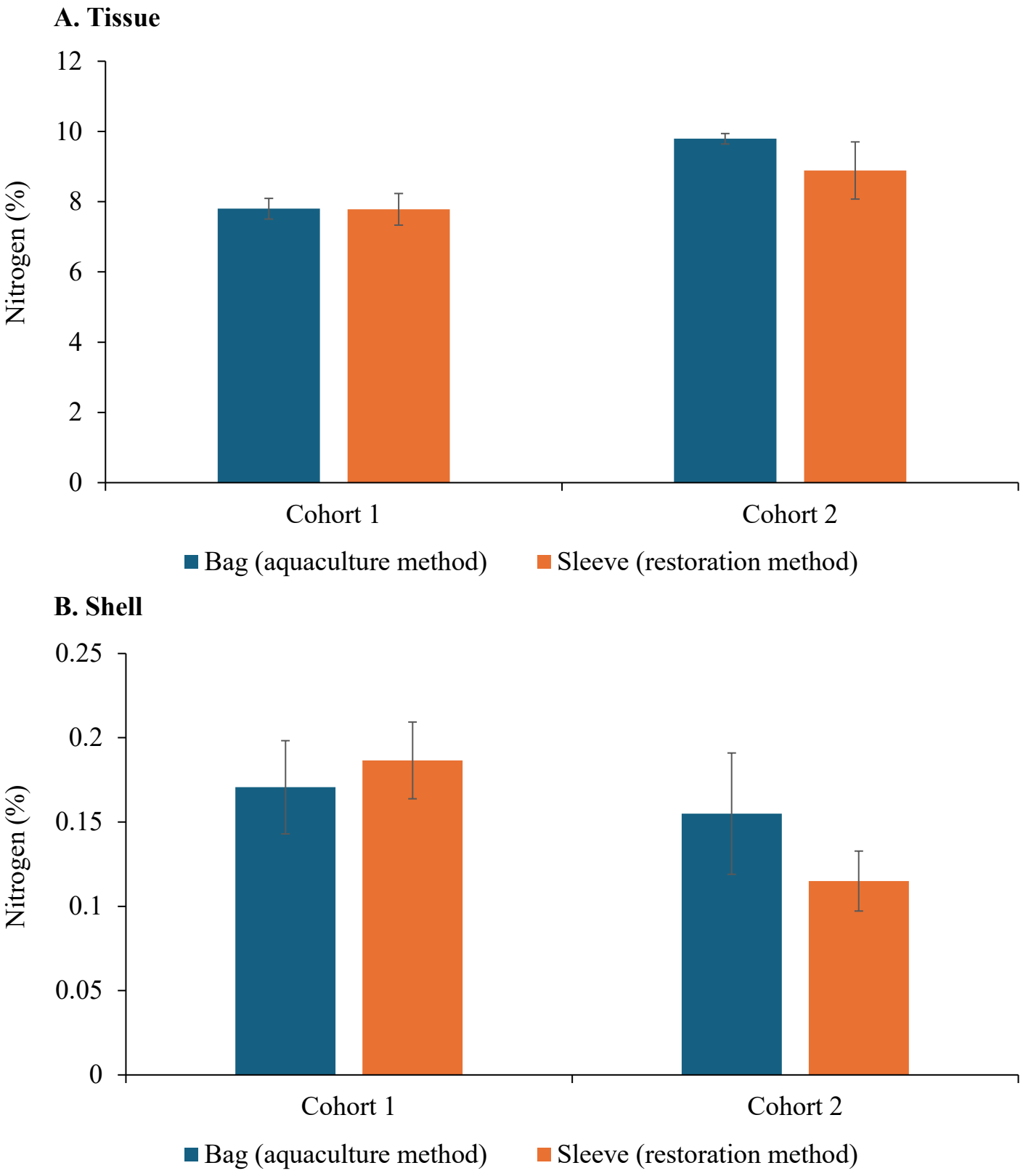


Figure 22. Nitrogen content of **(A)** oyster tissue and **(B)** oyster shell from oysters in commercial grow-out bags in cages (aquaculture method) and Vexar mesh sleeves (restoration method) at the East North Haven study sites in January 2026. Cohort #1 oysters were deployed as Spat-on-shell in June 2024, and cohort #2 oysters were deployed as spat-on-shell in July 2025. Error bars indicate standard error.

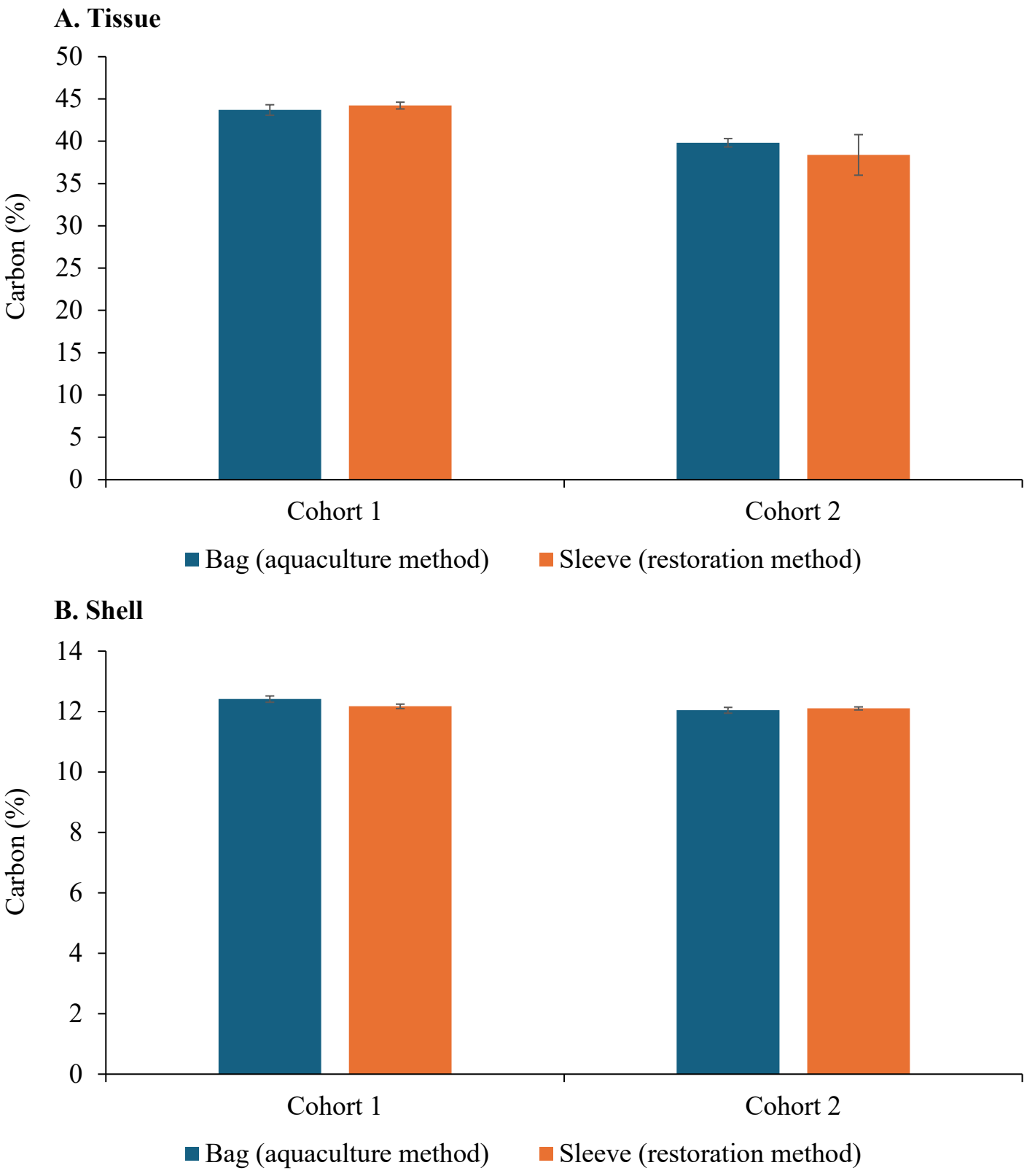


Figure 23. Carbon content of **(A)** oyster tissue and **(B)** oyster shell from oysters in commercial grow-out bags in cages (aquaculture method) and Vexar mesh sleeves (restoration method) at the East North Haven study sites in January 2026. Cohort #1 oysters were deployed as Spat-on-shell in June 2024, and cohort #2 oysters were deployed as spat-on-shell in July 2025. Error bars indicate standard error.

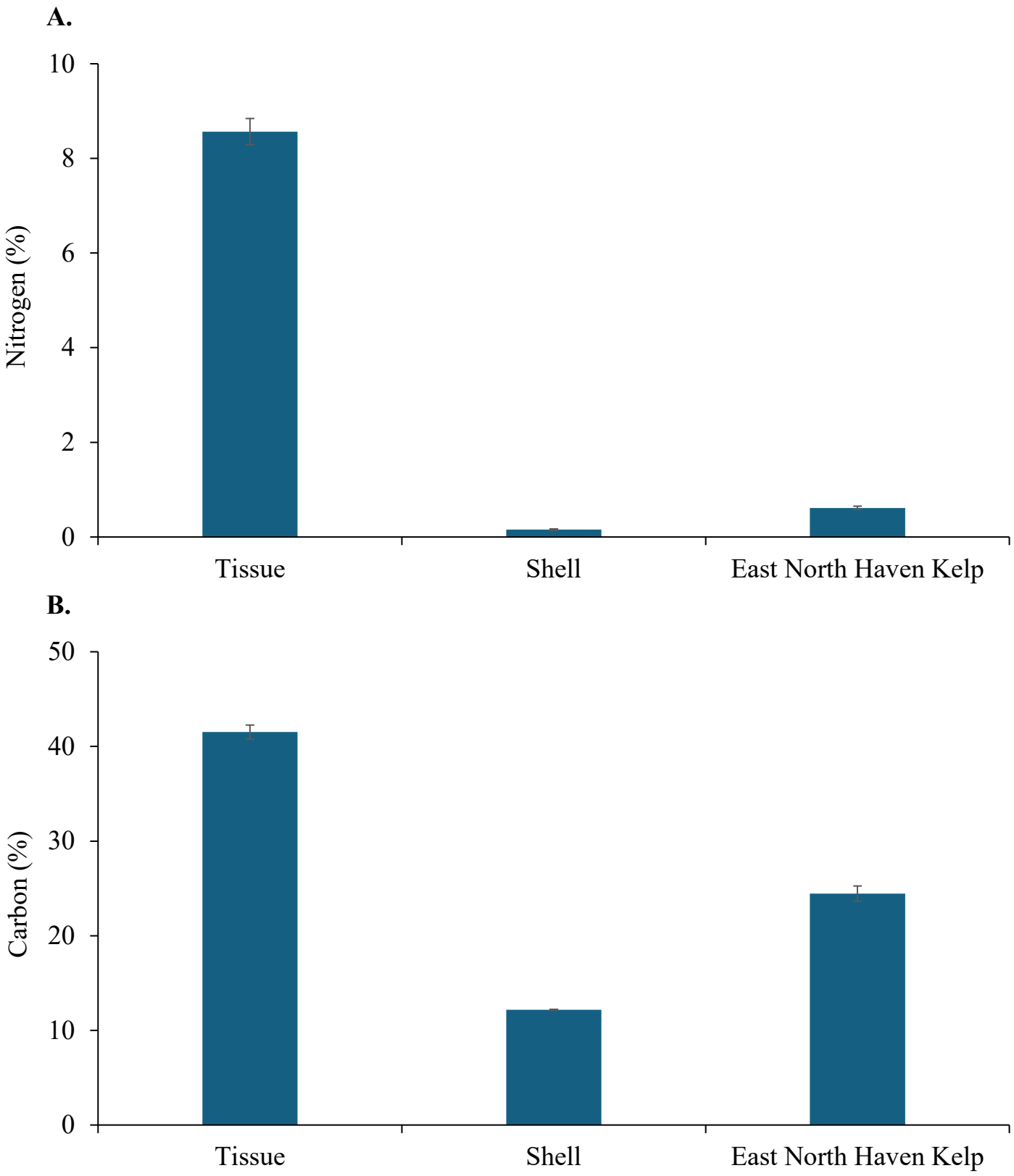


Figure 24. Comparison of **(A)** Nitrogen and **(B)** Carbon content (% dry mass) of oyster tissue, oyster shell, and kelp tissue at the East North Haven site. Error bars indicate standard error.

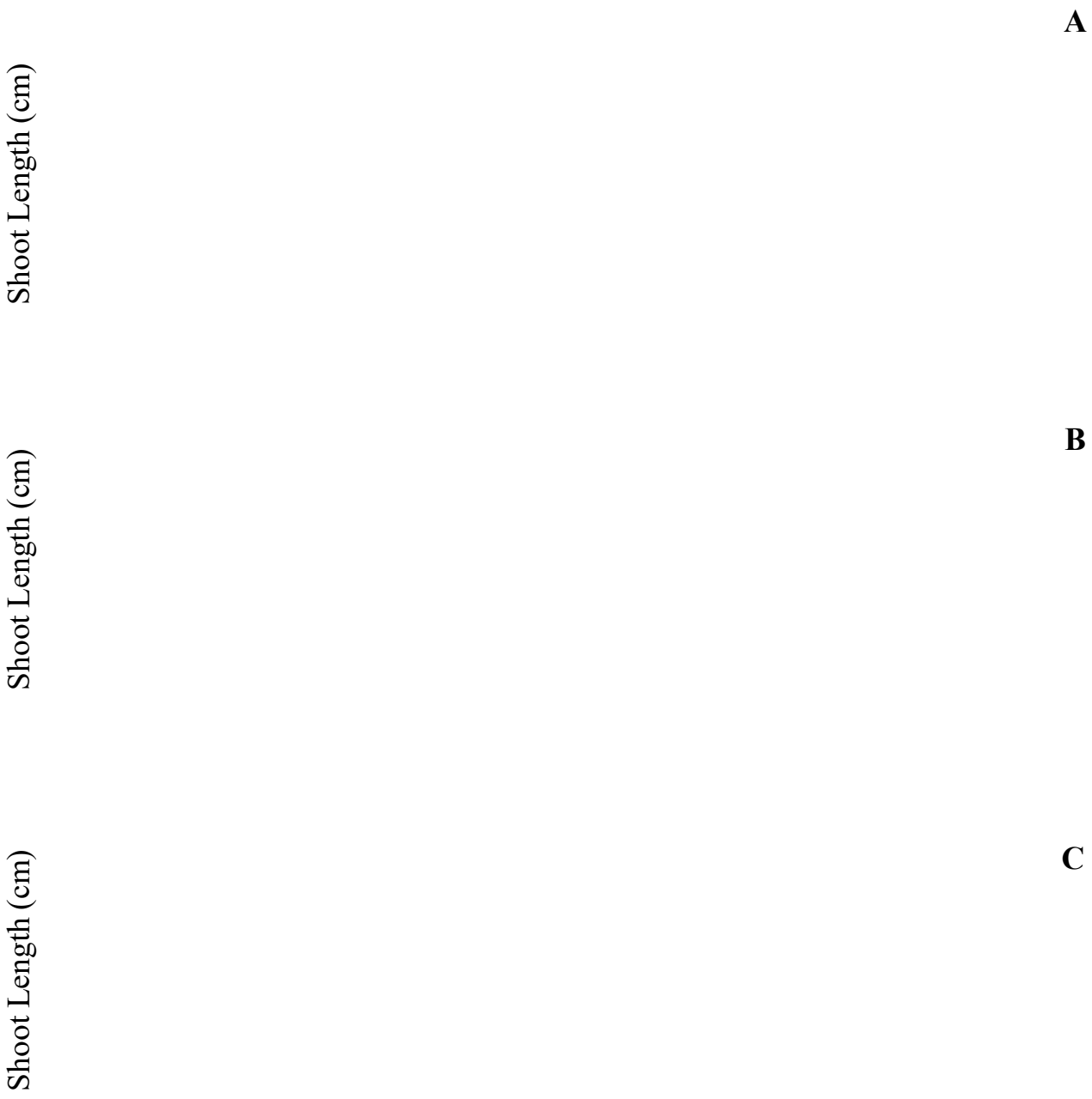


Figure 25. Average shoot length (cm) for **(A)** Barcelona Point (BP), **(B)** East North Haven (ENH), and **(C)** both study site for each patch across the growing season, as measured by the mean length of the longest leaf of 5 shoots within the patch.

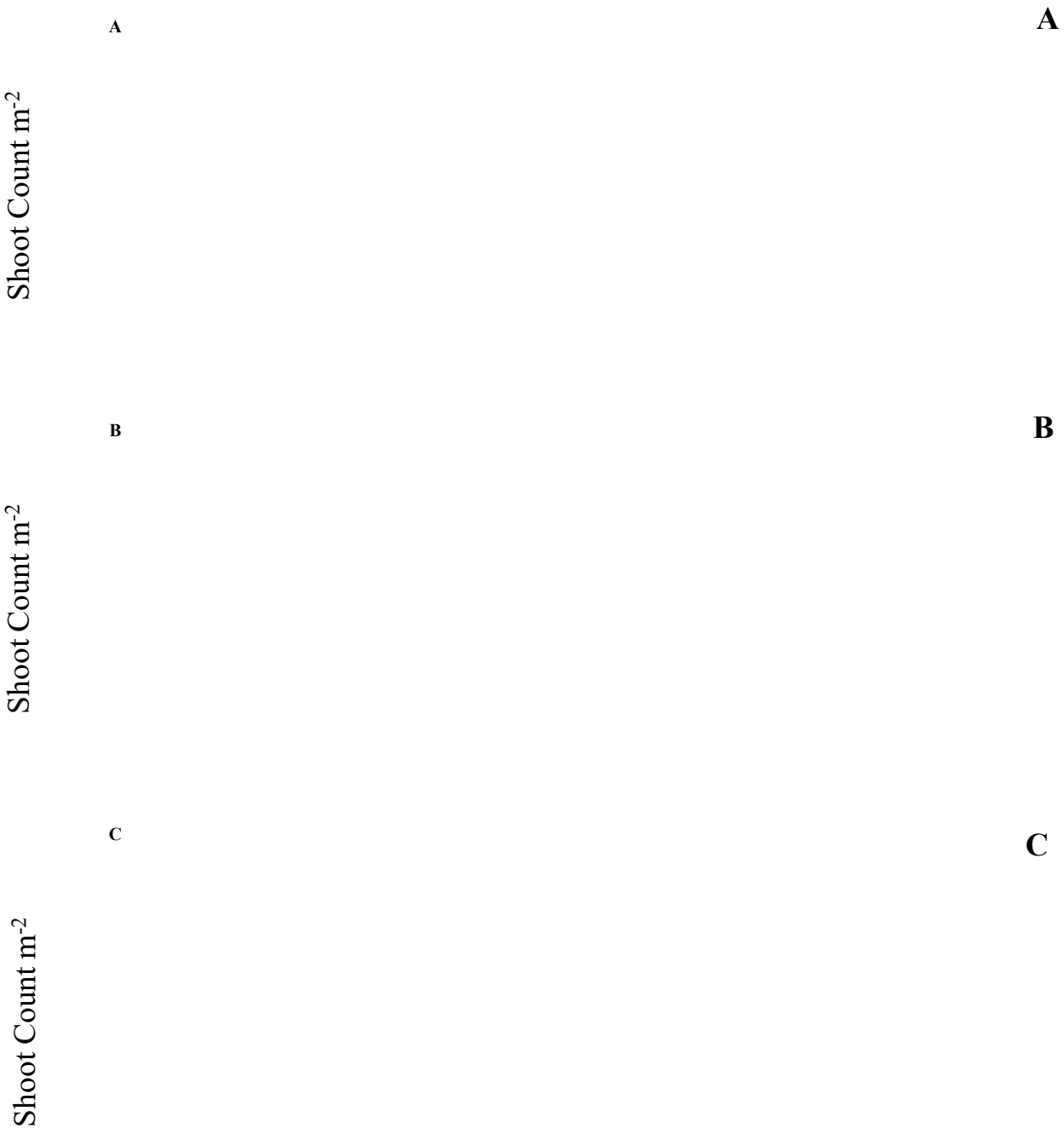


Figure 26. Shoot count m^{-2} at for **(A)** Barcelona Point (BP), **(B)** East North Haven (ENH), and **(C)** both sites throughout the growing season, separated by patch. Shoots were counted in 1/16 or ¼ m^2 quadrats in the center of the patch and multiplied by the appropriate factor to extrapolate shoots / m^2. Not all patches covered a full extent of 1 m^2.

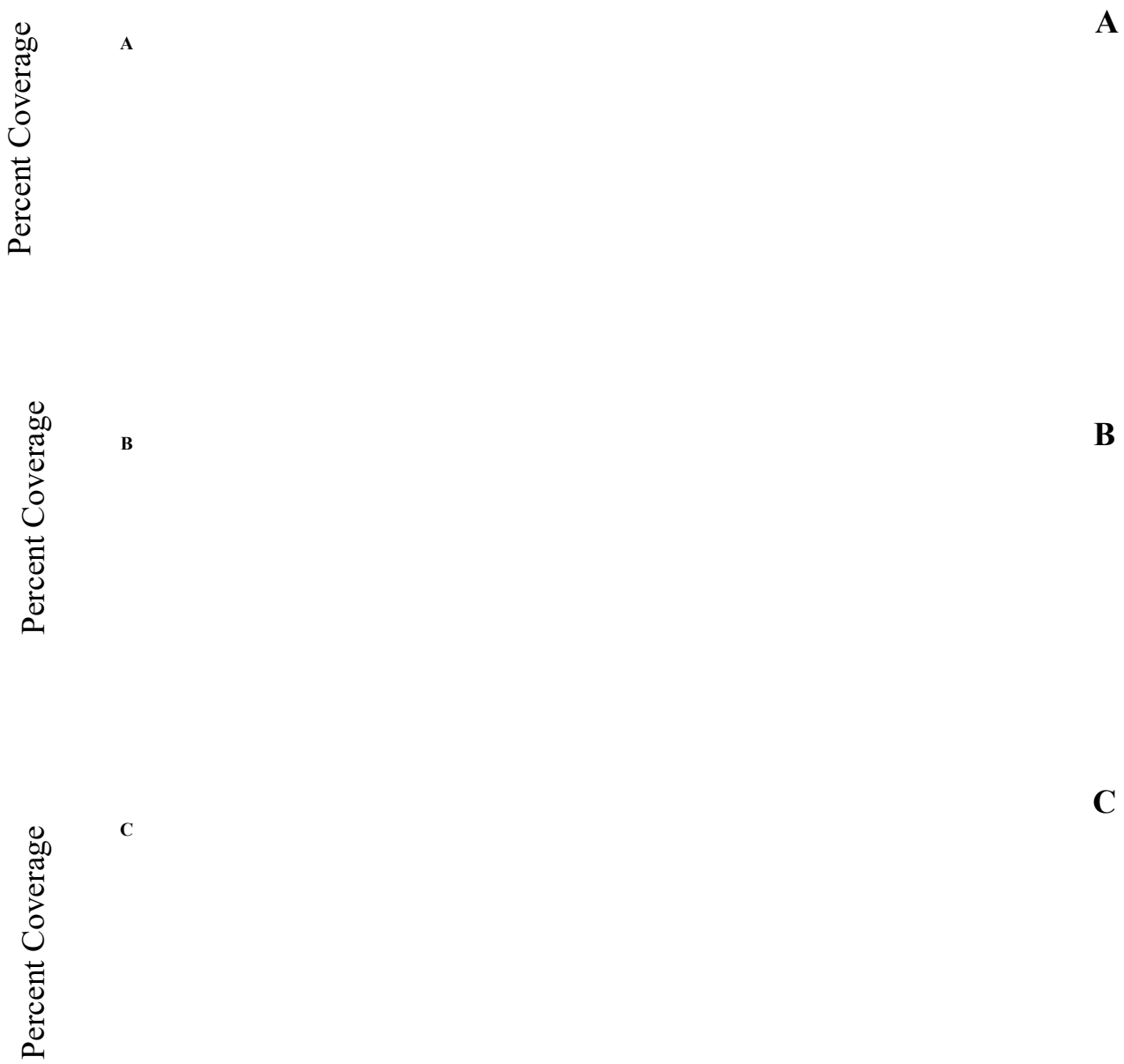


Figure 27. Percent coverage of *zostera marina* at for **(A)** Barcelona Point (BP), **(B)** East North Haven (ENH), and **(C)** both sites patch throughout the growing season. This metric was measured using ½ m^2 quadrats, placed in the center of the patch. Not all patches covered an areal extent of 0.5 m^2, and in these cases the existing grass was centered in the quadrat, and the measurement was still taken in respect to a full ½ m^2.



Figure 28. Leaf area index (LAI) for for **(A)** Barcelona Point (BP), **(B)** East North Haven (ENH), and **(C)** sites for each patch throughout the growing season. This metric was calculated on a per 1 m^2 basis, as the total area of photosynthetic material (m^2) in 1 m^2 of a given patch. Total shoot area was morphometrically measured for 12 shoots at each site, and the average shoot area for the site was multiplied by the shoot density (shoots/m^2) of each patch to yield total photosynthetic coverage for that site.

Macroalgae percent coverage

East North Haven

Barcelona Point

Figure 29. Percent cover of various macroalgae species at each site throughout the growing season, averaged across the whole site for each time period. Macroalgae percent cover was determined by considering the percentage of the existing seagrass fouled by macroalgae, as well as the percentage of the bare sand covered by macroalgae in a given ½ m^2 quadrat.



Figure 30. Epiphytic load (mg cm $^{-2}$) at **(A)** Barcelona Point and **(B)** East North Haven study sites throughout the study period, in dry weight of epiphytes per area of photosynthetic material of *Zostera marina*. After morphometric data was taken for 12 shoots sampled from each site, each shoot was scraped of epiphytes, which were then dried and weighed after 48 hours.



Figure 31. Biomass of *Zostera marina* in grams (g) dry weight across the growing season, averaged across the whole site. 12 shoots were sampled from each site at each time point, morphometrically analyzed, scraped of epiphytes, and dried in a drying oven for 48 hours to calculate dry weight.

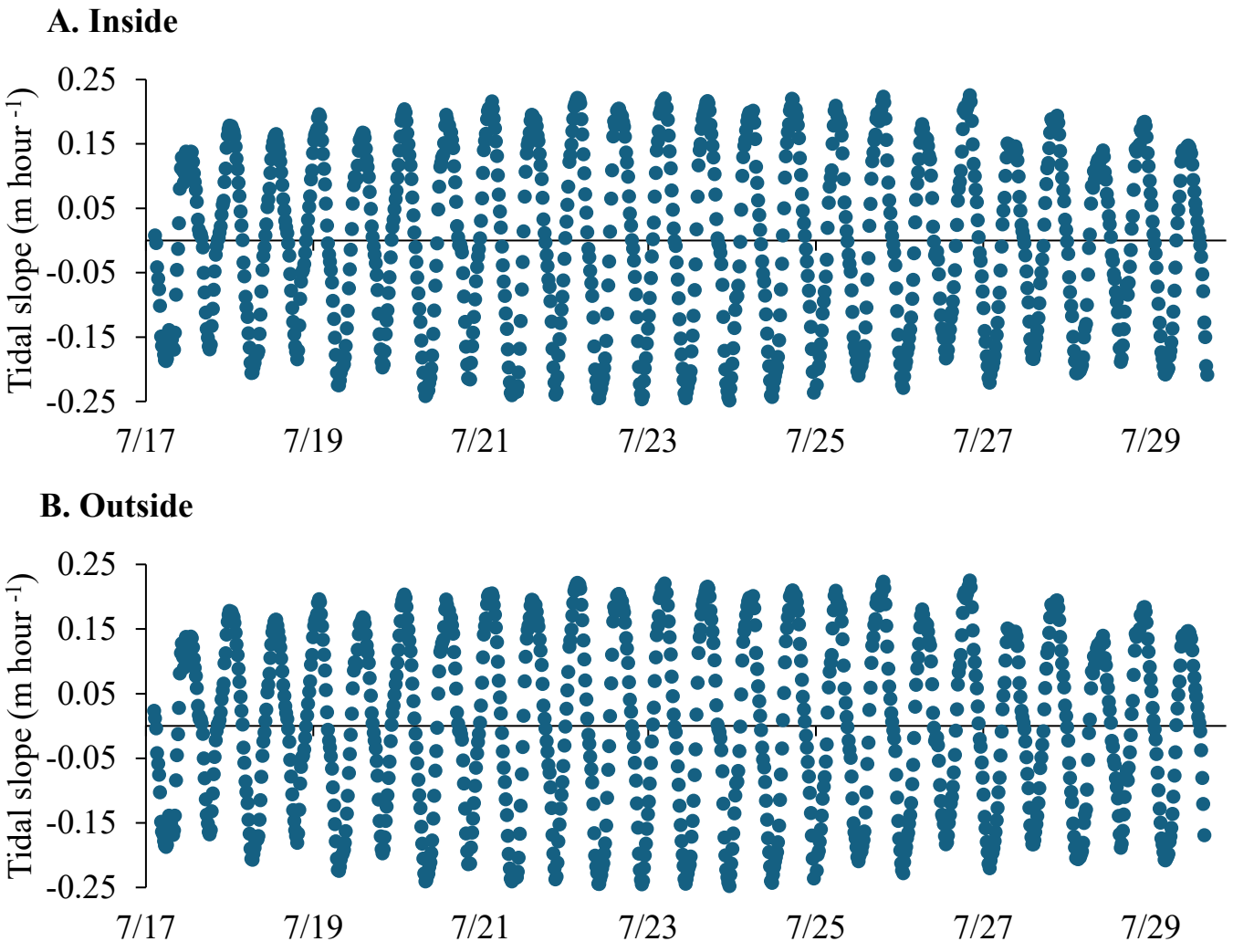


Figure 32 . Tidal slope (m hour^{-1}) depicting the tidal profile of **(A)** inside **(B)** outside the conservation area of the East North Haven study site in the Peconic Bays collected at 17-minute intervals using a RBR*solo*^{3} D: pressure (depth) wave attenuation sensor in July 2024.

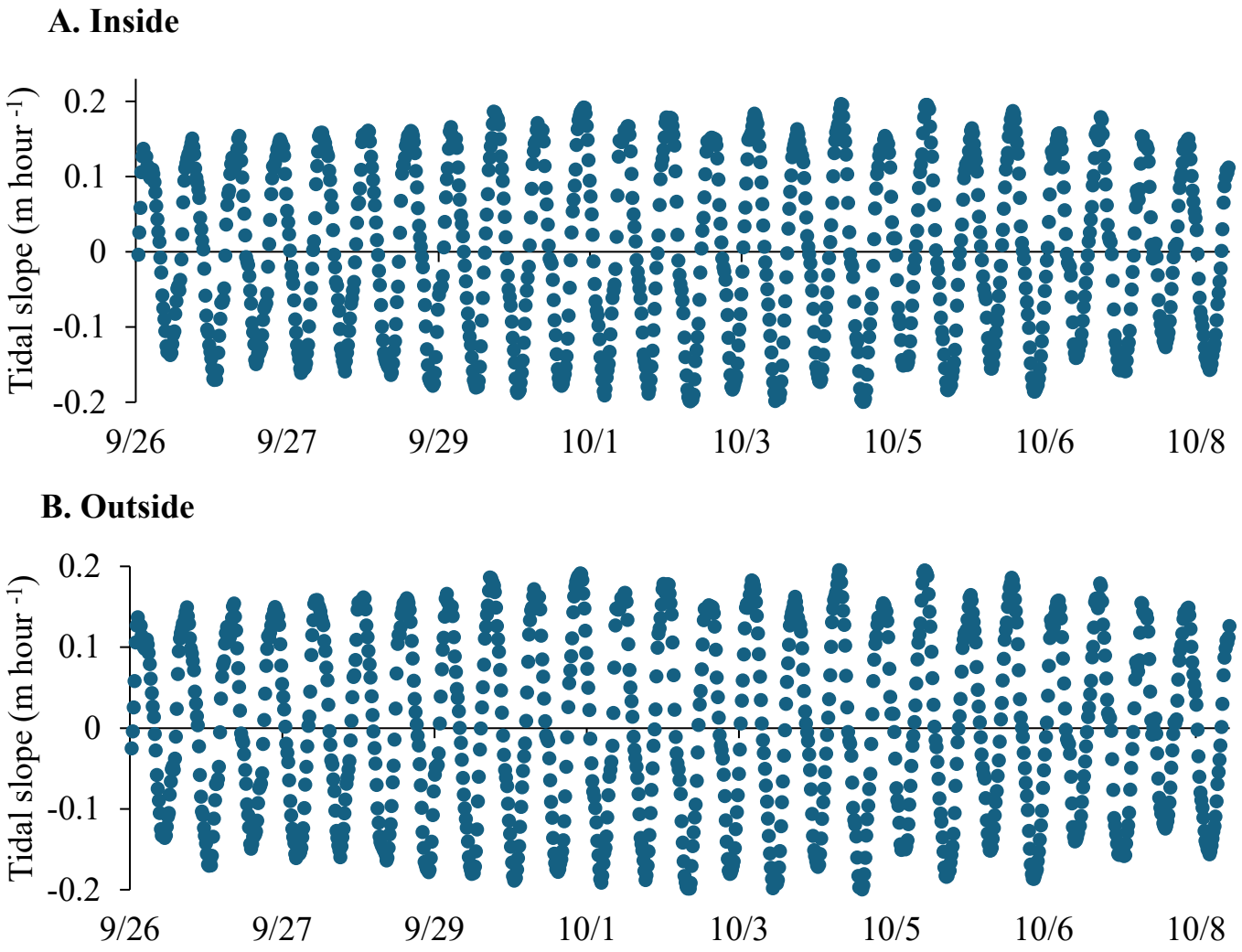


Figure 33 . Tidal slope (m hour^{-1}) depicting the tidal profile of **(A)** inside **(B)** outside the conservation area of the Sag Harbor Marina study site in the Peconic Bays collected at 17-minute intervals using a RBR*solo*^{3} D: pressure (depth) wave attenuation sensor in September 2024.

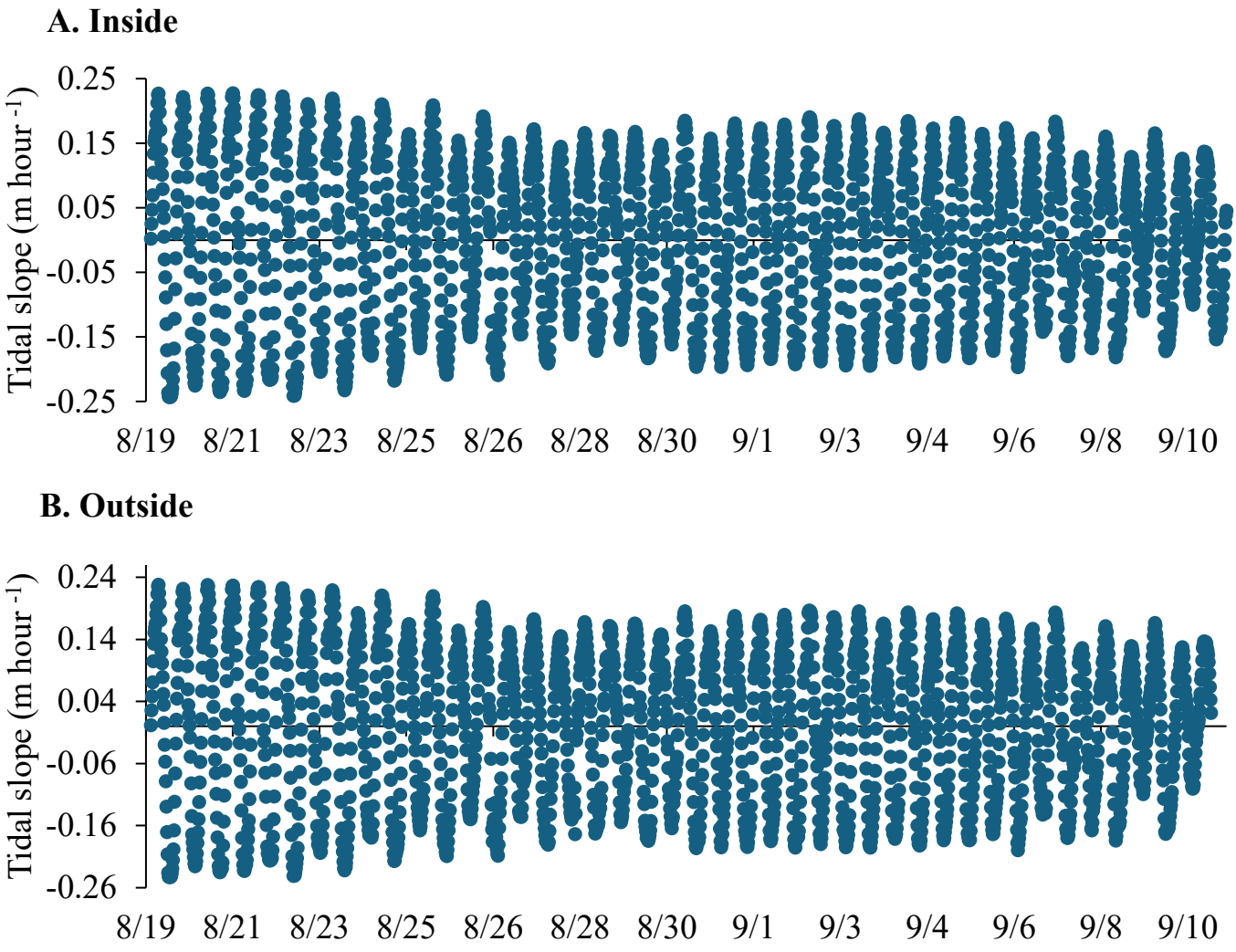


Figure 34. Tidal slope (m hour^{-1}) depicting the tidal profile of **(A)** inside **(B)** outside the conservation area of the South Haven study site in the Peconic Bays collected at 17-minute intervals using a RBR*solo*^{3} D: pressure (depth) wave attenuation sensor in August 2024.

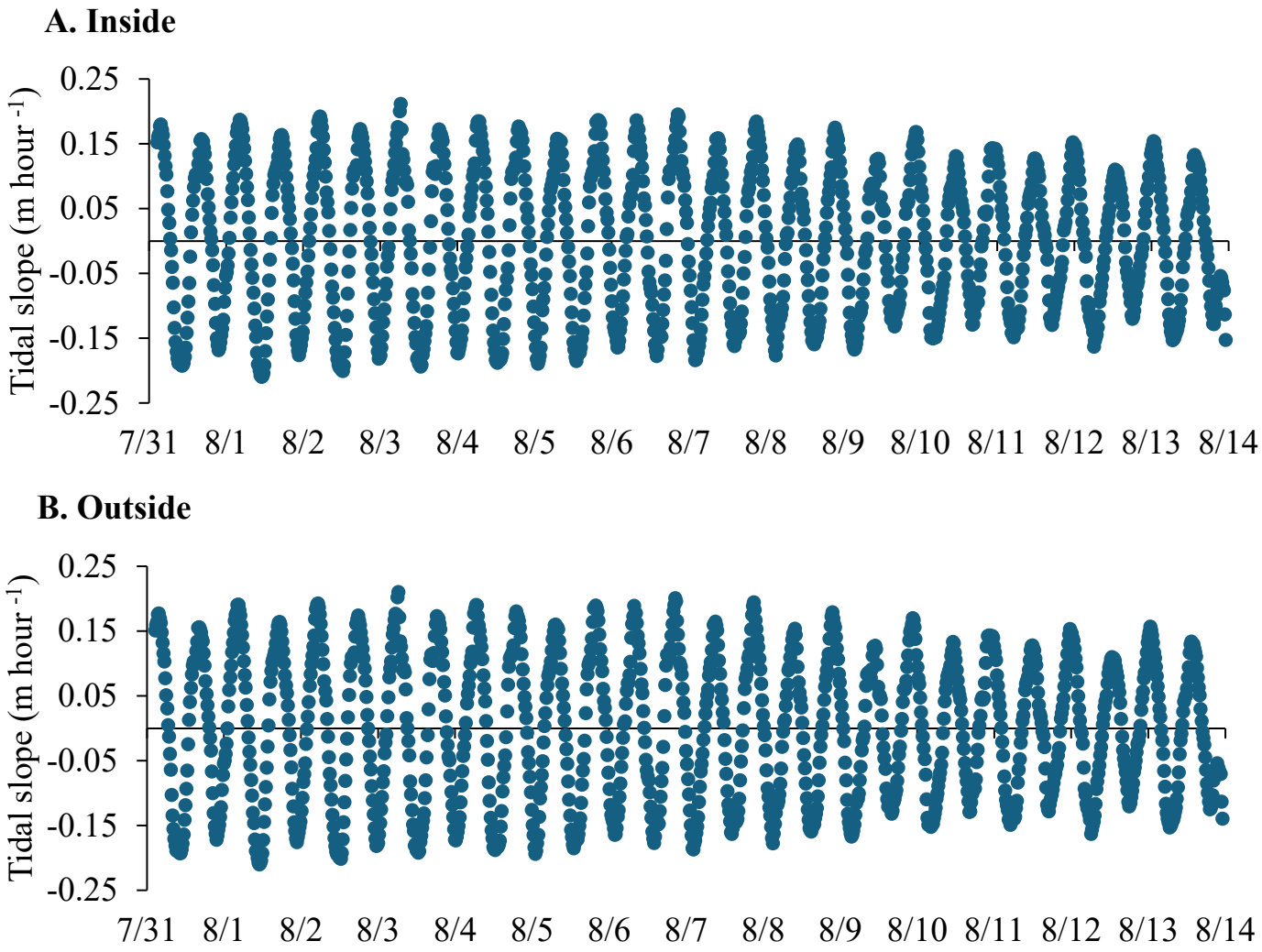


Figure 35. Tidal slope (m hour^{-1}) depicting the tidal profile of **(A)** inside **(B)** outside the conservation area of the Ganet Creek study site in the Peconic Bays collected at 17-minute intervals using a RBR*solo*^{3} D: pressure (depth) wave attenuation sensor in July 2024.

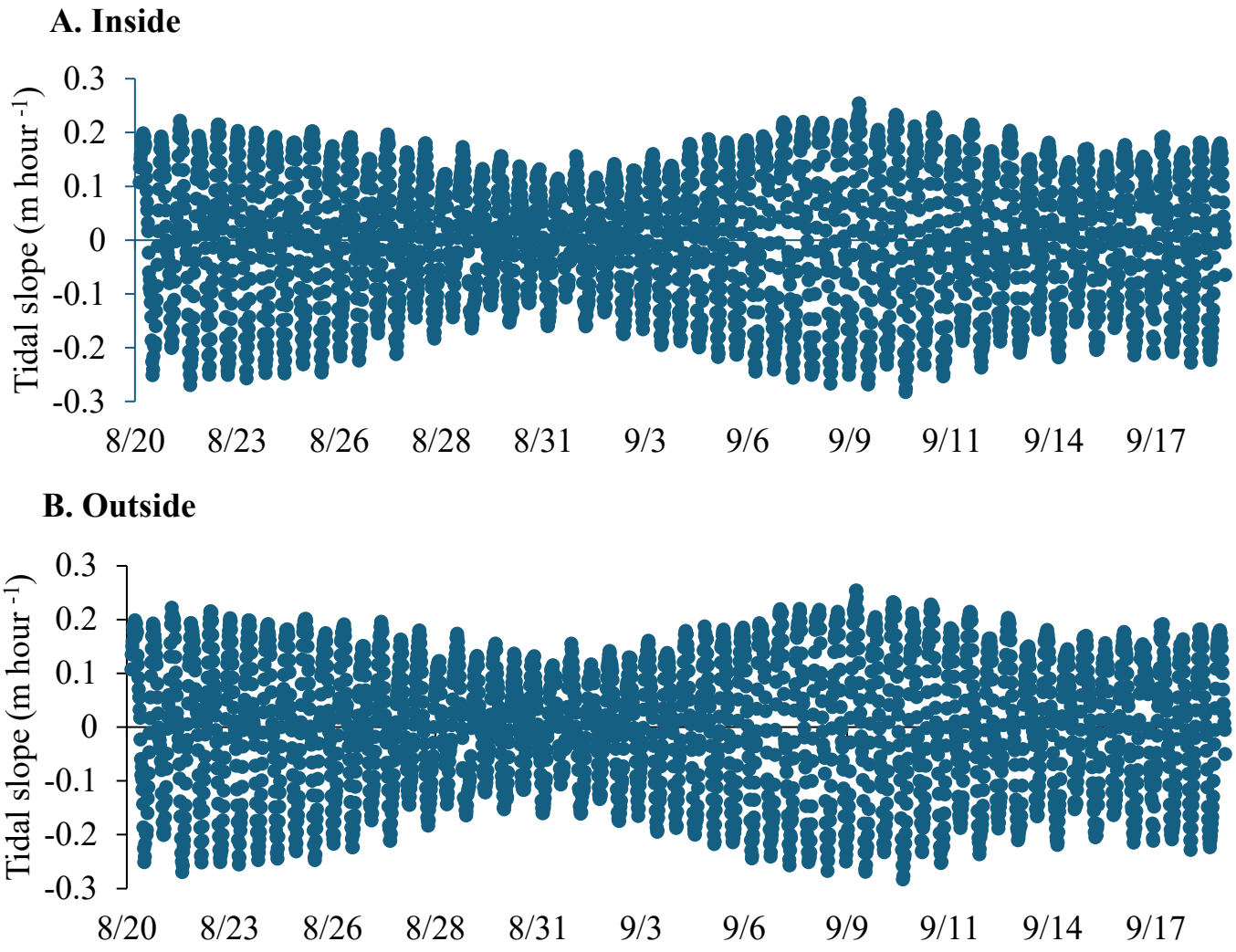


Figure 36. Tidal slope (m hour^{-1}) depicting the tidal profile of **(A)** inside **(B)** outside the conservation area of the East North Haven study site in the Peconic Bays collected at 17-minute intervals using a RBR*solo*^{3} D: pressure (depth) wave attenuation sensor in August 2025.

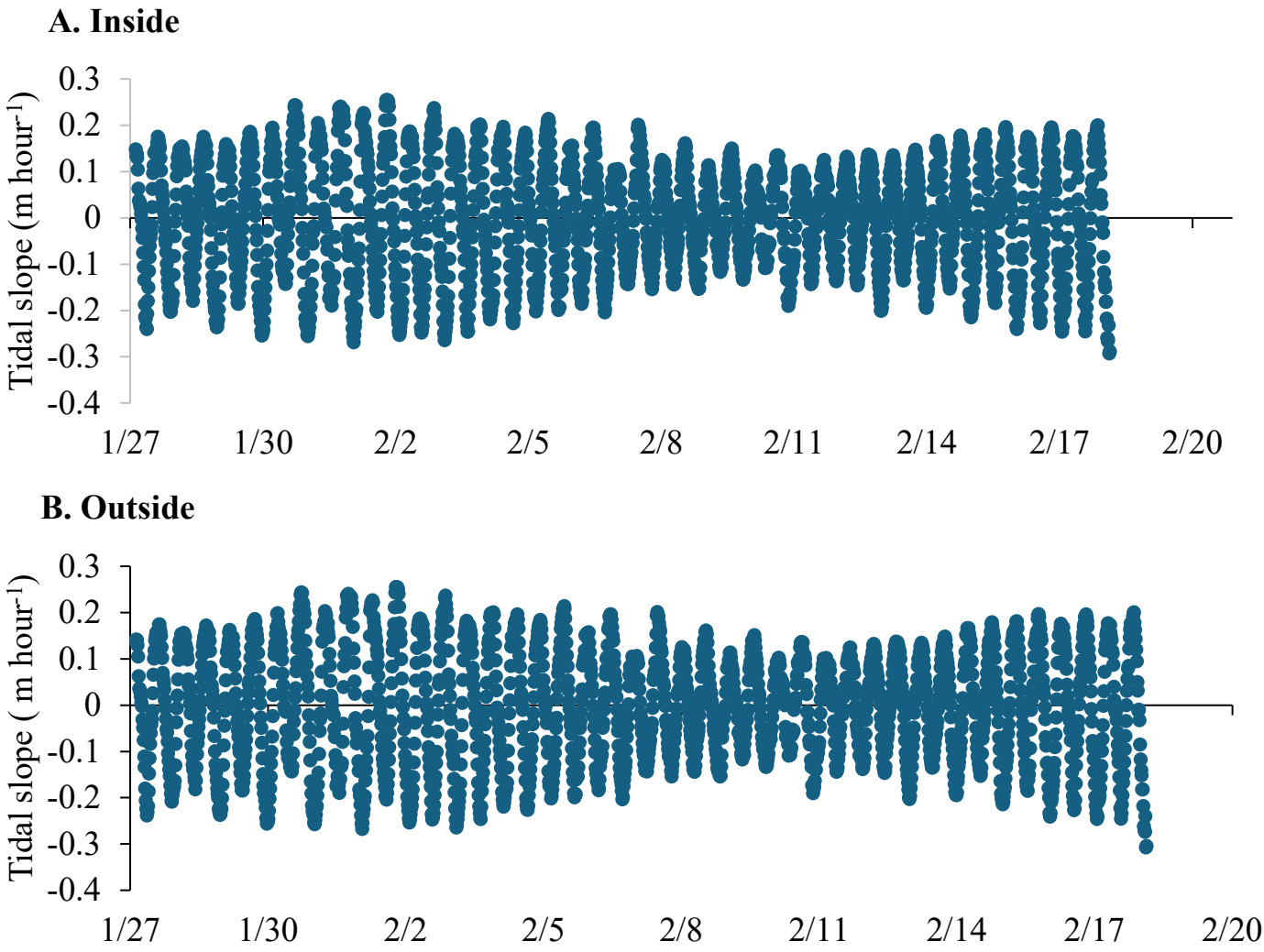


Figure 37. Tidal slope (m hour^{-1}) depicting the tidal profile of **(A)** inside **(B)** outside the conservation area of the East North Haven study site in the Peconic Bays collected at 17-minute intervals using a RBR*solo*^{3} D: pressure (depth) wave attenuation sensor in late January to late February 2026.

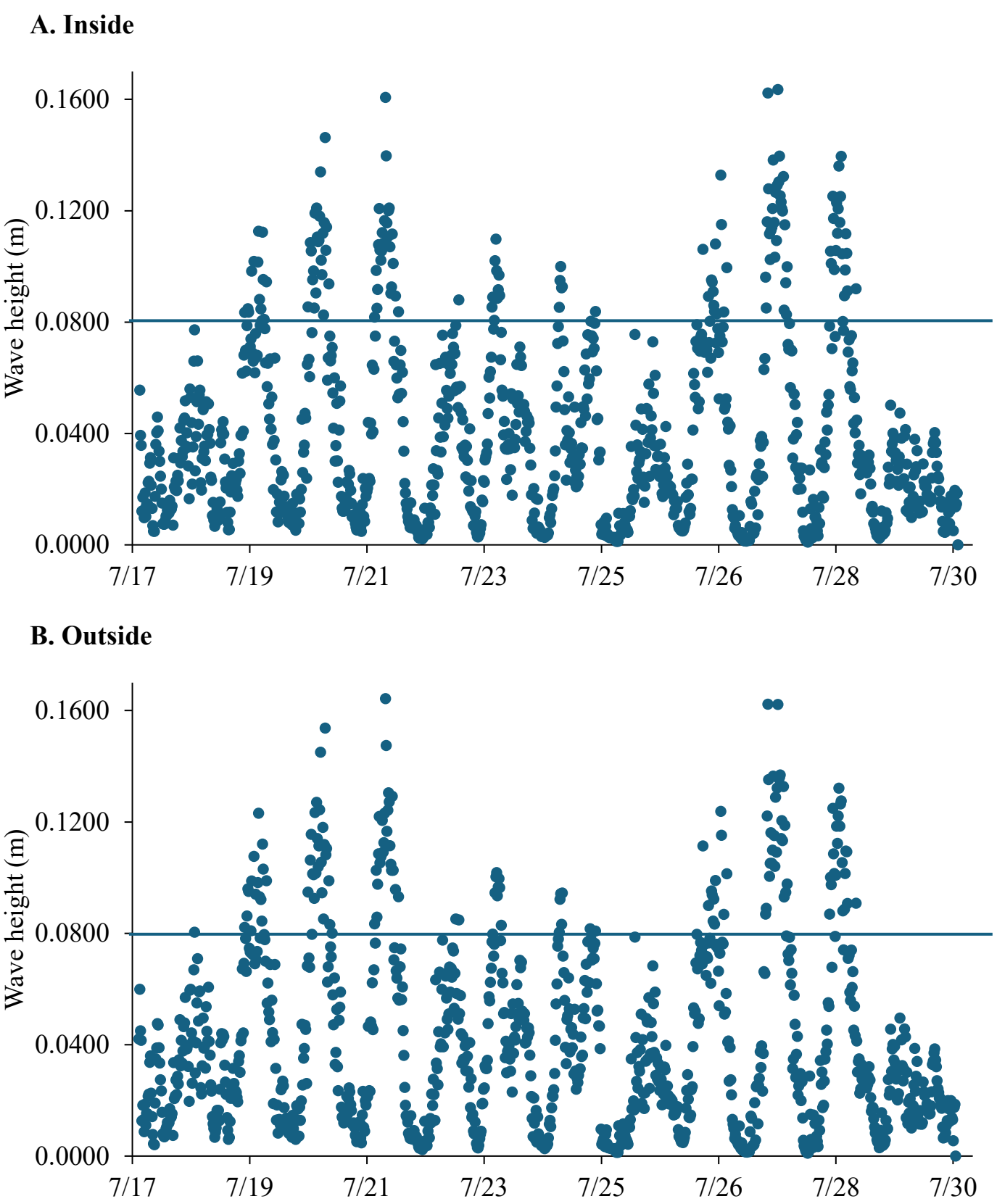


Figure 38. Average wave height (m) depicting general state of surface water of **(A)** inside **(B)** outside the conservation area of the East North Haven study site in the Peconic Bays collected at 17-minute intervals using a RBR*solo*³ D: pressure (depth) wave attenuation sensor in July 2024.

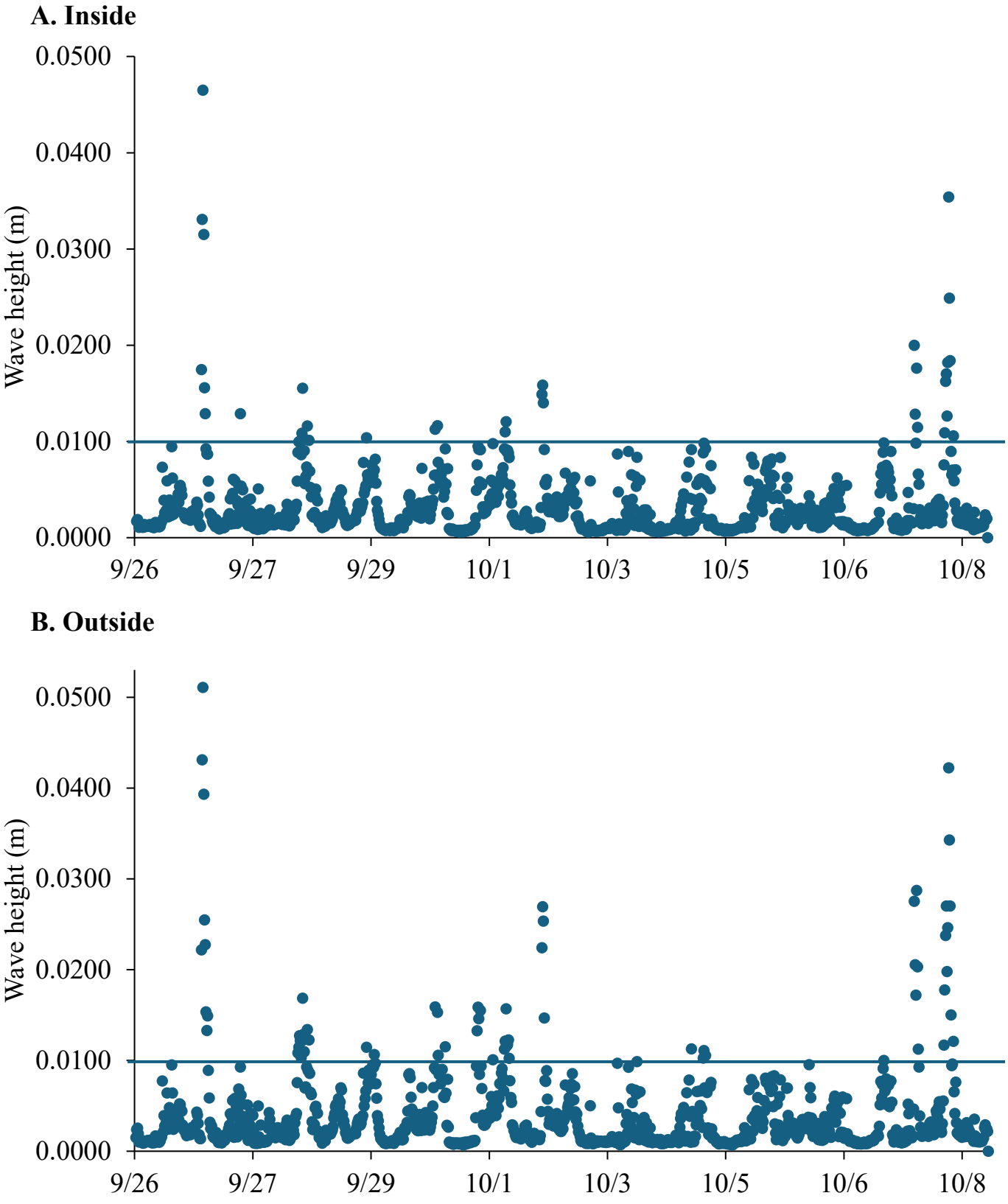


Figure 39. Average wave height (m) depicting general state of surface water of **(A)** inside **(B)** outside the conservation area of the Sag Harbor Marina study site in the Peconic Bays collected at 17-minute intervals using a RBR*solo*³ D: pressure (depth) wave attenuation sensor in September 2024.

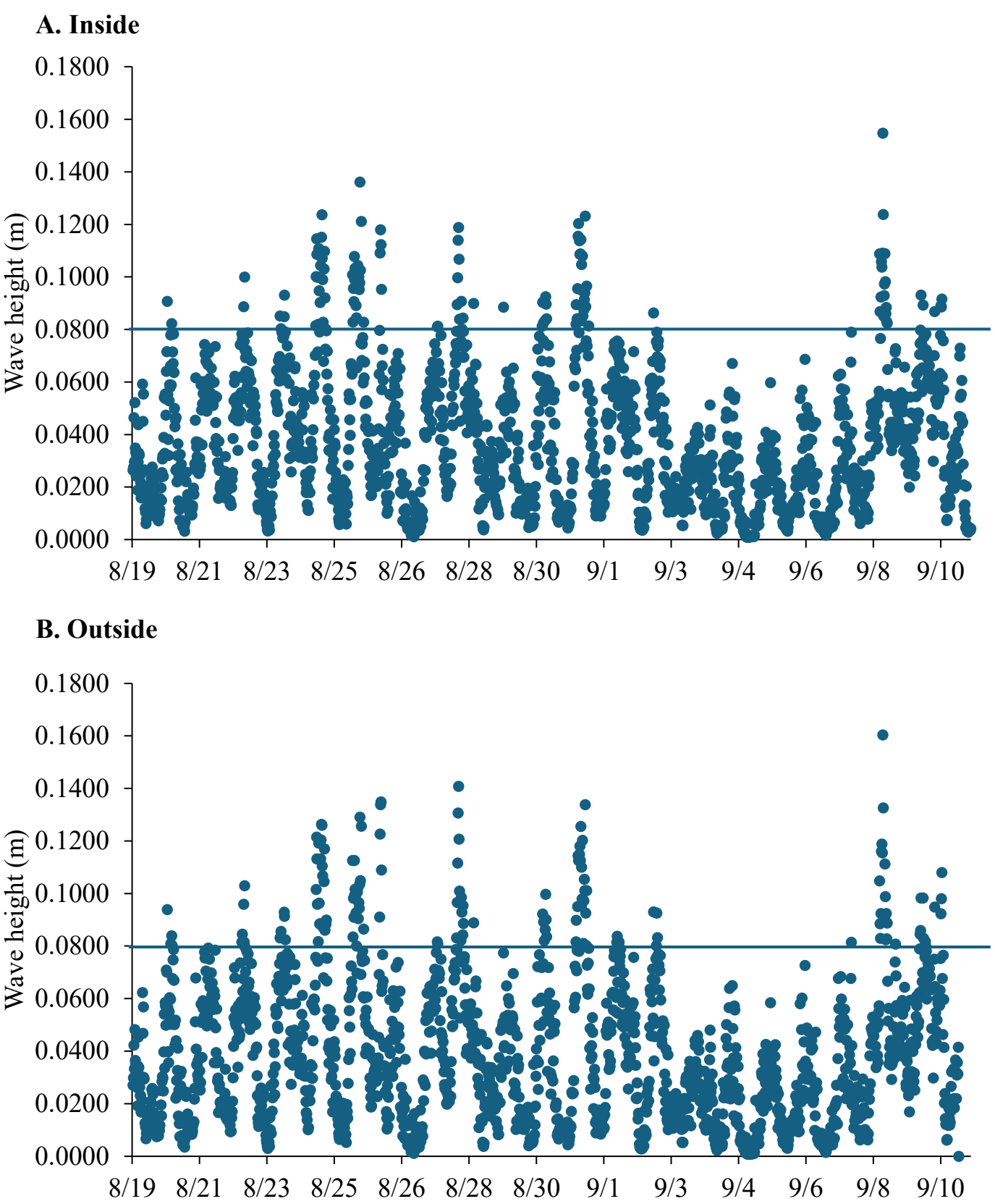


Figure 40. Average wave height (m) depicting general state of surface water of **(A)** inside **(B)** outside the conservation area of the South Haven study site in the Peconic Bays collected at 17-minute intervals using a RBR*solo*^{3} D: pressure (depth) wave attenuation sensor in August 2024.

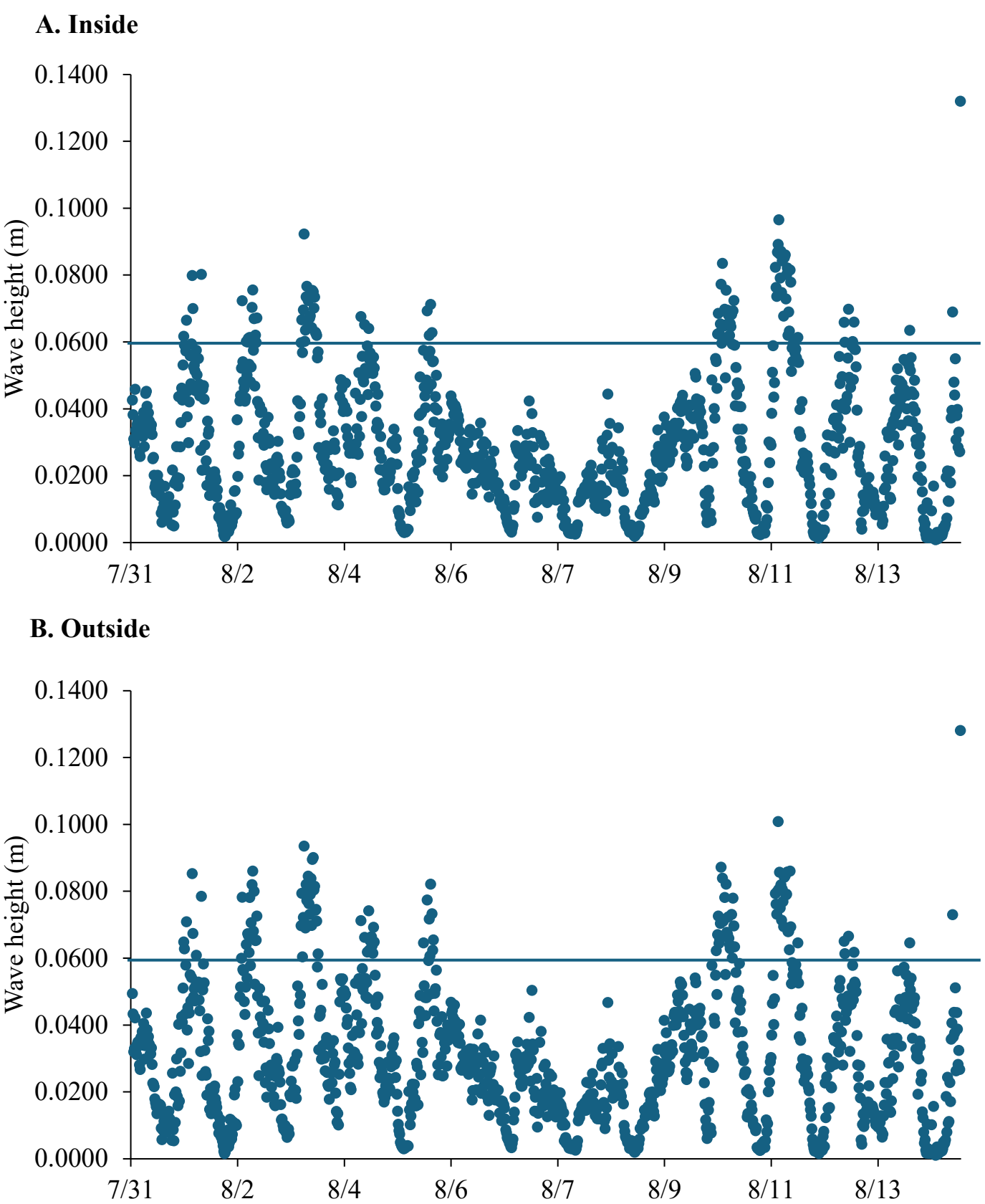


Figure 41. Average wave height (m) depicting general state of surface water **(A)** inside **(B)** outside the conservation area of the Ganet Creek study site in the Peconic Bays collected at 17-minute intervals using a RBR*solo*³ D: pressure (depth) wave attenuation sensor in July 2024.

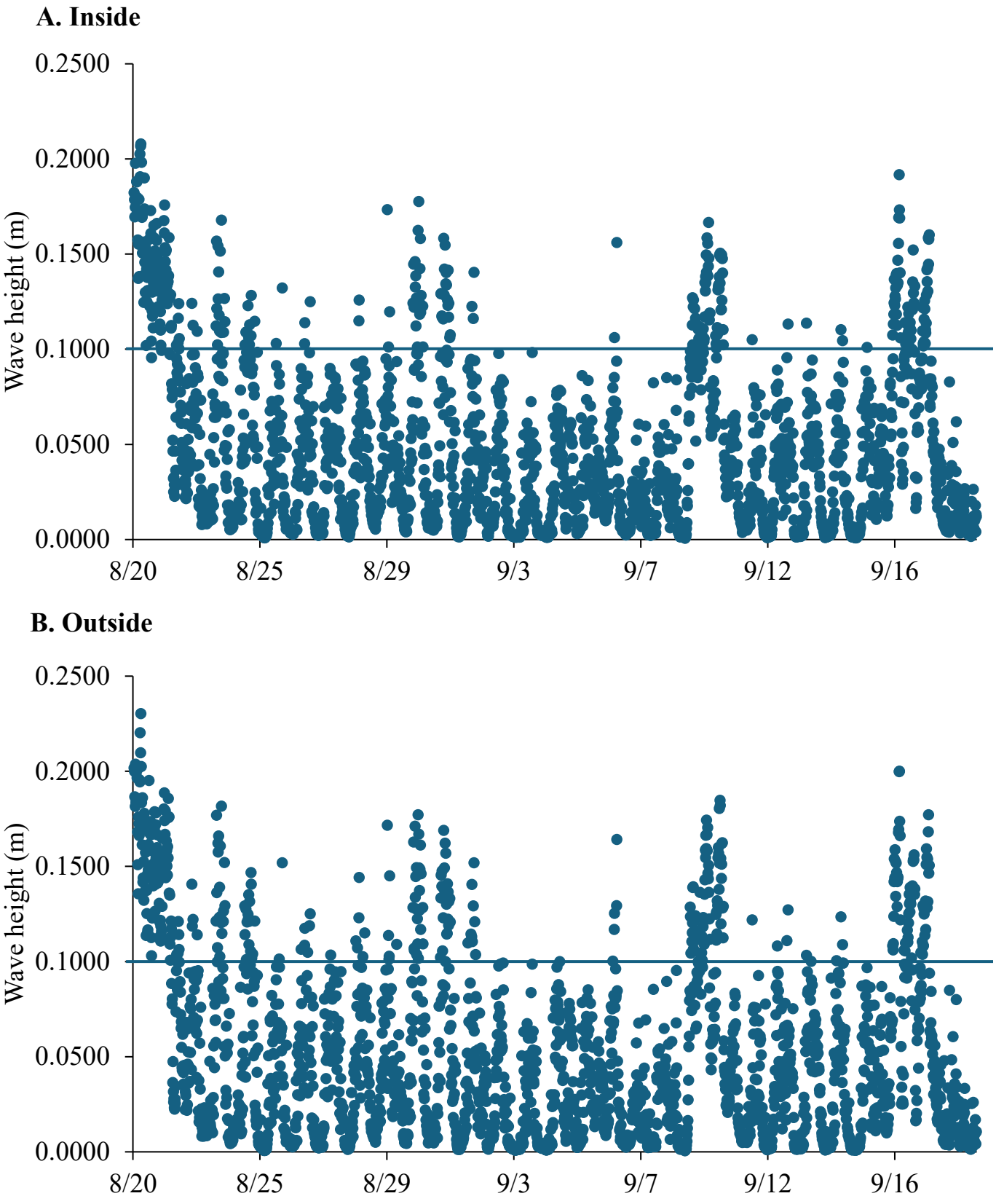


Figure 42. Average wave height (m) depicting general state of surface water of **(A)** inside **(B)** outside the conservation area of the East North Haven study site in the Peconic Bays collected at 17-minute intervals using a RBR*solo*³ D: pressure (depth) wave attenuation sensor in August 2025.

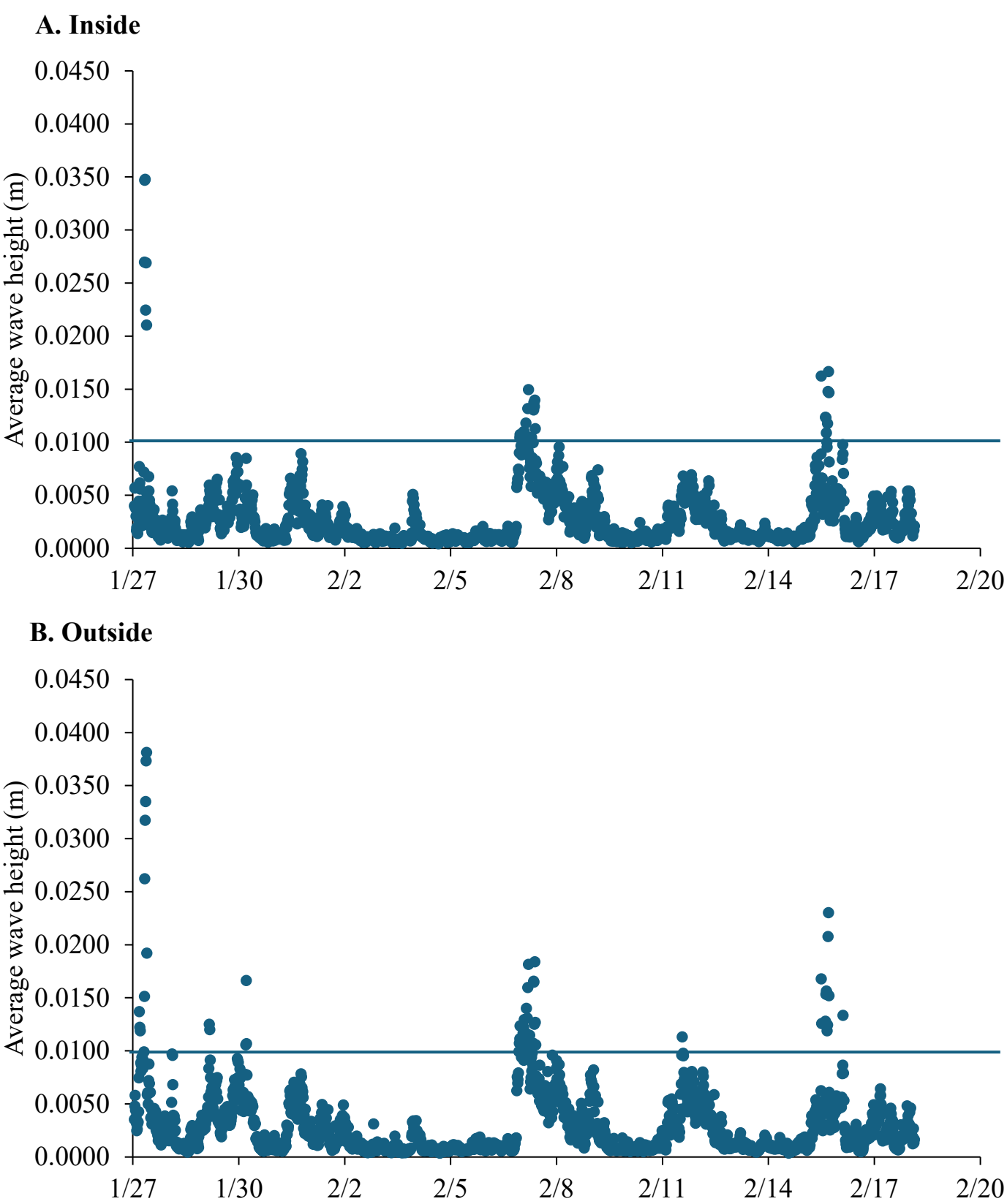


Figure 43. Average wave height (m) depicting general state of surface water of **(A)** inside **(B)** outside the conservation area of the East North Haven study site in the Peconic Bays collected at 17-minute intervals using a RBR*solo*³ D: pressure (depth) wave attenuation sensor in late January to late February 2026.

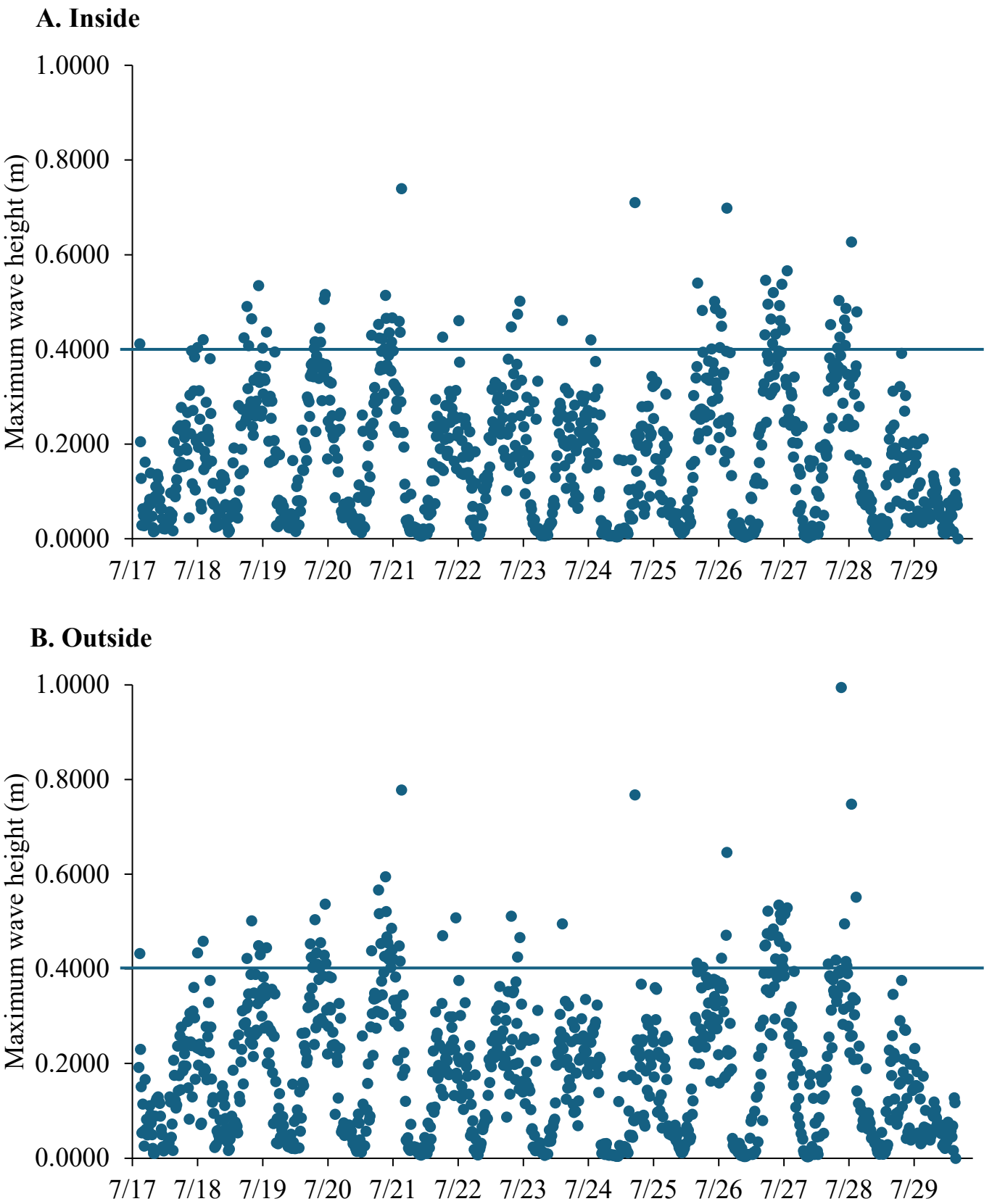


Figure 44. Maximum wave height (m) depicting wave damping caused by dissipative force of friction by the bottom cages in **(A)** inside and depicting boat wakes in **(B)** outside the conservation area of the East North Haven study site in the Peconic Bays collected at 17-minute intervals using a RBR*solo*^{3} D: pressure (depth) wave attenuation sensor in July 2024.

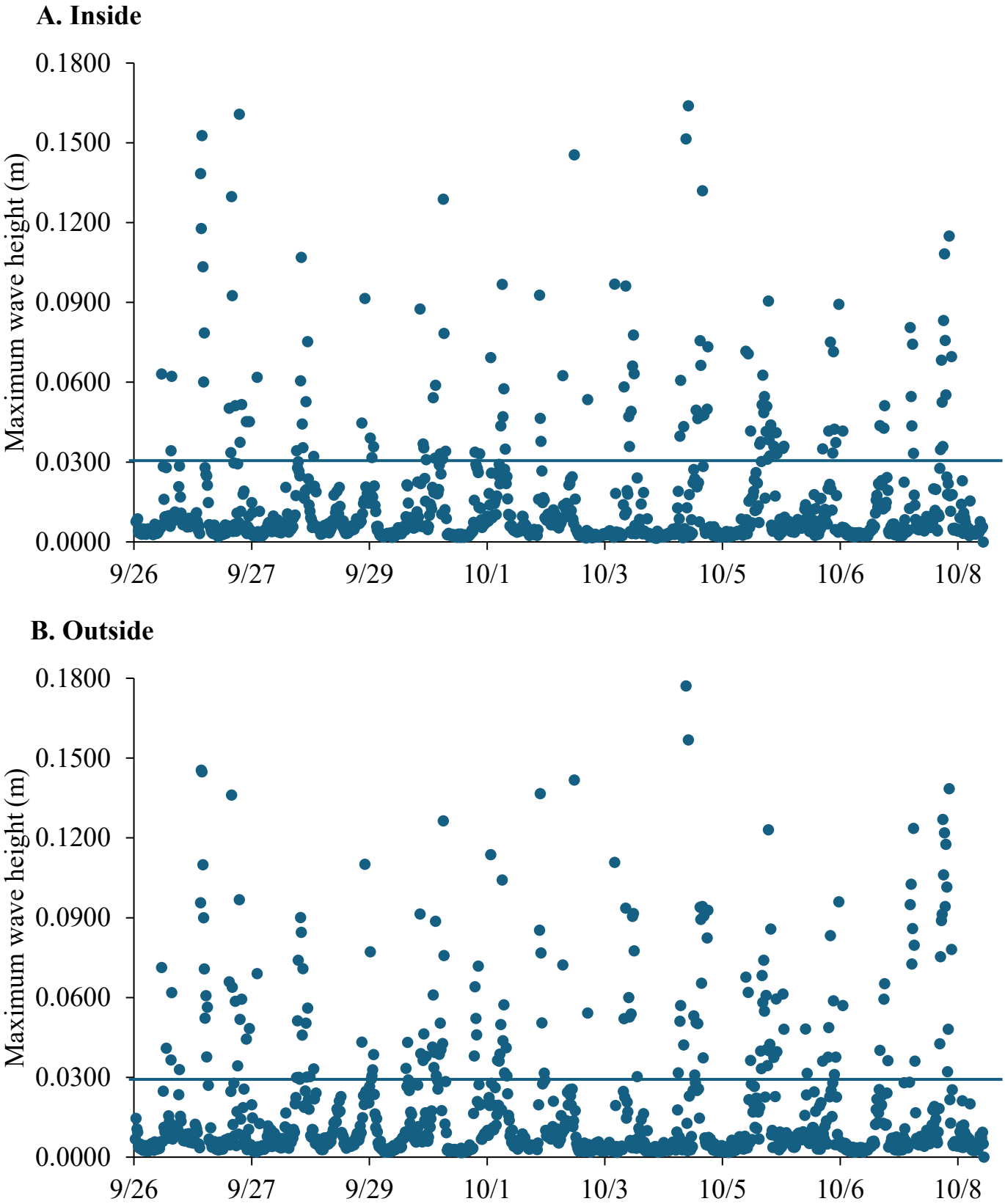


Figure 45. Maximum wave height (m) depicting wave damping caused by dissipative force of friction by the bottom cages in **(A)** inside and depicting boat wakes in **(B)** outside the conservation area of the Sag Harbor Marina study site in the Peconic Bays collected at 17-minute intervals using a RBR*solo*³ D: pressure (depth) wave attenuation sensor in September 2024.

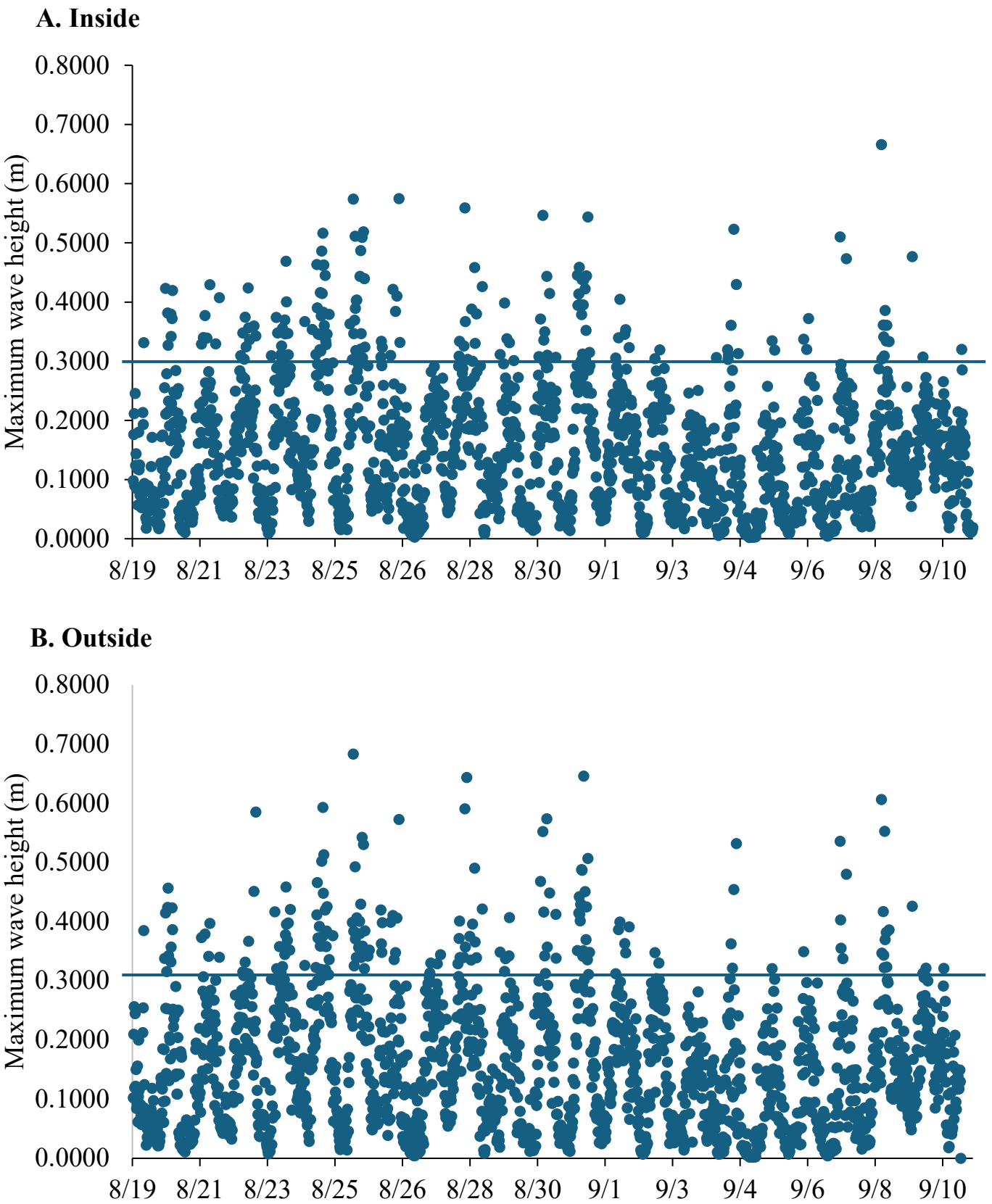


Figure 46. Maximum wave height (m) depicting wave damping caused by dissipative force of friction by the bottom cages in **(A)** inside and depicting boat wakes in **(B)** outside the conservation area of the South Haven study site in the Peconic Bays collected at 17-minute intervals using a RBR*solo*^{3} D: pressure (depth) wave attenuation sensor in August 2024.

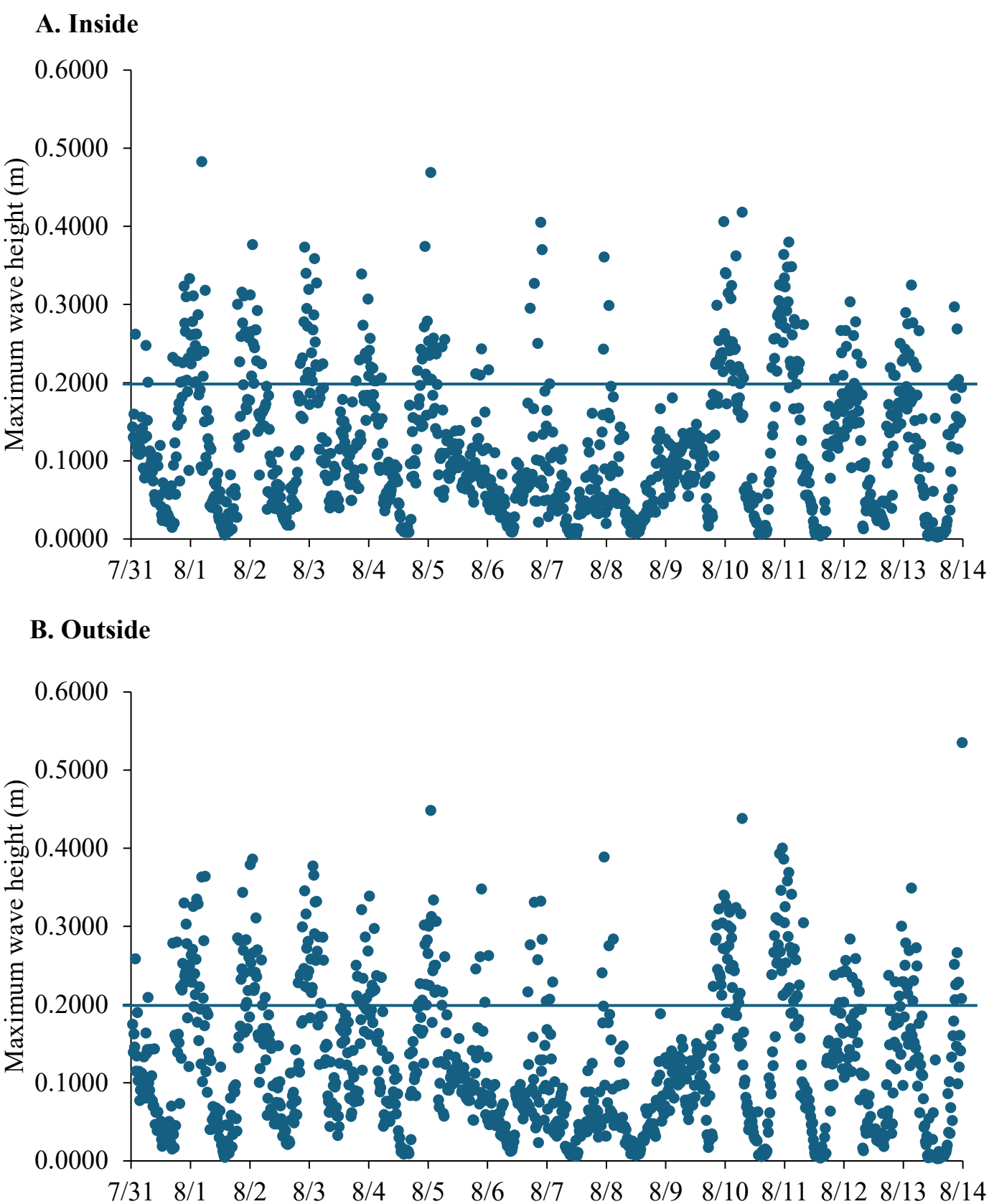


Figure 47. Maximum wave height (m) depicting wave damping caused by dissipative force of friction by the bottom cages in **(A)** inside and depicting boat wakes in **(B)**) outside the conservation area of the Ganet Creek study site in the Peconic Bays collected at 17-minute intervals using a RBR*solo*^{3} D: pressure (depth) wave attenuation sensor in July 2024.

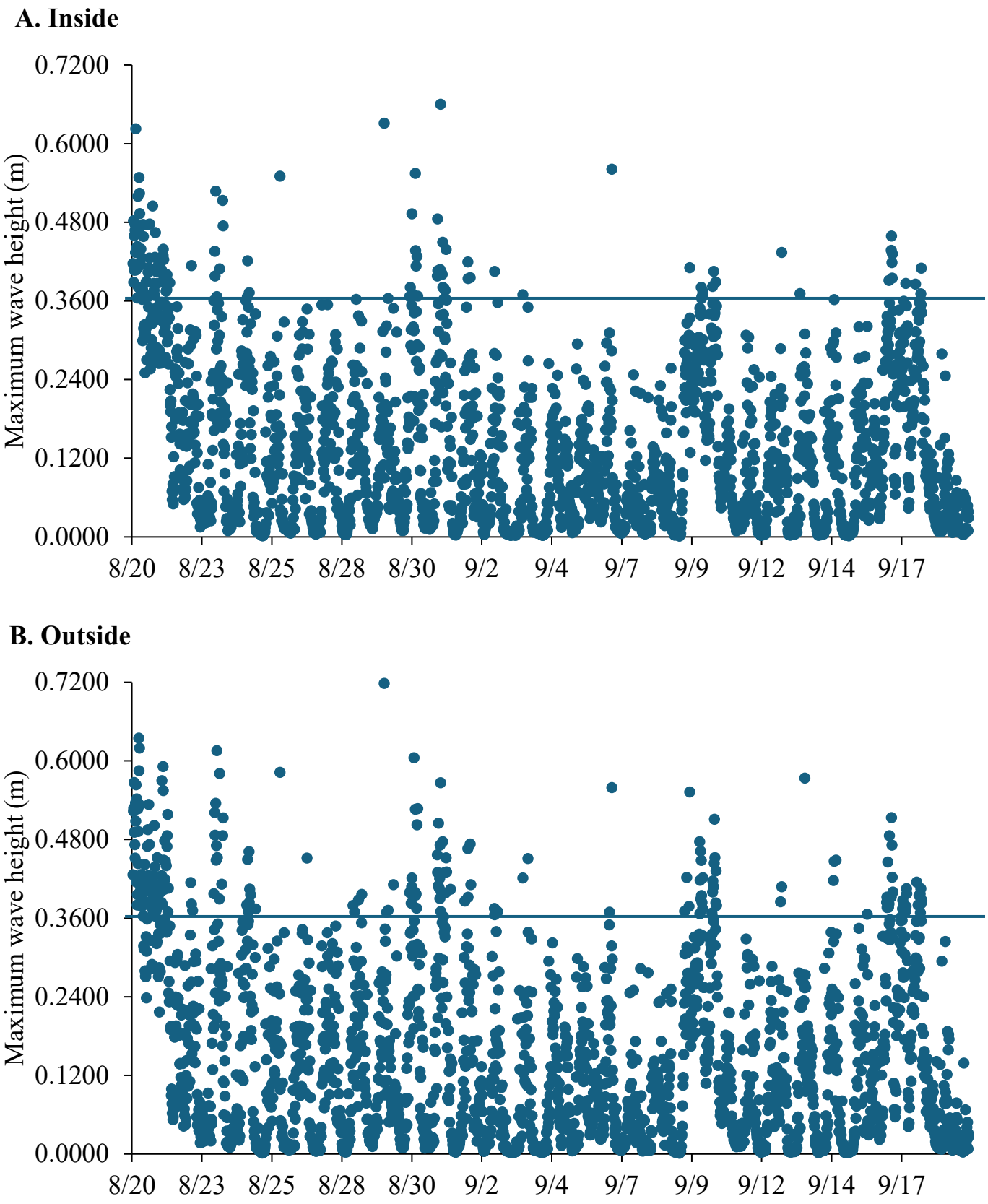


Figure 48. Maximum wave height (m) depicting wave damping caused by dissipative force of friction by the bottom cages in **(A)** inside and depicting boat wakes in **(B)** outside the conservation area of the East North Haven study site in the Peconic Bays collected at 17-minute intervals using a RBR*solo*³ D: pressure (depth) wave attenuation sensor in August 2025.

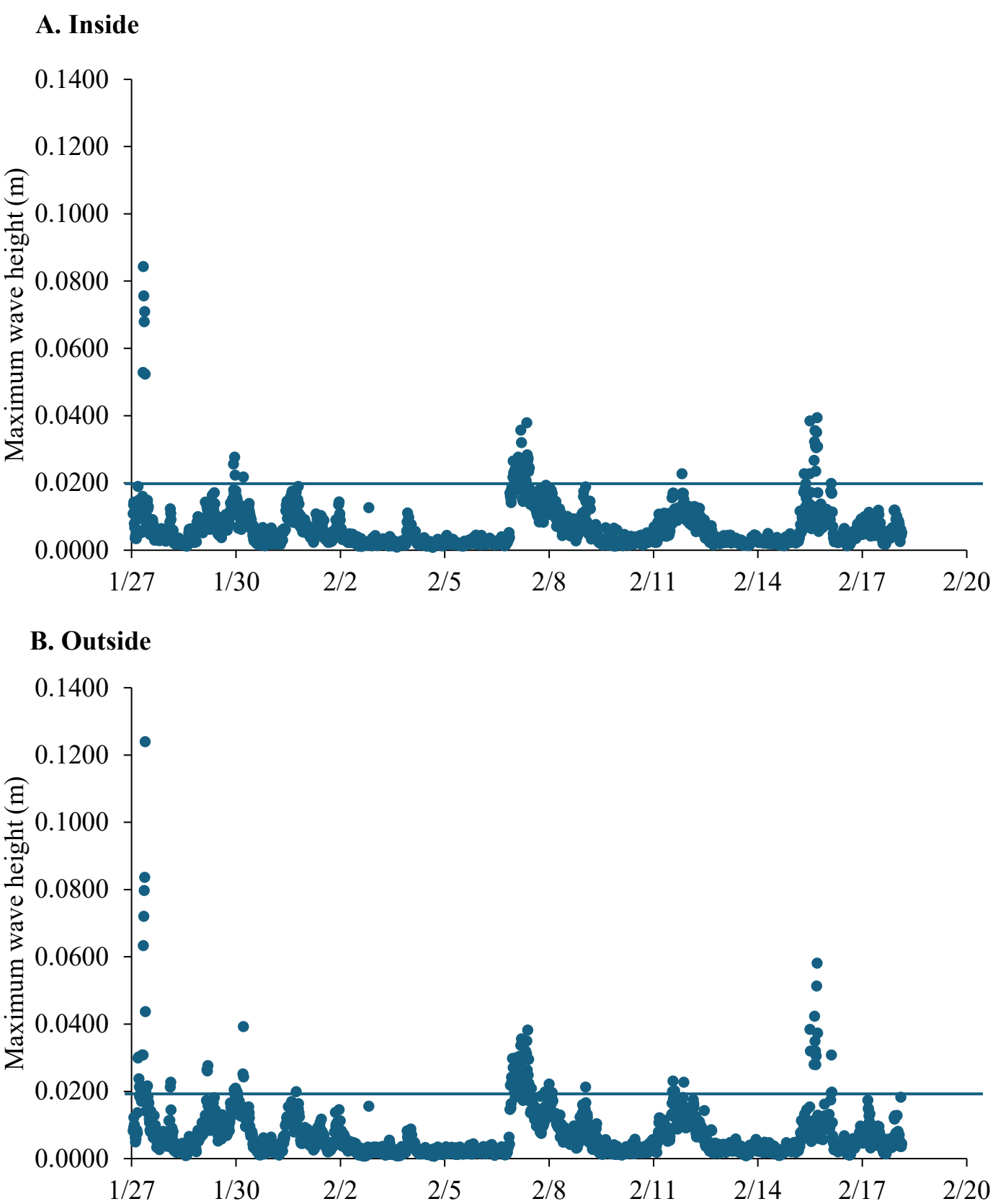


Figure 49. Maximum wave height (m) depicting wave damping caused by dissipative force of friction by the bottom cages in **(A)** inside and depicting boat wakes in **(B)** outside the conservation area of the East North Haven study site in the Peconic Bays collected at 17-minute intervals using a RBR*solo*^{3} D: pressure (depth) wave attenuation sensor in late January to late February 2026.

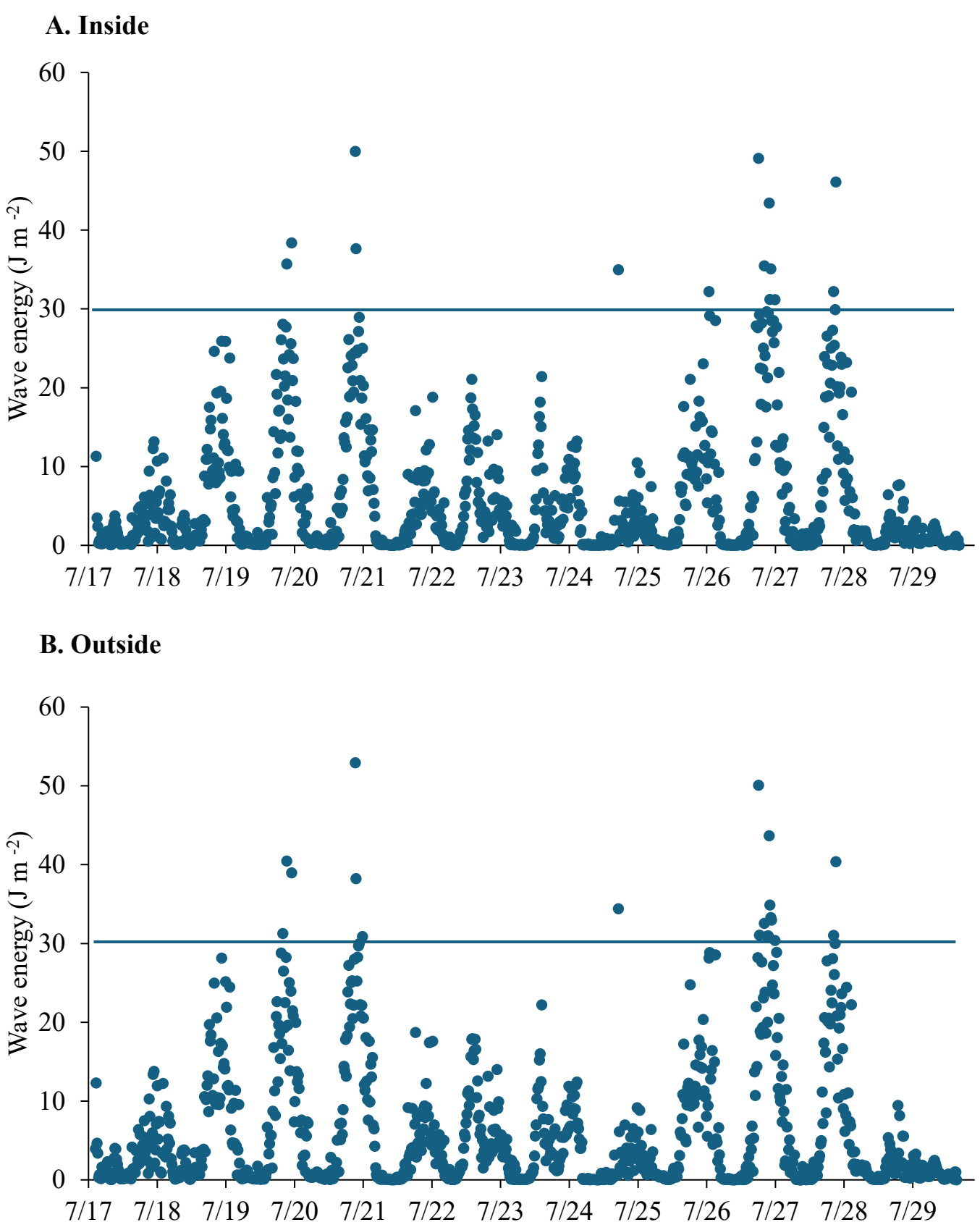


Figure 50. Wave energy (J m^{-2}) depicting total kinetic and potential energy per unit surface area of waves in **(A)** inside and in **(B)** outside the conservation area of the East North Haven study site in the Peconic Bays collected at 17-minute intervals using a RBR*solo*^{3} D: pressure (depth) wave attenuation sensor in July 2024.

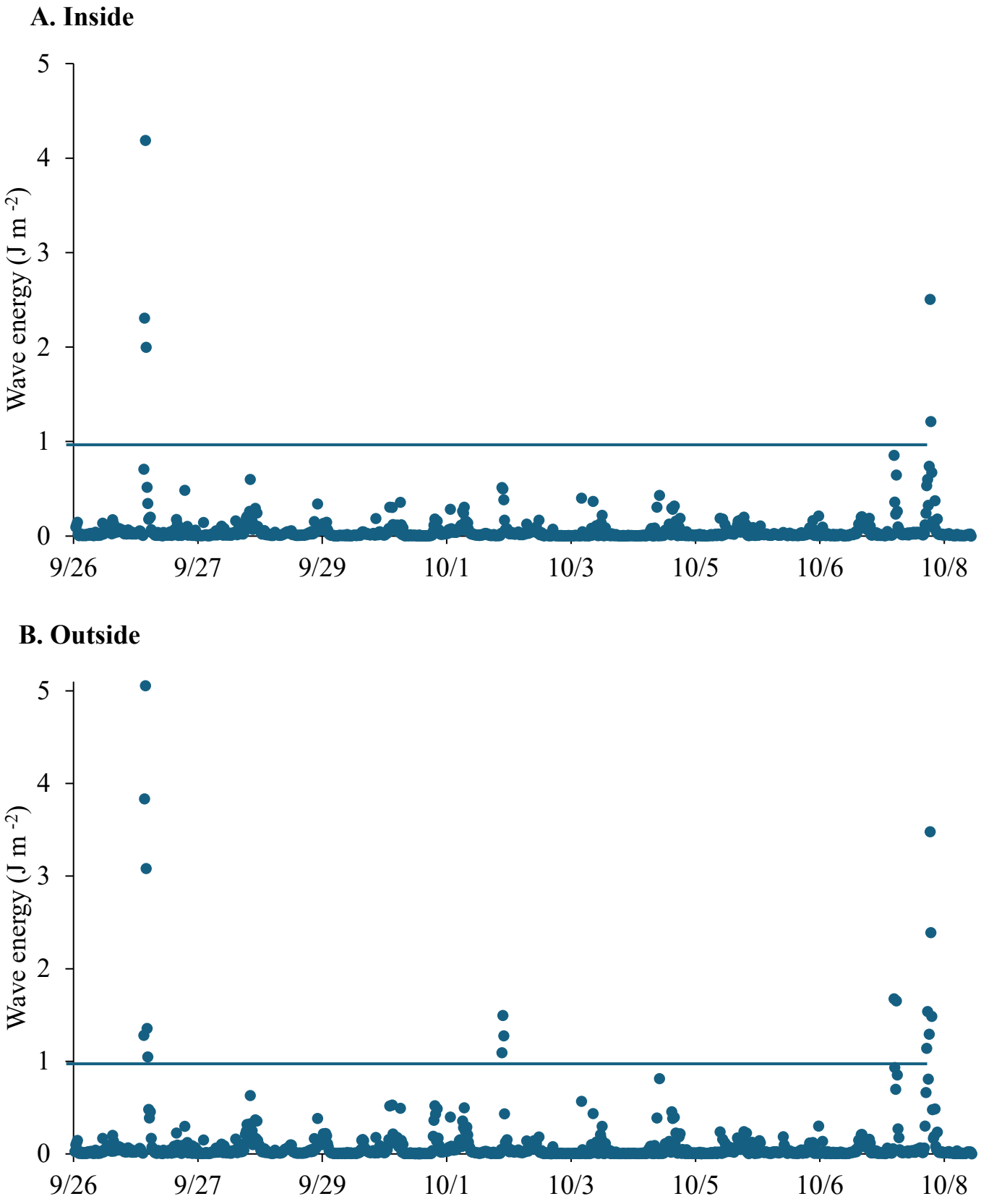


Figure 51. Wave energy (J m^{-2}) depicting total kinetic and potential energy per unit surface area of waves in **(A)** inside and in **(B)** outside the conservation area of the Sag Harbor Marina study site in the Peconic Bays collected at 17-minute intervals using a RBR*solo*^{3} D: pressure (depth) wave attenuation sensor in September 2024.

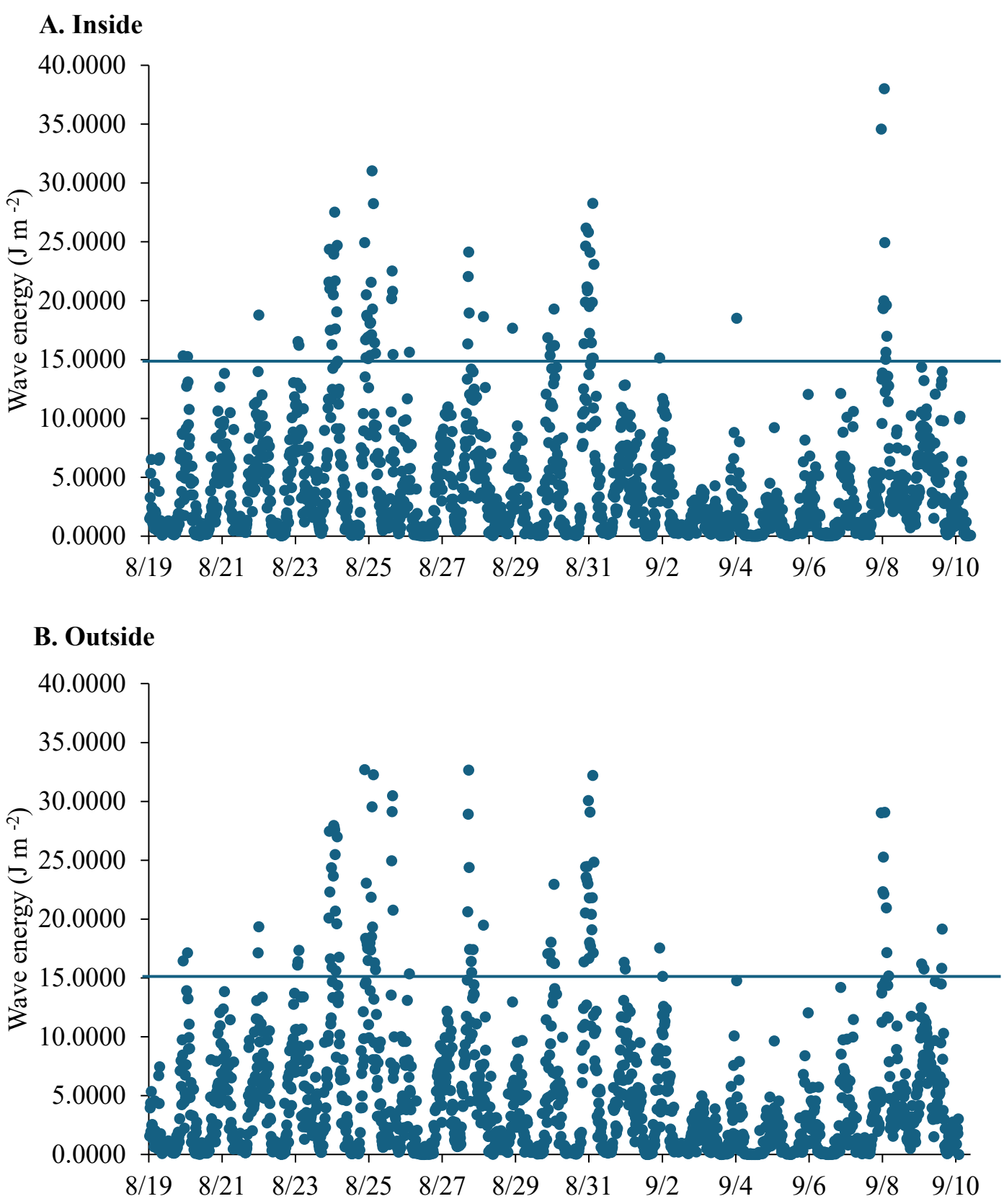


Figure 52. Wave energy (J m^{-2}) depicting total kinetic and potential energy per unit surface area of waves in **(A)** inside and in **(B)** outside the conservation area of the South Haven study site in the Peconic Bays collected at 17-minute intervals using a RBR*solo*^{3} D: pressure (depth) wave attenuation sensor in August 2024.

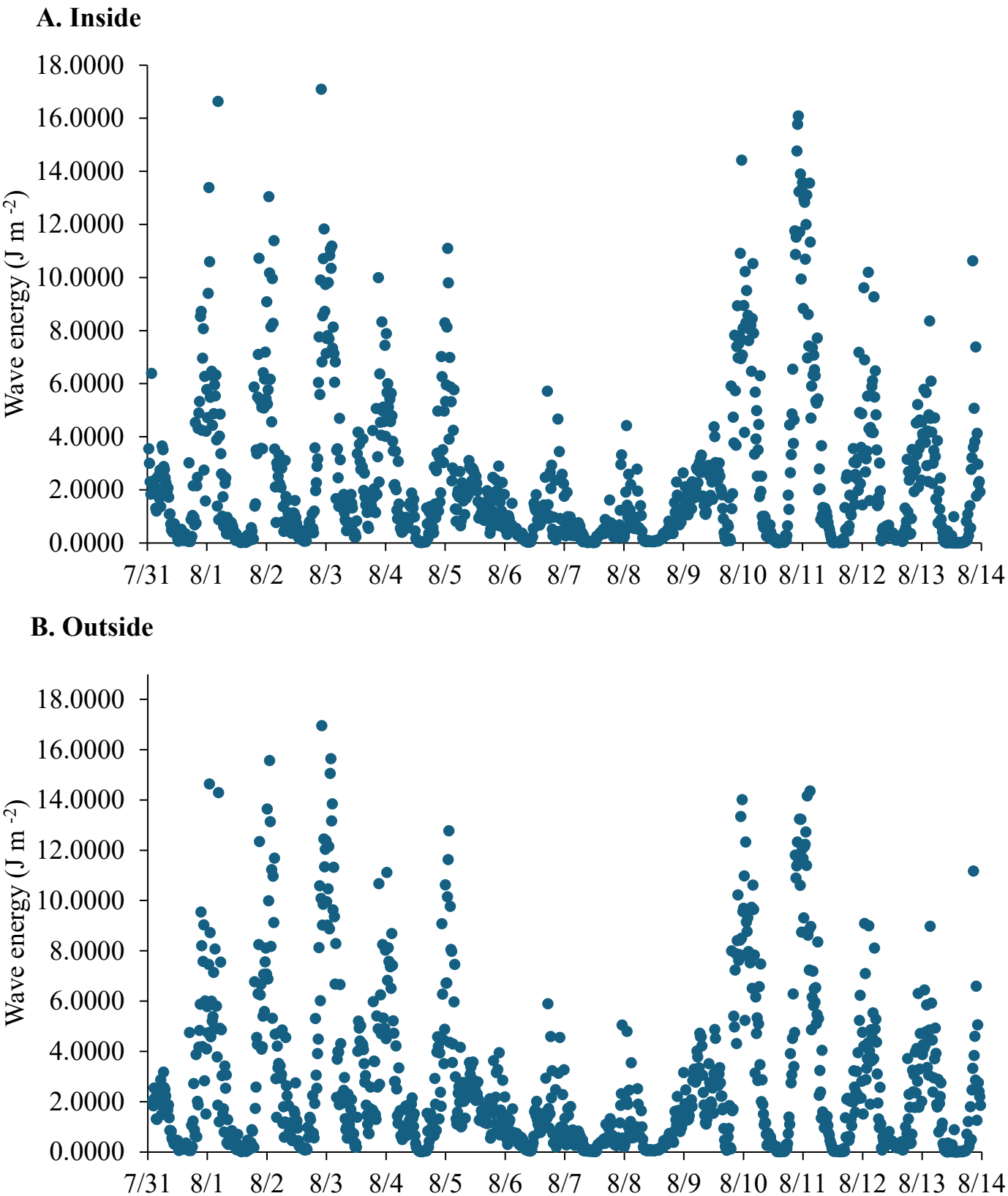


Figure 53. Wave energy (J m^{-2}) depicting total kinetic and potential energy per unit surface area of waves in **(A)** inside and in **(B)** outside the conservation area of the Ganet Creek study site in the Peconic Bays collected at 17-minute intervals using a RBR*solo*³ D: pressure (depth) wave attenuation sensor in July 2024.

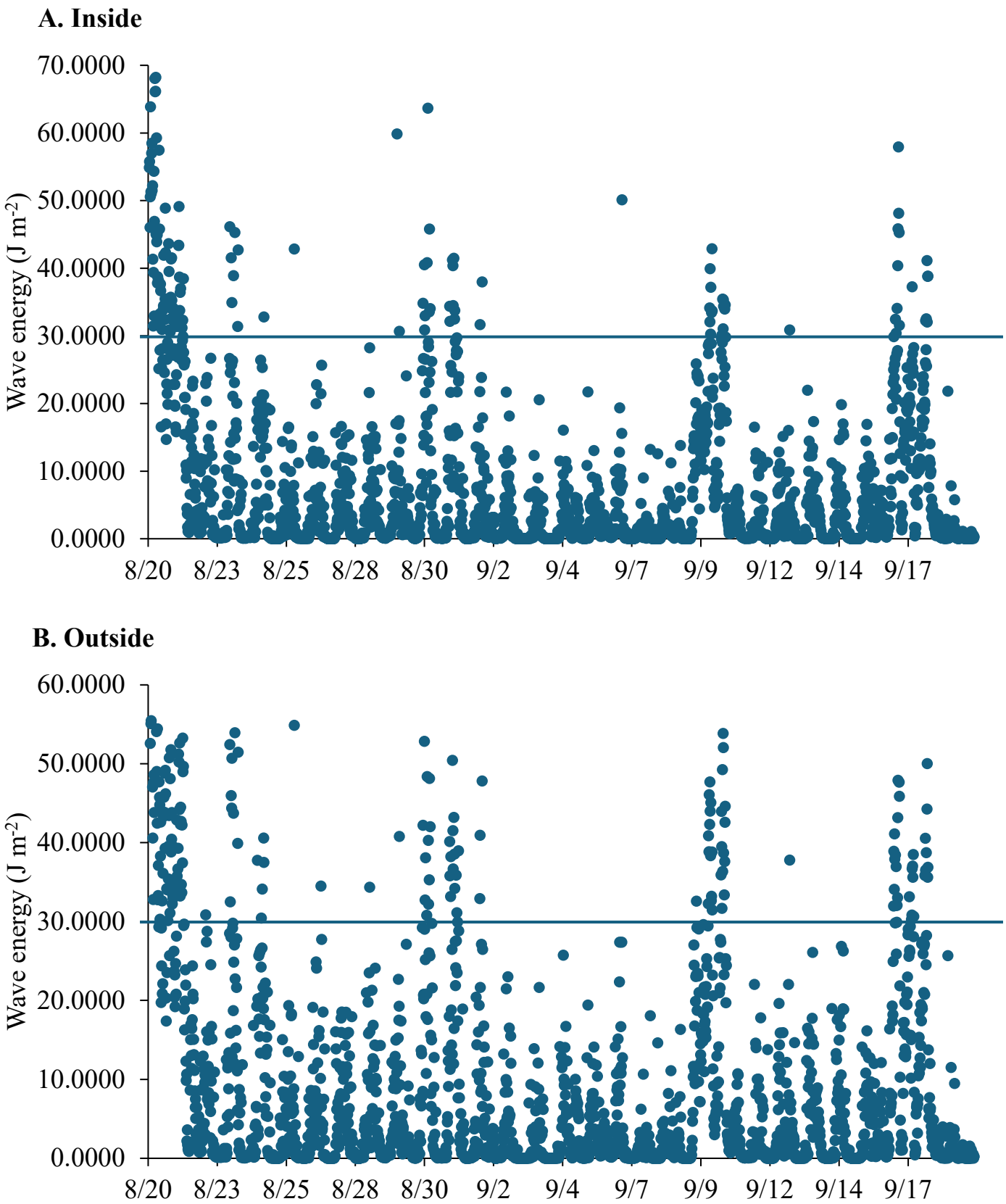


Figure 54. Wave energy (J m^{-2}) depicting total kinetic and potential energy per unit surface area of waves in **(A)** inside and in **(B)** outside the conservation area of the East North Haven study site in the Peconic Bays collected at 17-minute intervals using a RBR*solo*^{3} D: pressure (depth) wave attenuation sensor in August 2025.

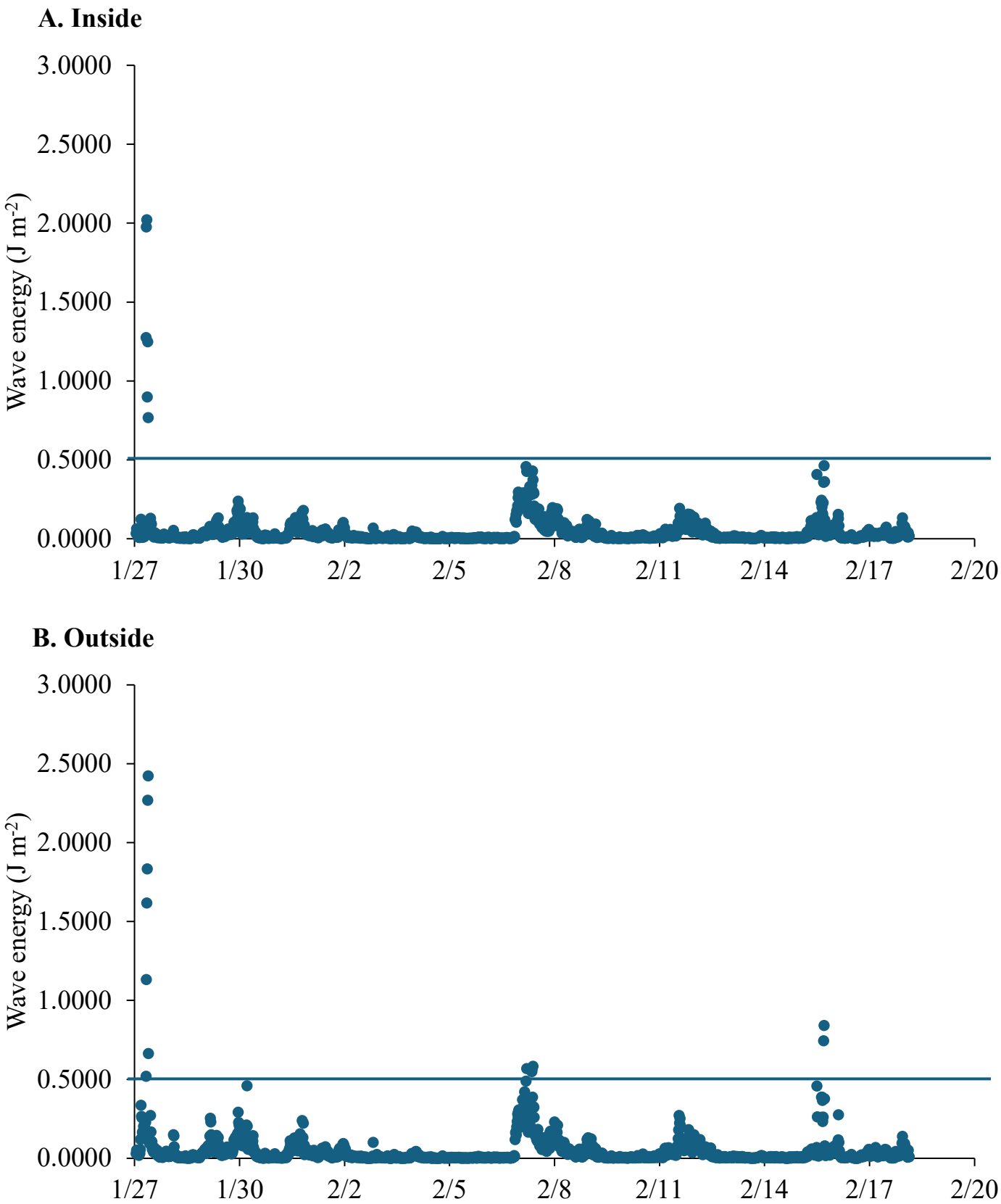


Figure 55. Wave energy (J m^{-2}) depicting total kinetic and potential energy per unit surface area of waves in **(A)** inside and in **(B)** outside the conservation area of the East North Haven study site in the Peconic Bays collected at 17-minute intervals using a RBR*solo*^{3} D: pressure (depth) wave attenuation sensor in late January to late February 2026.